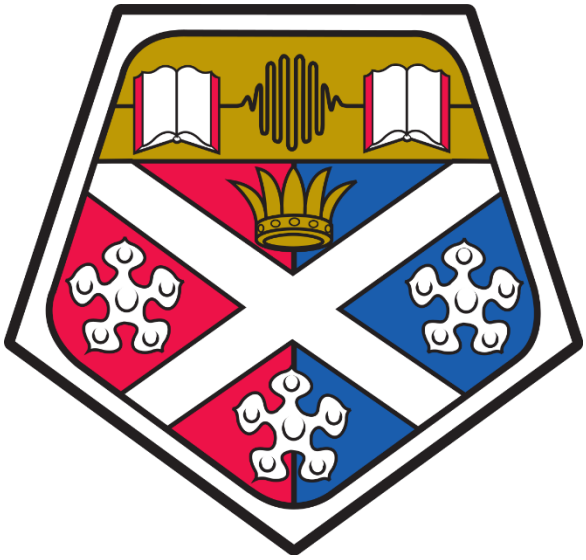

Analysis of the Effects of Forcefields on Adsorption Simulation in MOFs

MPhil Thesis

Kristina Sladekova

Department of Chemical and Process Engineering

University of Strathclyde, Glasgow

May 2022

This thesis is the result of the author's original research. It has been composed by the author and has not been previously submitted for examination which has led to the award of a degree.

Abstract

Metal-organic frameworks (MOFs) are crystalline and porous materials consisting of coordination bonds between transition-metal cations and organic ligands. The immense number of existing MOFs poses great challenges for experimental screening. Computational methods like Grand-Canonical Monte Carlo offer a viable alternative for screening, but they rely strongly on the accuracy of the underlying molecular model, or force field. In particular, the assignment of atomic point charges to each atom of the framework is required for modelling Coulombic interactions between the MOF and the adsorbate(s), which are crucial in adsorption of polar compounds. This thesis reports a systematic analysis of the effect of point charges on adsorption predictions by molecular modelling, with the results showing that the use of charges developed by periodic DFT methods produce the most accurate and consistent results.

Furthermore, conventional molecular models for adsorption in MOFs neglect important physics of the process, and thus can lead to inaccurate predictions. This is particularly the case for MOFs that possess open metal sites (OMS) – the complex interaction of these sites with particular adsorbate molecules is not captured by standard force fields. The impact of neglecting these interactions can be huge, particularly considering that MOFs that contain OMS are among the most promising materials for gas storage and separation applications, precisely due to these strong and selective binding sites. In this work, experimental adsorption measurements of ethane and ethylene on CuBTC (a widely studied MOF that contains OMS) were carried out and compared to simulations implementing a bespoke model previously developed by our group to account for OMS interactions. This thesis validated the model and demonstrated its robustness even at low temperatures.

In summary, the results of this work offer a more consistent way to assess the suitability of molecular models to provide more accurate adsorption predictions.

Publications arising from this work

Sladekova, K.; Campbell, C.; Grant, C.; Fletcher, A. J.; Gomes, J. R. B.; **Jorge, M.*** "The effect of atomic point charges on adsorption isotherms of CO_2 and water in metal organic frameworks" *Adsorption*, *26*, 663-685 (2020). DOI: 10.1007/s10450-019-00187-2.

Contents

List of Figures

List of Tables

1. Introduction

Metal-organic frameworks (MOFs) are porous crystalline materials consisting of coordination bonds between transition-metal cations and organic ligands (see Figure 1.1 for an example). A wide array of metals and organic linkers have been used to produce MOFs, giving rise to structures with different properties, which can be tailored to specific requirements or applications (Moghadam et al. 2017). The intrinsic properties of these materials include very high porosity (Furukawa et al. 2010) and surface areas (Farha et al. 2012), which can be employed in various applications, such as gas storage and separation (Ma and Zhou 2010), sensor devices (Li et al. 2012) or drug delivery (Farrusseng 2011). A wide array of metals and organic linkers have been used to produce MOFs, giving rise to structures with different properties, which can be tailored to specific requirements or applications. The sheer number of MOF variations becomes apparent when looking at the Cambridge Structural Database, which currently contains over 70,000 MOF structures.

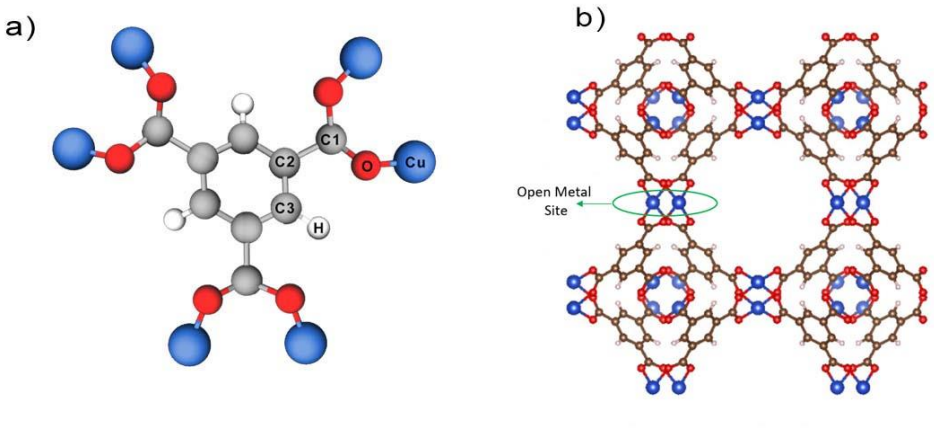

Figure 1.1 – a) CuBTC building block b) CuBTC framework structure with open metal sites highlighted in green.

A variety of processes is used in industry for gas separation. One of these processes is distillation which is based on the difference of boiling points in order to achieve separation. This process is very energy demanding for such mixtures that have similar boiling points, such as ethane/ethylene (Van Miltenburg et al. 2006).
The swing adsorption method utilizes the selectivity of the adsorbent material for a component in the gas mixture, therefore has the potential to be more energy efficient.

Examples of this method include the Pressure Swing Adsorption (PSA) and the Vacuum Swing Adsorption (VSA) (Maring & Webley 2013). Both are similar in their operating principle. PSA uses high pressures to achieve separation which are then lowered to regenerate the adsorbent, and VSA uses ambient pressures for adsorption and very low pressures for regeneration. There are many examples of MOFs being demonstrated as potential adsorbents of interest for PSA/VSA processes (Avci et al. 2018) (Altintas and Keskin, 2022).
Molecular simulations can be used to predict selectivity of the adsorbent for certain gases and therefore help in designing the separation processes described above (Nikolaidis et al. 2015) (Quaranta et al. 2021).

Some MOFs contain open metal sites (OMS) also known as coordinatively unsaturated sites. This occurs in MOFs when the metal site has additional valency outwith that occupied by the other framework components. Generally, this extra site is occupied by a guest molecule, such as solvent from synthesis. If the guest molecule is removed in a process called activation, however, the metal is left with a free unsaturated site (see green highlight in Figure 1.1b) and it can form strong bonds with certain adsorbates, such as unsaturated hydrocarbons, through electron donation from the π orbitals of the hydrocarbon to the metal site (Zhang et al. 2015). These sites have demonstrated selective adsorption for many practical applications, strongly adsorbing gases such as carbon dioxide (Britt et al. 2009), ethylene (Nechaev et al. 2014) and hydrogen (Chen et al. 2005). This unique adsorption mechanism puts OMS-containing MOFs in a prime position as potential adsorbents for gas separation processes. The OMS can exploit differences in electron donation capabilities for certain gas mixtures, such as ethane/ethylene, where only the ethylene gas will be able to form these coordination bonds with the MOF, producing a high gas selectivity (Nechaev et al. 2014). This selectivity feature is promising in the aforementioned case of olefin/paraffin separations, which are generally achieved through costly cryogenic distillation.

The presence of these OMS introduces additional complexity in simulations. The standard force fields for simulation were not developed to account for complex orbital interactions. As such, Grand Canonical Monte Carlo (GCMC) adsorption simulations using standard force fields fail in capturing the expected increase in adsorption of electron-donating compounds, observed in experiments. A new model, based on a combination of quantum mechanical (QM) calculations and GCMC, was developed by our group to overcome this issue (Jorge et al. 2014).

MOFs can also be categorized as rigid or flexible. In rigid MOFs, the framework structure does not change in response to external conditions and the porosity remains constant (Susumu and Mitsuru 1998). Flexible MOFs, on the other hand, have a non-rigid structure which can change conformation in a reversible way in response to external stimuli. Some of these stimuli include light, temperature or adsorption/desorption of guest molecules (Schneeman et al. 2014). A 'breathing effect' is observed where the structure changes in the right conditions and then reverts back to its original state when the stimuli are absent. This feature can lead to changes in pore volume and therefore adsorption capacity in flexible MOFs. Some of the applications of flexible MOFs include gas separation, as due to their flexibility they can act in a sieve-like manner (Bux et al. 2011). One such example is MIL-53, which can alternate between closed and open pores depending on the nature of adsorbate molecules (Chen et al. 2013). Framework flexibility also poses particular challenges to molecular modelling of adsorption in such MOFs, since the force field must account for the dynamic response of the framework upon adsorption (Coupry et al. 2016) (Bureekaew et al., 2013).

A particular application where MOFs have shown great potential is carbon dioxide capture, normally by designing new materials with high affinity for CO_2 (Kensari et al. 2013; Torrisi et al. 2010). In this context, however, a crucial and often overlooked aspect is the effect of the presence of trace amounts of water vapour in the feed stream on the performance of the process. Water, being a highly polar molecule, can compete with CO_2 for adsorption in strongly adsorbing sites of the MOF, and therefore affects the efficiency of carbon capture (Yazaydin et al. 2009). In particular, water will adsorb very strongly in MOFs that contain OMS, and the exact mechanism of competitive adsorption at these sites is still not fully understood.

Despite their great potential as adsorbents, the vast number and variety of MOF structures make it extremely time consuming and error prone to experimentally evaluate their properties. This obstacle is being increasingly overcome by using molecular simulation. This computational method allows high throughput screening of existing or hypothetical MOFs by modelling the MOF structure and its interactions with the adsorbate(s). It is therefore possible to efficiently identify materials with properties that are desirable for a specific application, for example their selectivity for a specific gas mixture, by simulating their adsorption behaviour. Once the best performing MOFs have been narrowed down, they can be investigated further by experimental methods. Watanabe and Sholl (2012) used this

approach to screen over 30,000 MOFs for CO_2/N_2 separation, and consequently identified 1163 promising materials to be further examined by computer modelling. Importantly, molecular simulation also allows testing of theoretical MOFs that have not been synthesized yet, thus making it possible to identify new hypothetical materials with desirable properties. For example, Wilmer et al. (2012) used computer modelling to screen 130,000 hypothetical MOFs for their CO_2 adsorption properties, while Haldoupis et al. (2012) screened ~500 MOFs for CO_2/N_2 selectivity, shortlisting 11 promising materials to be investigated further.

GCMC simulations are normally used to predict adsorption isotherms in MOFs. The accuracy of the predictions relies on determining the potential energy of the system, and thus it is crucial that the interactions between adsorbates and the MOF are described correctly. This is typically done by using force fields, a set of parameters describing the interactions between all atoms in the system. In the standard approach, repulsion and dispersion interactions are described by the Lennard-Jones (LJ) potential, while permanent electrostatic interactions are described by a set of atomic point charges. In this thesis, we assess the effect of framework point charge selection on the resulting adsorption isotherm predictions.
The electron density around a molecule consists of electrons that are constantly in motion, but they are likely to be found in some locations more than others. Electrostatic interactions thus arise from differences in electronegativity between atoms, and they are governed by Coulomb's law. For simulation purposes, the electrostatic potential is normally represented by assigning point charges to each atom to simplify the computation process. These are therefore important parameters in adsorption simulations, particularly with polar species such as water. CO_2 is a quadrupolar molecule – due to the difference in electronegativities, there is a partial positive charge on the carbon and partial negative charges on the oxygens. Due to this effect, the molecule will orient itself preferentially based on the interactions of these charges; therefore electrostatic interactions also have to be accounted for in simulations of CO_2 adsorption. To clarify, although strictly speaking most classical intermolecular interactions (including repulsion and dispersion) are electrostatic in origin, we use the term "electrostatic" in the context of this thesis to describe interactions arising from permanent molecular multipole moments, described through the use of effective atomic point charges.

The importance of inclusion and correct estimation of electrostatic interactions between the MOF and the adsorbate has been studied for various systems. Yang and Zhong (2006) showed the crucial effect of electrostatic interactions in CO_2/CH_4 adsorption simulations, which showed reversed selectivity depending on whether electrostatics were included or not.

The system showed selectivity for methane when the electrostatic interactions were not considered, however, higher selectivity for CO_2 was observed once these interactions were accounted for. This was particularly evident at higher pressures, when the long-range electrostatic interactions exerted their effect over the longer distances of multilayer adsorption. McDaniel et al. (2015) screened 424 MOFs for CO_2 and CH_4 uptake, followed by comparing REPEAT, Qeq (Kadantsev et al. 2013) and no charges to in-house Q_{sbu} charges for selected materials, finding slight underestimation by the QEq method and significantly lower uptake when no charges were used. Zheng et al. (2009) studied the influence of point charges on CO_2 adsorption in 20 MOFs with different structural properties by simulating the adsorption with and without electrostatics and calculating the contribution of framework point charges to CO_2 uptake. The results showed that the effect of framework charges was most significant at low pressures when the strongest CO_2 adsorption was occurring around the metal centres, reaching up to 40% of the total uptake for CuBTC at low pressure. These observations clearly demonstrate the importance of including framework point charges in the adsorption process and also the potential of selectivity enhancement in mixtures with different electrostatic interactions (Yang and Zhong 2006).

Walton et al. (2008) carried out a study on IRMOF-1, simulating CO_2 adsorption isotherms and comparing them to experimental data. They found that good agreement with experiment was obtained when adsorbate-adsorbate electrostatics were included in the model but, crucially, when adsorbate-MOF electrostatic interactions were omitted. Inclusion of point charges on the MOF was in fact deemed unnecessary because it led to a deterioration in agreement with experiment. This highlights the potential pitfalls, such as error cancellation, when comparing simulations against experimental adsorption isotherms. Watanabe et al. (2010) compared CO_2 adsorption isotherms using framework charges calculated using DDEC, REPEAT, CBAC and Hirshfeld methods, for a variety of Zn-based MOFs including IRMOF-1 and ZIF-90. They concluded that for some MOFs the adsorption behaviour is consistent even when different point charges are used, while for other materials a slight change in the point charges can cause significant deviations in adsorption predictions. Indeed, their results showed that while IRMOF-1 produced fairly similar adsorption isotherms, they were very different in ZIF-90, thus showing that the effect of framework point charges on the adsorption behaviour is dependent on the material and its structure. While Haldoupis et al. (2015) compared DDEC and LoProp charges in M-MOF-74 (M = Mn, Co, Ni, Cu) resulting in significantly different adsorption isotherms, Borycz et al. (2016) compared DDEC and CM5 charges in M-IRMOF-10, finding that although DDEC charges were significantly larger in magnitude than CM5 charges, they both led to similar

adsorption isotherms. Babarao et al. (2011) compared CO_2 adsorption on ZIF-68 and ZIF-69 using CHELPG and Mulliken point charges. The results showed that while Mulliken charges led to slight overestimation of adsorption, the difference was not significant. However, as only two structurally similar materials and two sets of charges were employed, this result does not offer a wide overview of the effect of different framework point charges on adsorption behaviour.

Prolonged exposure can result in degradation of the MOF structure. Understanding water adsorption in CuBTC has been a topic of many studies, both experimental and theoretical. It has been shown that the open metal sites play a crucial role in water adsorption. Previous work by Yang et al. (2007) has demonstrated that in CO_2/N_2 mixture adsorption simulations, the Cu metal centres will preferentially adsorb CO_2 due to its larger quadrupole moment. However, their affinity for water is expected to be even higher, as water has a large dipole moment. Yazaydin et al. (2009) have demonstrated this in their GCMC simulations, along with high sensitivity of the point charge on the Cu atom for modelling water adsorption. All these findings lead to the conclusion that the open metal sites play a crucial role in adsorption in MOFs.

A set of DDEC point charges for over 2000 MOFs was developed by Nazarian et al. (2016), who also compared these charges to those obtained by the CBAC and EQeq methods. Their findings showed that higher charges on the metal centre were produced consistently by the CBAC method. Comparison to the semi-empirical EQeq method showed large differences to the charges calculated by the DDEC method, leading to possible inaccuracies in adsorption modelling. Hamad et. al found that simulations with different charges led to difference in thermal expansion results, thus showing that the choice of framework point charges can also affect modelling of structural properties of MOFs (Hamad et al. 2015).

Although the importance of including and accurately defining electrostatic interactions has been demonstrated, the precise effect of different framework point charges on adsorption isotherm predictions has not yet been systematically studied over a wide enough range of MOF topologies. Instead, the comparison of point charges has mostly been carried out for the same group of materials, such as Zn-based MOFs. In this work, we performed a detailed and systematic investigation of the effect of framework point charges on GCMC adsorption predictions in MOFs (Chapter 3). We simulated adsorption of both CO_2 and water, as it has been demonstrated that for these adsorbates the electrostatic interactions are of crucial

importance in the adsorption process, and due to their relevance for carbon capture applications. To gain a wider perspective and a deeper understanding, we have included MOF materials with different composition and structural properties, representing the most important MOF families. We intentionally included MOFs with and without OMS, to see whether this structural property would have an impact on the results. However, we excluded MOFs that exhibit significant framework flexibility (e.g. "breathing"); modelling adsorption in such MOFs is a research topic of its own, and would introduce an unnecessary level of complexity in our assessment of the effect of point charges.

Methods for point charge assignment investigated in this thesis covered the most important classes and were based on QM calculations at different levels of theory and with different structural model approaches (e.g., periodic vs cluster) – see Chapter 2 for details. In order to isolate the effect of framework point charges, and decouple it from other sources of error and variation in simulated adsorption isotherms, we have: i) selected well-established and widely used adsorbate-adsorbate potentials for CO_2 and water, and kept them identical in all simulations; ii) selected a widely used model (DREIDING) for the framework LJ contribution, together with Lorentz-Berthelot combining rules (Allen and Tildesley 1987), and kept the adsorbate-adsorbent LJ parameters constant in all simulations; iii) run our simulations with always the same set of technical parameters (run lengths, type and probability of MC moves, etc.) so that they are directly comparable to each other. In the first results chapter (Chapter 3), we have intentionally avoided a direct comparison with experimental data. This way, we also eliminate any uncertainty arising from variability in experimental measurements of adsorption isotherms in MOFs, which has been shown to be quite large (Park et al, 2017) and may have otherwise obscured the analysis we wish to carry out. However, the wider aim of this work is to put in place a robust framework for validation of molecular models of adsorption in MOFs, which includes experimental characterisation and adsorption measurements. In Chapter 4, we present preliminary experimental work on a prototype MOF, HKUST-1 or CuBTC, aiming to validate the techniques employed.

References

Allen, M.P., Tildesley, D.J.: Computer simulation of liquids. Clarendon Press, Oxford (1987)

Altintas, C. and Keskin, S.: MOF adsorbents for flue gas separation: Comparison of material ranking approaches. Chemical Engineering Research and Design, 179, pp.308-318 (2022)

Avci, G., Velioglu, S. and Keskin, S.: High-Throughput Screening of MOF Adsorbents and Membranes for H2 Purification and CO2 Capture. ACS Applied Materials & Interfaces, 10(39), pp.33693-33706 (2018)

Babarao, R., Dai, S., Jiang, D.: Effect of Pore Topology and Accessibility on Gas Adsorption Capacity in Zeolitic−Imidazolate Frameworks: Bringing Molecular Simulation Close to Experiment. J. Phys. Chem. C 115, 8126-8135 (2011)

Borycz, J., Tiana, D., Haldoupis, E., Sung, J., Farha, O., Siepmann, J., Gagliardi, L.: CO_2 Adsorption in M-IRMOF-10 (M = Mg, Ca, Fe, Cu, Zn, Ge, Sr, Cd, Sn, Ba). J. Phys. Chem. C 120,12819-12830 (2016)

Britt, D., Furukawa, H., Wang, B., Glover, T. and Yaghi, O.: Highly efficient separation of carbon dioxide by a metal-organic framework replete with open metal sites. Proceedings of the National Academy of Sciences, 106(49), pp.20637-20640 (2009)

Bureekaew, S., Amirjalayer, S., Tafipolsky, M., Spickermann, C., Roy, T. and Schmid, R.: MOF-FF - A flexible first-principles derived force field for metal-organic frameworks. physica status solidi (b), 250(6), pp.1128-1141 (2013)

Bux, H., Chmelik, C., Krishna, R., Caro, J.: Ethene/ethane separation by the MOF membrane ZIF-8: Molecular correlation of permeation, adsorption, diffusion. Journal of Membrane Science. 369(1), 284-9 (2011)

Campbell, C., Gomes, J., Fischer, M., Jorge, M.: New Model for Predicting Adsorption of Polar Molecules in Metal–Organic Frameworks with Unsaturated Metal Sites. J. Phys. Chem. Lett. 12, 3544-3553 (2018)

Chen, B., Ockwig, N., Millward, A., Contreras, D. and Yaghi, O.: High H2 Adsorption in a Microporous Metal-Organic Framework with Open Metal Sites. Angewandte Chemie, 117(30), pp.4823-4827 (2009)

Chen, L., Mowat, J., Fairen-Jimenez, D., Morrison, C., Thompson, S., Wright, P.: Elucidating the Breathing of the Metal–Organic Framework MIL-53(Sc) with ab Initio Molecular Dynamics Simulations and in Situ X-ray Powder Diffraction Experiments. J Am Chem Soc., 135(42), 15763-73 (2013)

Coupry, D., Addicoat, M. and Heine, T.: Extension of the Universal Force Field for Metal–Organic Frameworks. Journal of Chemical Theory and Computation, 12(10), pp.5215-5225 (2009)

Farha, O. K.; Eryazici, I.; Jeong, N. C.; Hauser, B. G.; Wilmer, C. E.; Sarjeant, A. A.; Snurr, R. Q.; Nguyen, S. T.; Yazaydın, A. O¨.; Hupp, J. T.: Metal−Organic Framework Materials with Ultrahigh Surface Areas: Is the Sky the Limit? J. Am. Chem. Soc. 134, 15016−15021 (2012)

Farrusseng, D.: Metal-organic Frameworks: Applications from Catalysis to Gas Storage. Wiley (2011)

Furukawa, H.; Ko, N.; Go, Y. B.; Aratani, N.; Choi, S. B.; Choi, E.; Yazaydin, A. O¨.; Snurr, R. Q.; O'Keeffe, M.; Kim, J.: Ultrahigh Porosity in Metal-Organic Frameworks. Science 329, 424−428 (2010)

Haldoupis, E., Nair, S., Sholl, D.S.: Finding MOFs for Highly Selective CO_2/N_2 Adsorption Using Materials Screening Based on Efficient Assignment of Atomic Point Charges. J. Am. Chem. Soc. 134, 4313-432 (2012)

Hamad, S., Balestra, S., Bueno-Perez, R., Calero, S., Ruiz-Salvador, A.: Atomic charges for modeling metal–organic frameworks: Why and how. J. Solid State Chem. 223, 144-151 (2015)

Jorge, M., Fischer, M., Gomes, J., Siquet, C., Santos, J., Rodrigues, A.: Accurate Model for Predicting Adsorption of Olefins and Paraffins on MOFs with Open Metal Sites. Industrial & Engineering Chemistry Research 53.40, pp. 15475–15487 (2014)

Kadantsev, E. S.; Boyd, P. G.; Daff, T. D.; Woo, T. K.: Fast and Accurate Electrostatics in Metal Organic Frameworks with a Robust Charge Equilibration Parameterization for High-Throughput Virtual Screening of Gas Adsorption. J. Phys. Chem. Lett. 4, 3056−3061 (2013)

Kenarsari, S., Yang, D., Jiang, G., Zhang, S., Wang, J., Russell, A., Wei, Q., Fan, M.: Review of recent advances in carbon dioxide separation and capture. RSC Advances 3, 22739 (2013)

Li, J.-R.; Sculley, J.; Zhou, H.-C.: Metal−organic frameworks for separations. Chem. Rev. 112, 869-932 (2012)

Ma, S.; Zhou, H.C.: Gas storage in porous metal−organic frameworks for clean energy applications. Chem. Comm. 46, 44-53 (2010)

Maring, B.J and Webley, P.A: A new simplified pressure/- vacuum swing adsorption model for rapid adsorbent screening for CO2 capture applications. International Journal of Greenhouse Gas Control 15.0, pp. 16–31 (2013)

McDaniel, J., Li, S., Tylianakis, E., Snurr, R., Schmidt, J.: Evaluation of Force Field Performance for High-Throughput Screening of Gas Uptake in Metal–Organic Frameworks. J. Phys. Chem 119, 3143-3152 (2015)

Van Miltenburg, A., Zhu, W., Kapteijn, F. and Moulijn, J.A: Adsorptive Separation of Light Olefin/Paraffin Mixtures. Chemical Engineering Research and Design 84.5, pp. 350 –354 (2006)

Moghadam, P. Z.; Li, A.; Wiggin, S. B.; Tao, A.; Maloney, A. G. P.; Wood, P. A.; Ward, S. C.; Fairen-Jimenez, D.: Development of a Cambridge Structural Database Subset: A Collection of Metal− Organic Frameworks for Past, Present, and Future. Chem. Mater. 29, 2618-2625 (2017)

Nazarian, D., Camp, J., Sholl, D.: A Comprehensive Set of High-Quality Point Charges for Simulations of Metal–Organic Frameworks. Chem. Mater. 28,785-793 (2016)

Nechaev, M., Rayón, V., Frenking, G.: Energy Partitioning Analysis of the Bonding in Ethylene and Acetylene Complexes of Group 6, 8, and 11 Metals: (CO)5TM-C2Hx and Cl4TM-C2Hx (TM = Cr, Mo, W), (CO)4TM-C2Hx (TM = Fe, Ru, Os), and TM+-C2Hx (TM = Cu, Ag, Au).” The Journal of Physical Chemistry A 108.15, pp. 3134–3142 (2014)

Nikolaidis, G., Kikkinides, E. and Georgiadis, M.: Modelling and Simulation of Pressure Swing Adsorption (PSA) Processes for post-combustion Carbon Dioxide (CO_2) capture from flue gas. 12th International Symposium on Process Systems Engineering and 25th European Symposium on Computer Aided Process Engineering, pp.287-292 (2015)

Park, J., Howe, J., Sholl, D.: How Reproducible Are Isotherm Measurements in Metal–Organic Frameworks? Chem. Mater. 29, 10487-10495 (2017)

Quaranta, I., Pinheiro, L., Gonçalves, D., Peixoto, H. and Lucena, S.: Multiscale design of a pressure swing adsorption process for natural gas purification. Adsorption, 27(7), pp.1055-1066 (2021)

Schneemann, A., Bon, V., Schwedler, I., Senkovska, I., Kaskel, S., Fischer, R.A.: Flexible metal-organic frameworks. Chem. Soc. Rev. 43 (16), 6062–6096 (2014)

Susumu, K., Mitsuru, K.: Functional Micropore Chemistry of Crystalline Metal Complex-Assembled Compounds. Bull Chem Soc Jrn. 71(8), 1739-53, (1998)

Torrisi, A., Bell, R., Mellot-Draznieks, C.: Functionalized MOFs for Enhanced CO_2 Capture. Cryst. Growth Des., 10, 2839-2841 (2010)

Walton, K.S., Millward, A. R., Dubbeldam, D., Frost, H., Low, J.J., Yaghi, O.M., Snurr, R.Q.: Understanding Inflections and Steps in Carbon Dioxide Adsorption Isotherms in Metal-Organic Frameworks. J. Am. Chem. Soc.130, 406-407 (2008)

Watanabe, T., Sholl, D.: Accelerating Applications of Metal–Organic Frameworks for Gas Adsorption and Separation by Computational Screening of Materials. Langmuir 28, 14114-14128 (2012)

Wilmer, C. E.; Kim, K. C.; Snurr, R. Q.: An extended charge equilibration method. J. Phys. Chem. Lett. 3, 2506−2511 (2012)

Yang, Q., Zhong, C.: Molecular Simulation of Carbon Dioxide/Methane/Hydrogen Mixture Adsorption in Metal−Organic Frameworks. J. Phys. Chem. 110, 17776-17783 (2006)

Yang, Q., Xue, C., Zhong, C., Chen, J.: Molecular simulation of separation of CO_2 from flue gases in Cu-BTC metal-organic framework. AIChE Journal 53,.2832-2840 (2007)

Yazaydın, A., Benin, A., Faheem, S., Jakubczak, P., Low, J., Willis, R., Snurr, R.: Enhanced CO_2 Adsorption in Metal-Organic Frameworks via Occupation of Open-Metal Sites by Coordinated Water Molecules. Chem. Mater. 21, 1425-1430 (2009)

Zhang, Y., Li, B., Krishna, R., Wu, Z., Ma, D., Shi, Z., Pham, T., Forrest, K., Space, B., Ma, S.: Highly Selective Adsorption of Ethylene Over Ethane in a MOF Featuring the Combination of Open Metal Site and [Small pi]-Complexation. Chem. Comm. 51, 2714-2717 (2015)

Zheng, C., Liu, D., Yang, Q., Zhong, C. and Mi, J.: Computational Study on the Influences of Framework Charges on CO_2 Uptake in Metal−Organic Frameworks. Industrial Eng. Chem. Res. 48, 10479-10484 (2009)

2. ***Methodology***

This chapter will begin by looking into the basics of the adsorption processes and describing adsorption theory. It will then explain how to obtain information about porous materials using various characterization techniques. It will introduce molecular simulation methods with particular focus on the Grand-Canonical Monte Carlo (GCMC) method. This section will also provide a brief overview of Quantum theory calculations; although they were not carried out in this work, they are important to discuss in relation with obtaining point charges for adsorption simulations.

2.1 Adsorption

Adsorption is a surface phenomenon in which particles (molecules, ions or dissolved solids) are attached to a surface. The reverse process is called desorption. The substance that adsorbs is called adsorbate and the material to which it attaches is the adsorbent. The adsorbent is most commonly a porous material (Figure 2.1). Porous materials can be classified into macroporous, mesoporous or microporous (Sing et al. 1985). Microporous materials are those with pores of an internal diameter less than 2 nm. If the pores are between 2 and 50 nm in diameter, then the material would be classified as mesoporous. Pores with diameter higher than 50nm characterize macroporous materials.

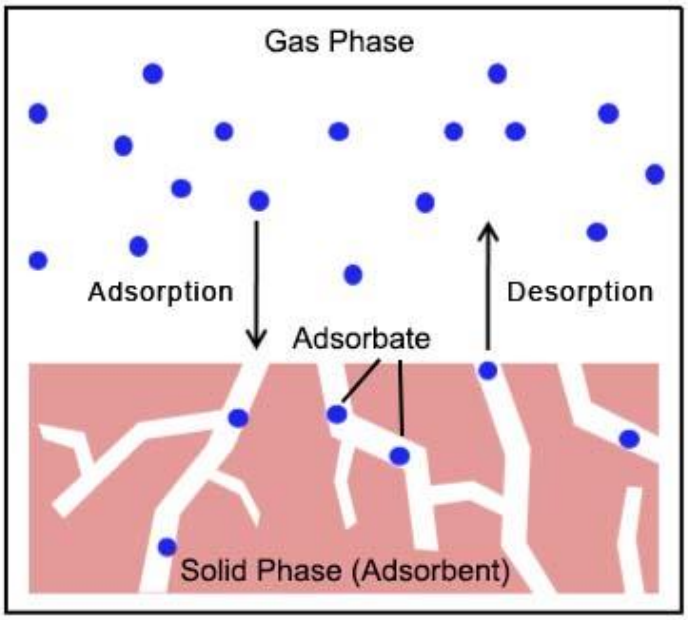

Figure 2.1 – Illustration of the adsorption process

The adsorption process is categorized into physisorption (physical adsorption) and chemisorption (chemical adsorption) (Thommes et al. 2015). In physical adsorption, the adsorbate and the adsorbent are bonded through Van der Waals interactions to form multilayers of the adsorbate. Higher surface area typically leads to higher adsorption uptake. Adsorption can also be enhanced with the effect of polar functional groups, electrostatic charges or pore shape and dimensions. On the other hand, in chemisorption the adsorbate is bonded to the adsorbent material through much stronger chemical bonds. The reactions are reversible, but it can take significant amount of energy to desorb the adsorbate and it can be altered upon regeneration. The main differences between these two types of adsorption are listed in Table 2.1.

Table 2.1 – Differences between Physisorption and chemisorption (Atkins 1994)

	Physisorption	**Chemisorption**
Forces	Weak	Strong
Heat of adsorption (kJ mol^{-1})	20-40	> 80
No. of adsorbed layers	Mono or Multilayers	Monolayer
Effect of increasing temperature	Uptake decreases	Uptake increases
Desorption	Easy (reducing pressure or increasing temperature)	Difficult (E required to break chemical bonds)
Desorbate	Unchanged	Can be altered
Specificity	Mostly non-specific	Very specific

2.1.1 Adsorption Isotherms

An adsorption isotherm is defined as the relation between the amount adsorbed and the equilibrium pressure of the gas (Thommes 2015). The adsorption isotherms are classified into 6 types and these are shown in Figure 2.2 (Sing et al. 1985). The shape of the adsorption

isotherm can convey valuable information about the pore characteristics of the adsorbent material and the nature of the adsorbate-adsorbent interactions.

A Type I isotherm corresponds to microporous materials. A steep uptake is observed at low p/p_0 which is due to the enhanced adsorbent-adsorbate interaction in the micropores. The uptake is dictated by the accessible micropore volume.

Type II Isotherms are observed when the adsorbent is a nonporous or a microporous material. In this case, monolayer and multilayer formations occur, leading to high uptake up to high p/p_0.

Similarly, type III isotherm is also associated with nonporous or microporous materials. However, in this case, the adsorbate-adsorbent interactions are weak and the monolayer formation does not complete before the multilayer formation begins by clustering of molecules at the most favourable sites.

Type IV isotherms are typical for mesoporous adsorbents. Initially, monolayer and multilayer formation occurs in the mesopores and this is then followed by pore condensation. This occurs when a gas condenses into a liquid-like state in a pore, where the pressure is less than the saturation pressure of the bulk liquid (p_0).

The Type V isotherm is similar to that of Type III in the low p/p_0 range, reflecting weak adsorbent-adsorbate interactions. Molecular clustering and pore filling occur at higher p/p_0. This type of isotherm is typically observed for water adsorption in hydrophobic materials.

The Type VI isotherm is typical for highly uniform adsorbents. A layer-by-layer adsorption occurs with each step indicating a layer completion. The height of the steps indicates the adsorption capacity for each layer. (Thommes 2015)

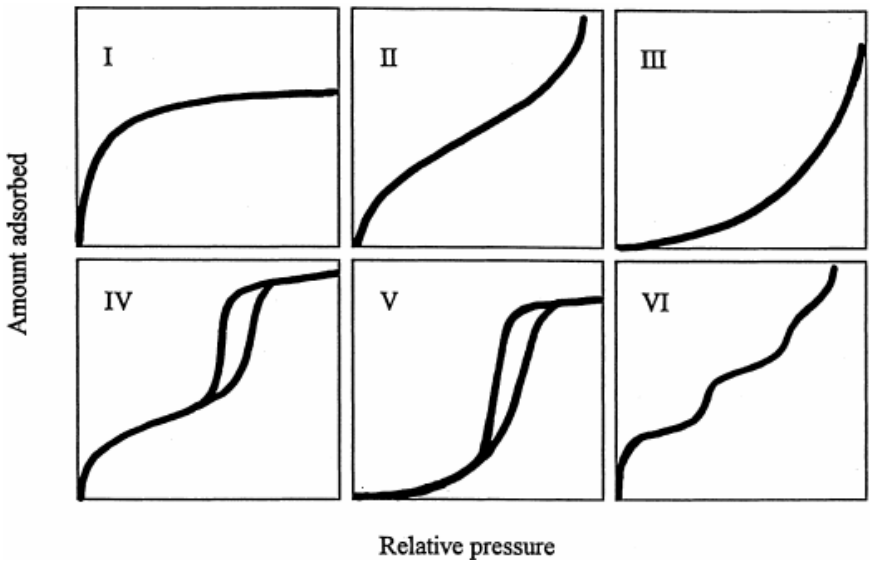

Figure 2.2 -- Isotherm types (Sing et al. 1985)

2.1.2 Langmuir Theory

The Langmuir Theory is a model developed to describe the adsorption of species onto simple surfaces, derived by Irving Langmuir in 1916 (Langmuir 1916). The Langmuir theory describes the relationship between the numbers of active sites for adsorption on the surface as a function of pressure.

$$\theta = \frac{KP}{1+KP} \qquad \text{Equation 2.1}$$

Where

θ – Fractional coverage of surface

K – Langmuir adsorption constant

P – Pressure

The fractional coverage of the surface represents the ratio of the volume of adsorbate adsorbed onto the surface compared to the volume of adsorbate monolayer covering the whole surface when completely occupied.

Langmuir theory implements the following assumptions:

1. Adsorption is localized to the available sites
2. Only one monolayer forms

3. No interaction between adsorbed molecules
4. All sites are energetically equivalent

The accuracy of Langmuir theory depends on the adsorbed gas behaving ideally, which occurs only in the low-pressure regions.

2.1.3 Brunauer-Emmett-Teller (BET) Theory

BET theory is an extension to Langmuir adsorption theory (Brunauer et al. 1938). The Langmuir adsorption model only considered adsorption in the monolayer whereas BET focuses on multilayer adsorption. The BET equation is expressed as:

$$\frac{1}{V[(P_0/P)-1]} = \frac{1}{V_m C} + \frac{(C-1)}{V_m C}\frac{P}{P_0} \qquad \text{Equation 2.2}$$

Where
P – equilibrium pressure of adsorbate
P_0 – saturation pressure of adsorbate
V – volume of adsorbate
V_m – Volume of adsorbate needed to form a monolayer
C – equilibrium constant

The BET equation can be plotted and used to determine surface area, as will be described in Section 2.1.5.

BET theory assumes the following hypotheses:

1. Adsorbed molecules do not interact laterally
2. Molecules can adsorb on a solid in multilayers
3. The Langmuir theory can be applied to each layer
4. The enthalpy of the first layer is constant and greater than subsequent layers
5. The second and subsequent layers have interparticle interaction with the same energy as would apply in the liquid state

2.1.4 Ideal Adsorbed Solution Theory

Adsorption measurements for gas mixtures can be challenging to carry out experimentally. The Ideal Adsorbed Solution Theory (IAST), developed by Myers and Prausnitz (1965) addresses this issue. IAST is a computational method which can be used to predict adsorption behaviour of multi-component gas mixtures from single component adsorption isotherms. IAST implements the following assumptions:

1. The gas components behave ideally
2. The adsorbed phase behaves as an ideal mixture
3. The adsorbent surface is homogenous and equally accessible to all adsorbates

This approach can be a useful tool for screening different adsorbents for selectivity without the need to carry out time-consuming experiments and has been shown to perform well for various systems (Chen et al. 2011). One of the drawbacks is that the prediction of multicomponent adsorption requires extrapolation of the single component data up to high pressures. This introduces a degree of error, particularly for the component adsorbed to a lower amount. This can be particularly challenging when studying mixtures where the selectivity is high, i.e., there is a large difference between the individual components' adsorption (Cessford et al. 2012).

2.1.5 Adsorption measurements

There are two main methods to measure adsorption and these are volumetric and gravimetric methods. The volumetric method measures the change in pressure of the gas in a known volume, and the gravimetric method directly measures the change in the mass of the solid.

The volumetric method for the measurement of high-pressure pure gas adsorption isotherms gives an indirect measurement of the amount adsorbed. A known amount of the adsorbate (typically nitrogen gas) is introduced to an evacuated chamber holding the adsorbent at constant temperature (the standard being 77 K for nitrogen adsorption). A reduction in the pressure of the chamber occurs as the gas is adsorbed onto the surface of the adsorbate until equilibrium is reached. The amount of gas adsorbed at this equilibrium pressure can then be measured. The advantage of the volumetric method is that it's relatively cheap and can be easily implemented for high pressure measurements. However,

it can be prone to various errors due to the indirect measurements of adsorbed quantities (Belmabkhout et al. 2004).

Gravimetric analysis is the direct measurement of sample weight which provides information about the amount of gas adsorbed. The instrument can be set up to capture data in real-time, so that it gives information about the adsorption kinetics and can show whether equilibrium was reached. Another benefit of this method is the ability to reach pre-defined equilibrium pressures. An advantage of this method is that all variables are measured independently, however, the equipment is more expensive and more complex to operate. The most significant error in this measurement method results from the determination of buoyancy (Belmabkhout et al. 2004).

2.2 Porous Material Characterization Methods

2.2.1 Fourier Transform Infrared Spectroscopy

Infrared (IR) spectroscopy studies interactions between infrared radiation and matter. Infrared light is an electromagnetic radiation, which has a longer wavelength than visible light (Figure 2.3).

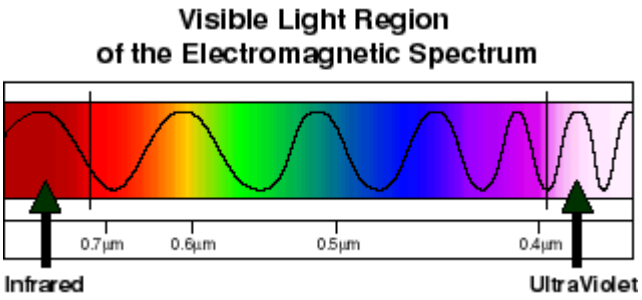

Figure 2.3 – Electromagnetic spectrum (NASA 2022)

IR light interacts with matter and it can trigger vibrations in specific bonds depending on energy levels. Different kinds of vibrations are symmetric and anti-symmetric bond stretching and bond bending (Figure 2.4).

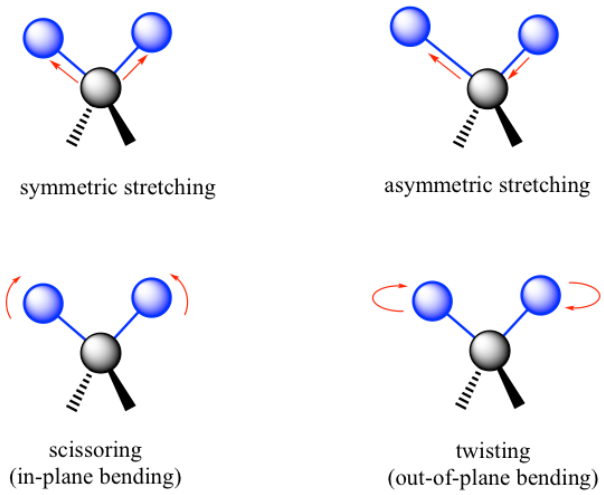

Figure 2.4 – Stretching and bending of bonds (Libretext 2021)

An IR source emits IR light into the sample. Some light will be reflected but a larger fraction will travel through the sample, and specific parts will be absorbed by the sample. The part of the light that is transmitted is collected by the detector and is converted into an electronic signal.

FTIR spectroscopy is an improved form of IR spectroscopy. Here, the instrument contains an interferometer, which allows for the spectral information of all wavelengths to be acquired simultaneously, more accurately and with an improved signal to noise ratio (Larkin 2018). First, the spectrum is measured without the sample to eliminate any environmental influences such as water vapour or CO_2. This is called the reference spectrum. Then, a spectrum of the sample is taken and the reference spectrum is subtracted. This gives the FTIR spectrum of the sample. The spectrum is formed of absorption peaks, which correspond to the frequencies of energy gaps between the vibrational states of the molecules making up the material.

Most of the bands that indicate which functional groups are present are found in the region from 4000 cm^{-1} to 1300 cm^{-1}. Their bands can be identified and used to determine the functional groups of an unknown compound. The peaks can be assigned by looking up typical absorption values for particular types of bonds. Some of these are illustrated in Figure 2.5. Bands that are unique to each molecule, similar to a fingerprint, are found in the fingerprint region, from 1300 cm^{-1} to 400 cm^{-1}. These bands are only used to compare the spectra of one compound to another (Larkin 2018).

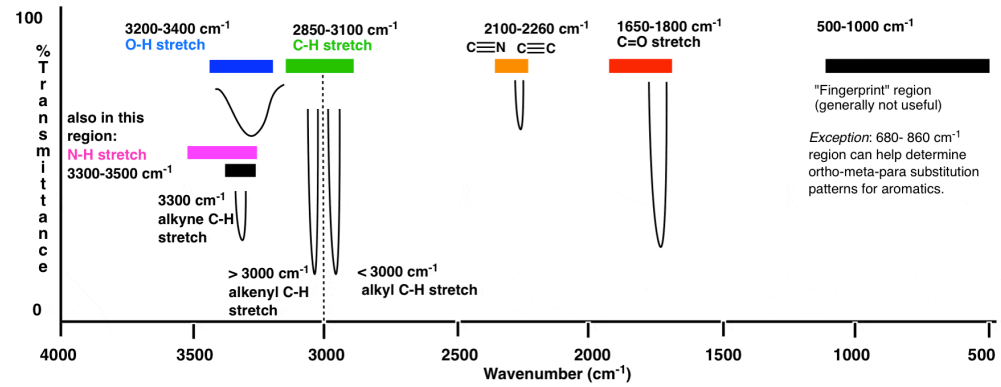

Figure 2.5 – Typical absorption values for various types of bonds (Master Organic Chemistry 2020)

2.2.2 Thermogravimetric Analysis

Thermogravimetric analysis (TGA) is a precise technique, which measures the mass of a sample as a function of temperature. In a typical case, the heating of the sample results in a change in mass, which can be attributed to several effects (Gabbot 2008). Some of these include:

- Evaporation of volatile constituents
- Drying
- Desorption and adsorption of gases
- Oxidation of metals in air or oxygen
- Oxidative decomposition of organic substances in air or oxygen

In porous materials, the initial mass loss is typically due to the removal of adsorbed solvent molecules, from either the synthesis or the washing procedure. As well, some materials (particularly hydrophilic materials, such as CuBTC) adsorb moisture from the atmosphere when exposed, which can be seen on a TGA measurement. The thermal stability (or decomposition temperature) of the material is also measured using TGA. Typically, a large mass loss at relatively high temperatures indicates the combustion of the organic content, leaving behind the inorganic residue in the form of a metal oxide. Using the information provided from this measurement, the activation temperature can be determined.

The main components of a TGA instrument are:

1. A high precision microbalance
2. Furnace with temperature programming facility.

3. Atmosphere control (inert or oxidizing)
4. A computer for data collection

The data is displayed as a TGA curve, where the mass or % mass is plotted against temperature or time. The mass change occurs when the sample material loses mass or reacts with the atmosphere. These stages can be seen on the TGA curve.

A different way to look at the data is to plot a DTG curve, which is the first derivative of the TGA curve with respect to temperature or time. In this representation, the rate of mass change is shown and the mass changes are represented as peaks (Figure 2.6).

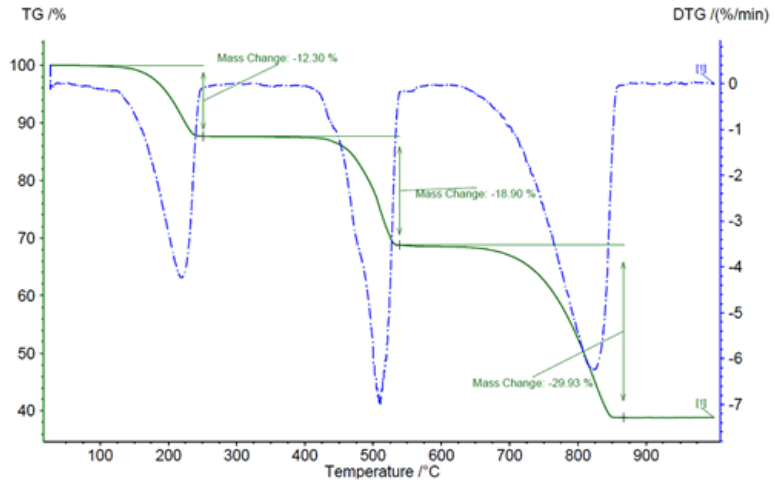

Figure 2.6 – A sample plot containing TGA and DTG curves for calcium oxalate, indicating mass change events and rate (Ebatco 2020)

2.2.3 BET - Surface Area Measurement

BET theory is largely used to determine the specific surface area of a solid substrate. A standard procedure to do so incorporates the use of nitrogen at its boiling temperature (77 K) to determine the adsorption in the first layer. The measured data can be plotted based on the BET equation (Section 2.1.3) to give a linear plot as described in Figure 2.7.

$$\frac{1}{v\left[\left(\frac{p_0}{p}\right)-1\right]} = \frac{c-1}{v_m c}\left(\frac{p}{p_0}\right) + \frac{1}{v_m c}$$

$$y = mx + b$$

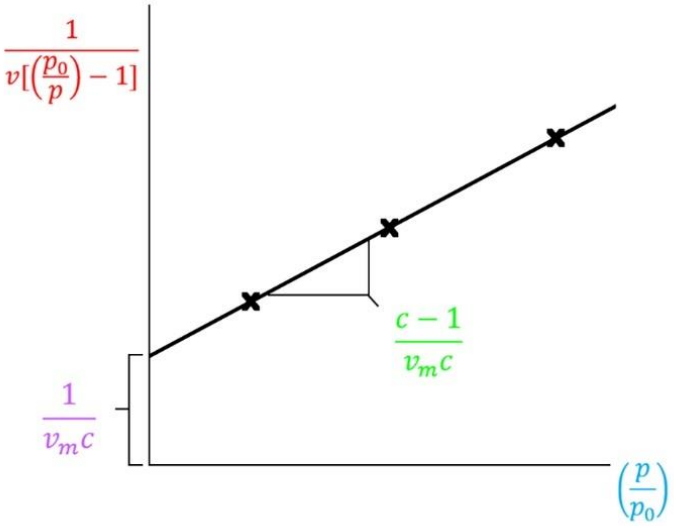

Figure 2.7 – Illustration of the BET equation

$$\frac{1}{v\left[\left(\frac{p_0}{p}\right)-1\right]} = \frac{c-1}{v_m c}\left(\frac{p}{p_0}\right) + \frac{1}{v_m c} \qquad \text{Equation 2.3}$$

From here, the values of C and V_m can be obtained as follows:

$$slope = \frac{c-1}{V_m C} \qquad \text{Equation 2.4}$$

$$intercept = \frac{1}{V_m C} \qquad \text{Equation 2.5}$$

$$V_m = \frac{1}{slope + intercept} \qquad \text{Equation 2.6}$$

$$C = 1 + \frac{slope}{intercept} \qquad \text{Equation 2.7}$$

With these values obtained, total and specific surface area can be determined as follows:

$$S_{total} = \frac{V_m N s}{V} \qquad \text{Equation 2.8}$$

where

N – Avogadro's number

s – cross-sectional area of adsorbed gas molecule

V – molar volume of adsorbate

$$S_{BET} = \frac{S_{total}}{m} \qquad \text{Equation 2.9}$$

where

m – mass of sample

For accurate BET measurement, it is essential to select the correct partial pressure range where a linear trend is observed. The typically used region is between 0.05-0.30 (Figure 2.8), but the most effective range can vary with different materials and their porosity (Thommes et al. 2015). It is important to select this region with care so that meaningful results are obtained. The following criteria can be used to find the linear range (Thommes et al. 2015):

1. The value of the C constant should be positive
2. BET equation should only be applied to the range where $V(1-P/P_0)$ increases with P/P_0
3. The P/P_0 value corresponding to V_m should fall into the selected range

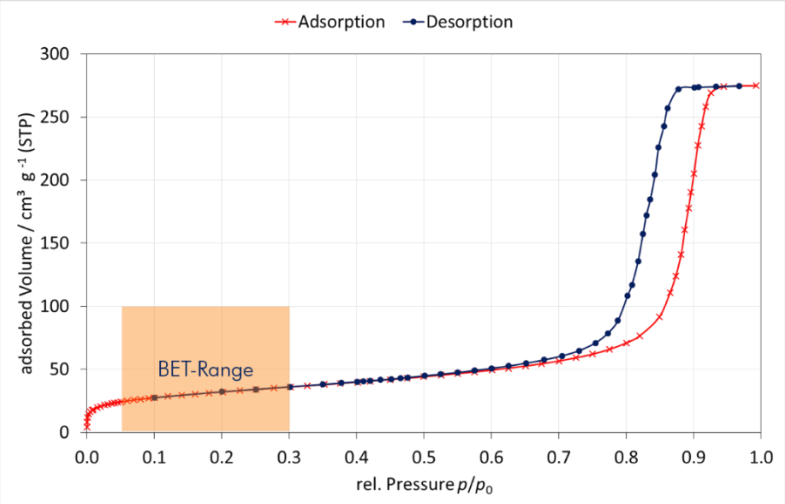

Figure 2.8 – The typically used partial pressure region for BET measurement

2.2.4 BET – Total Pore Volume Measurement

The total pore volume is typically determined from the amount of gas adsorbed at a relative pressure close to unity where it is assumed that the pores of the adsorbent material are filled

with liquid nitrogen at 77K. The validity of the Gurvich rule is assumed (Gurvich 1915), i.e., the molar volume of liquid nitrogen is the same regardless of the shape and size of the pore within which it is condensed.

The commonly used approach to determine the pore volume involves measuring the nitrogen uptake just before it starts to condense outside the material (typically 0.9-0.95 P/P_0). (Mason et al. 2014) The amount of adsorption can be used to calculate total pore volume by converting molar uptake (mol/g) to mass (g/g), followed by Equation 2.10:

$$V_p = \frac{m}{\rho} \qquad \text{Equation 2.10}$$

where

ρ – liquid density (0.808 g/cm^3 for N_2)

2.3 Molecular Simulations

Molecular simulations are computational methods used to study and predict behaviour of molecules or molecular systems. This then allows one to calculate macroscopic properties using the equations of statistical mechanics. Of particular importance for this thesis is the use of molecular simulations to understand the interactions between MOFs and adsorbates, and to predict their adsorption performance, which is a promising avenue for screening and potentially designing MOFs for particular applications. This computational technique allows to efficiently identify materials with properties that are desirable for a specific application, for example their selectivity for a specific gas mixture, by simulating their adsorption behaviour.

Typical methods for studying and characterizing MOFs include molecular dynamics (MD) and Monte Carlo (MC) simulations. In this context, Grand-Canonical Monte Carlo (GCMC) enables one to compare simulated adsorption isotherms with experimental data while providing a degree of molecular level detail that is difficult to obtain in experiments. In this thesis, GCMC will be used to predict MOF adsorption properties. As such, only a brief explanation of MD will be provided, and the reader is directed to Allen and Tildesley (1987) and Frenkel and Smit (2002) for further details.

2.3.1 Statistical Mechanics

The main goal of molecular modelling is to capture the macroscopic behaviour of a system based on microscopic interaction models between molecules. Statistical mechanics relates these microscopic properties to macroscopic properties. A basic concept of statistical mechanics is the ensemble. An ensemble is a set of large number of microstates of a system which is defined by specific thermodynamic conditions. A microstate of a system contains complete information about the instantaneous positions and momenta of all molecules and atoms. On the macroscopic level, the system is characterised by averages across the ensemble. It is common to refer to an ensemble by the set of thermodynamic constraints that define its macroscopic state. Some important ensembles are (Figure 2.9):

- Microcanonical ensemble (*NVE*): the system is isolated with fixed number of molecules, volume and energy
- Canonical ensemble (*NVT*): the system is connected to a heat bath with fixed number of molecules, volume and temperature
- Isothermal-isobaric ensemble (*NPT*): where the number of molecules, pressure and temperature are constant
- Grand-canonical ensemble (μVT): where the number of molecules is allowed to fluctuate while the chemical potential, volume and temperature are kept constant

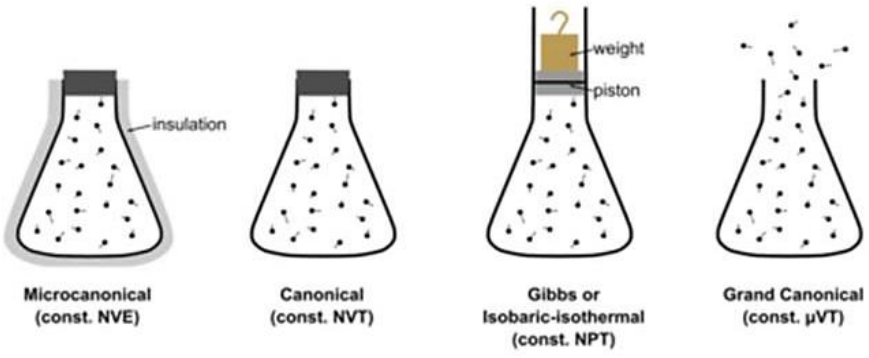

Figure 2.9 – Statistical ensembles (Wikipedia 2021)

A frequently used ensemble is the Canonical ensemble. This is a system of constant volume and temperature, surrounded by an infinite reservoir with which it exchanges energy. The probability of a microstate occurring in the system is dependent on its energy and is

proportional to the Boltzmann factor. It can be derived from the partition function, which represents all possible microstates of the system (Equation 2.11).

$$Q(N,V,T) = \frac{1}{\Lambda^{3N}N!} \int drN \,.\exp\left[-\beta.U(r^N)\right] \qquad \text{Equation 2.11}$$

where

Q – Canonical partition function

N - Number of atoms

Λ - Thermal de Broglie wavelength

β - $1/k_b$.T (k_b = Boltzmann constant)

U - Energy of the system

r - Distance between atoms

The partition function is a normalizing factor which relates the energy of any chosen microstate to those of all the possible microstates of the system (Frenkel and Smit 2002).

2.3.2 Molecular Dynamics

As explained previously, a macrostate describes the state of the system based on its macroscopic properties such as pressure, volume or temperature. It does not give information about individual particles of the system. A microstate is a specific microscopic arrangement of all particles in the system based on their quantum state (e.g. positions and velocities). These properties change rapidly over time as the particles interact, however the macrostate remains unchanged. Therefore, many possible microstates can exist for a given macrostate and by averaging these microstates it is possible to predict the macroscopic properties of the system. This theory is implemented by Molecular Dynamics (MD). MD is a deterministic simulation method that analyses the temporal evolution of the molecular system and yields the system trajectory (Gelpi et al. 2015). Sets of microstates are generated by solving Newton's equations of motion for all the atoms and molecules that interact within the system, which produces the system trajectory represented by the variation of atomic positions and velocities over time. The intermolecular forces and potential energies are calculated using their interatomic potentials (described in detail in section 2.4).

The process is divided into time steps which are typically of the order of femtoseconds (10^{-15} s). During each time step, the forces acting on each particle are calculated and their new positions and velocities are updated. This allows us to work out the evolution of the system

over time from the initial configuration and predict observable properties from averaging the sets of microstates over time. In this aspect, this method relates to a real-life experiment, as in such the values of a measured property (i.e. temperature) are also averaged over time. This method allows calculation of both equilibrium and dynamic properties of the system (some of the dynamic properties that can be investigated by MD include diffusion processes in pores or membranes, phase change dynamics or reaction kinetics). However, reaching the equilibrium can be very computationally expensive using this method, therefore a different method called Monte Carlo (MC) can be used if it is only the final equilibrium state that is being studied (Frenkel and Smit 2002).

2.3.3 Monte Carlo

Monte Carlo is a stochastic method which uses random points for function evaluation and, unlike MD, does not offer a system trajectory over time. The MC method implements the concept of probability. Random points are generated with probability proportional to the Boltzmann factor. First the initial atom configuration is specified, denoted r^N, with the Boltzmann factor $exp\ [-\beta[U(r^N)]$. Then a new configuration is generated by slightly perturbing the system and either accepting or rejecting this perturbation. The system can access its previous state with the same probability as moving to a new state – this condition is called detailed balance (Frenkel and Smit 2002). MC therefore aims to minimize the free energy of the system through iterations (steps). The iterations are independent and the system does not retain memory of previously accessed states. After enough iterations are carried out, the energy average versus the number of iterations stabilizes, indicating convergence to equilibrium. This simulation method yields information about thermodynamic properties of the system by sampling over the relevant microstates for the chosen ensemble.

A key step is to decide whether the move will be accepted or rejected -– this depends on how energetically favourable the move would be (Equation 2.12). If the move is energetically favourable (i.e. the energy of the new state is lower than that of the old state), the move is always accepted. If the move is energetically unfavourable, it can still be accepted with a certain probability. There are many rules for making this decision; in this thesis we utilize the most common Metropolis method (Metropolis et al. 1953):

1. A particle is selected at random and its energy $U(r^N)$ calculated

2. A random displacement of the particle is applied, r'= r+Δ and its new energy $U(r'^N)$ is calculated
3. The move from r^N to r'^N is accepted with the probability

$$acc(r \rightarrow r') = \min (1, \exp \{-\beta[U(r'^N) - u(r^N)]\}) \quad \text{Equation 2.12}$$

If the move is rejected, the original position is maintained and the process repeated. The old position must be counted. In practice, to determine whether a move will be accepted or rejected, a random number R between 0-1 is generated. If R < acc (r→r') then the move is accepted, if R > acc (r→r') then the move will be rejected.

This randomized acceptance allows the system to move out of local energy minima. This step is crucial in allowing access to energetically unfavourable locations and so maintaining ergodicity of the system. Ergodicity means that every microstate in the system must be accessible.

2.3.4 Grand-Canonical Monte Carlo

The Grand Canonical ensemble is derived from the Canonical ensemble and it is the one used in this thesis. It is commonly used for adsorption studies. This is a system which has constant volume and temperature, surrounded by an infinite reservoir with which it exchanges both energy and molecules (Figure 2.10). As the temperature and the chemical potential remain constant, the number of particles in the system can fluctuate. This makes it different to other ensembles where the number of molecules is fixed. With this setup the Grand Canonical ensemble replicates experimental conditions where an equilibrium exists between the adsorbed gas and the gas in the reservoir, meaning that the chemical potential and temperature of both gases are equal. From these values it is possible to determine the equilibrium concentration of the adsorbate for a given set of thermodynamic conditions (e.g. temperature and pressure of the bulk gas phase).

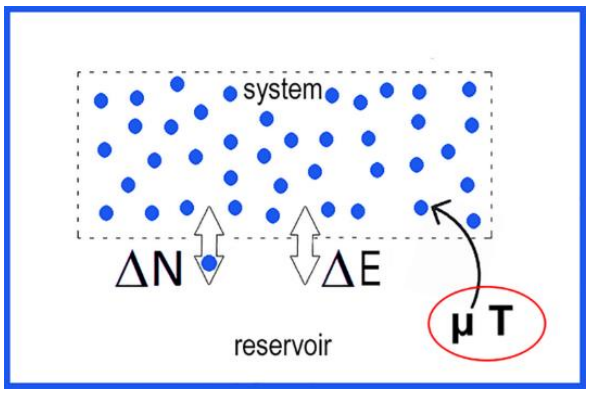

Figure 2.10 – μVT ensemble where the reservoir exchanges particles and energy with the adsorbent and so imposes constant chemical potential and temperature.

This system is described by a more complex variation of the Canonical ensemble partition function to account for the change in the number of molecules (Equation 2.13).

$$Q(\mu,V,T) = \sum_{\infty}^{N=0} \frac{\exp\left[\beta.\mu.N\right]V^N}{\Lambda^{3N}N!} \int dr^N . \exp\left[-\beta . U(r^N)\right] \quad \text{Equation 2.13}$$

where

μ - Chemical potential

Adsorbate molecules are randomly displaced into the rigid structure of the porous material using 3 types of move – translation, insertion and deletion. Using the Metropolis method, the moves are either rejected or accepted depending on the change in potential energy. Further details about calculating the potential energy will be explained in section 2.4. The acceptance ratio for translation is the same as in the previously discussed canonical ensemble (Equation 2.12). The expressions for insertion and deletion of particles must include two new terms to account for the difference in volume resulting from the change in the number of particles (Equations 2.14-2.16).

Translation:

$$acc(r \rightarrow r') = \min\left(1, \exp\left\{-\beta[U(r'^N) - U(r^N)]\right\}\right) \quad \text{Equation 2.14}$$

Insertion:

$$acc(N \rightarrow N+1) = \min\left(1, \frac{V}{\Lambda^3(N+1)} \exp\left\{-\beta\left[\mu - U(N+1) + U(N)\right]\right\}\right) \quad \text{Equation 2.15}$$

Deletion:

$$acc(N \rightarrow N\text{-}1) = \min\left(1, \frac{\Lambda^3 N}{V} \exp\{-\beta[\mu + U(N\text{-}1) - U(N)]\}\right) \quad \text{Equation 2.16}$$

As mentioned previously, if a particle moves into an energetically favourable state, the move is always accepted. If the move is less energetically favourable, it will be accepted given a certain probability according to the Boltzmann weighting. In GCMC simulations it is possible that a particle will be moved to a position that is already occupied by a framework atom or another particle, in which case the move will be highly energetically unfavourable and will be rejected. Special techniques can be used to mitigate this problem. One of these is cavity biasing (CB). The cavity bias method (Mezei 1980) is a sampling method which attempts insertion of particles only at locations with cavities of sufficient radius to accept the particle. This tends to increase the likelihood of accepted insertion moves. In this work, this method was applied to potential energy. The grid-like potential maps (discussed in Section 2.5.1) generated prior to running GCMC simulation were used to identify energetically favourable positions, resulting in a greater acceptance rate for the insertion and deletion moves.

Accumulating information about all the configurations and their potential energies allows us to predict adsorption properties and generate adsorption isotherms for a particular adsorbent and adsorbate species.

GCMC simulation yields the absolute amount adsorbed, which has to be converted into excess adsorption for comparison with experimental data (Coudert and Fuchs 2016). This is because absolute adsorption cannot be measured experimentally, as it is not possible to distinguish between adsorbed molecules and bulk molecules. Bulk gas molecules are molecules that would naturally exist in the available pore volume in the absence of the surface. It is determined using Equation 2.17:

$$Nex = N_{abs} - Vp.\rho b \quad \text{Equation 2.17}$$

where

N_{abs} - Total adsorbed amount
Vp - Pore volume
ρb - Bulk gas density

Adsorption data is generated in the form of number of molecules per unit cell, this is then converted to specified units (e.g. mmol/g) for comparison with experimental data.

To conclude this section, the author would like to recommend the publication of Frenkel and Smit (2002) for a more in-depth discussion of the MC method and different statistical mechanical ensembles.

2.3.5 Periodic Boundary Conditions

In any numerical method, boundary conditions need to be specified, and MC is no exception. To be able to simulate a large system, periodic boundary conditions (PBC) are used to eliminate the limitations resulting from boundaries (Watanabe et al. 2001). This method generates copies of the simulation unit cell along each axis, effectively creating an infinitely periodic system (Figure 2.11). This effect is ideal for use in crystalline systems such as MOFs or zeolites which are inherently periodic. However, for use in simulations of liquids or amorphous solids this is less convenient, as they do not possess long-range order. However, it is possible to decrease these finite size effects by using a sufficiently large simulation unit cell.

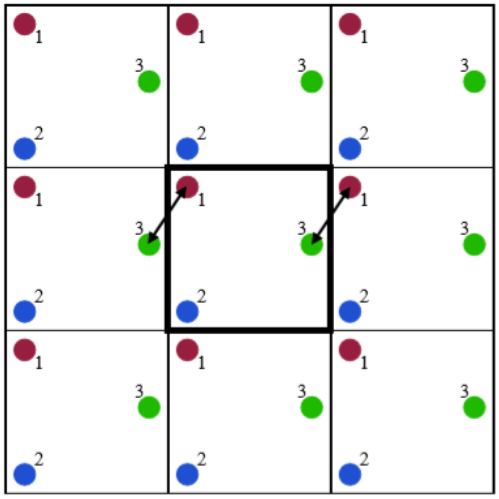

Figure 2.11 – Illustration of Periodic Boundary Conditions

Figure 2.11 shows a central unit cell surrounded by copies of itself. As particles move within the unit cell, their corresponding copies in surrounding boxes move identically. If a move

results in the molecule leaving through one side of the central unit cell, a corresponding molecule then enters the unit cell from the opposite side.

PBC ensure that the molecules are free to move across the system without being limited by the boundaries and that the correct number of molecules is maintained. It also allows simulating infinite systems using only the particles in the central simulation box, thus saving computer cost.

To avoid multiple interactions of a molecule with copies of itself or other molecules as a result of PBC, the minimum image convention is used in simulations to ensure that a specific interaction between the pair of molecules is only counted once. Minimum image convention limits the interactions between species to those which are the closest to each other and it is achieved by limiting the interaction distance in the simulation to less than half of the shortest edge of the simulation unit cell.

2.4 Intermolecular Forces

Grand Canonical Monte Carlo simulations are used to gain an insight into the intrinsic characteristics of the porous materials, predict adsorption and assess their suitability for specific applications. To be able to obtain reliable results in these simulations, the adsorbent-adsorbate interactions have to be accurately defined. These interactions are commonly characterized by a parametrized force field consisting of Van der Waals and electrostatic interactions, the former typically represented by a Lennard-Jones potential.

2.4.1 Force fields in Adsorption

A force field is a collection of potentials or models used in computational modelling to describe intermolecular interactions. The force fields can be empirical, Quantum-mechanical (QM)-based or hybrid.

The empirical approach tunes the force field parameters in order to replicate certain experimental observables. There can be various parameters for the same species, depending on which experimental observable is to be modelled. One of such force fields is Transferable Potentials for Phase Equilibria (TraPPe) (Martin and Siepmann 1998), which is used in this work to model fluid-fluid interactions. This force field was derived to capture the vapour/liquid phase equilibria and it is suitable for adsorption simulation studies. Other

examples are the Universal Force Field (UFF) (Rappe et al. 1992) and DREIDING (Mayo et al. 1990) force fields, which this thesis uses to model solid-fluid interactions. These force fields are commonly used for adsorption simulation in MOFs. The UFF force field is typically used to obtain parameters for the metal atoms of the MOFs, since it covers the entire periodic table. Specific details about force fields used will be listed in each corresponding chapter.

The force field parameters are typically divided into bonded and non-bonded interactions. Bonded interactions include bond stretching, bond bending and torsion, while non-bonded interactions typically account for repulsion, dispersion and electrostatics.

2.4.2 Bonded Interactions

Bonded interactions exist between covalently bonded atoms and affect the potential energy through changes in internal arrangement of the molecule. The intramolecular configuration is usually described by bond lengths, bond angles and dihedral angles. These properties give rise to the intramolecular interactions which include bond bending, stretching and torsion (Figure 2.12).

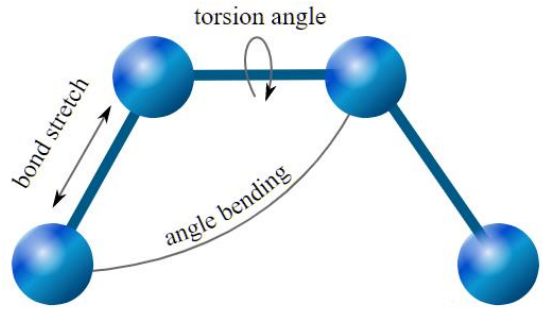

Figure 2.12 – Intramolecular interactions (MMB group 2022)

Bonding interactions are described by Hooke's law, where the bonds are treated as springs and the atoms as spheres. Bonds between particles are treated as harmonic oscillators.

1. Bond stretching

$$V_{stretch} = 1/2k_s(l - l_0)^2 \qquad \text{Equation 2.18}$$

where

k_s – Stretching force constant

l – Instantaneous bond length

l_0 – Equilibrium bond length

2. Angle bending

$$V_{bend} = 1/2k_b(\theta - \theta_0)^2 \qquad \text{Equation 2.19}$$

where

K_b - Bending force constant

Θ - Angle

θ_0 - Equilibrium angle

3. Torsion

$$V_{torsion} = 1/2V_0(1 + \cos n\omega) \qquad \text{Equation 2.20}$$

where

V_0 - Torsional constant

n - Periodicity of rotation

ω - Torsion angle

Equations 2.18 to 2.20 show how these interactions are typically calculated. In this thesis, all species were treated as rigid in the simulations, therefore the intramolecular interactions were not taken into account.

2.4.3 Non-bonded Interactions

Non-bonded interactions describe van der Waals forces and include four sub-categories:

Repulsion – Repulsive interactions are also known as Pauli repulsion and they arise from electron orbitals approaching each other and overlapping, resulting in a strong repulsion. They are based on the Pauli Exclusion Principle which states that two or more identical particles with half-integer spin cannot occupy the same quantum state at the same time within a system, hence as the electron orbitals come into proximity, they repel each other. These are very short-range intermolecular forces as the orbitals have to be in close proximity for the overlap to occur (Pauli 1925).

Dispersion – Dispersive interactions (also known as London dispersion forces) are longer range interactions which are always attractive and are brought about by temporary induced dipoles in neighbouring atoms. They arise when electrons, which are in constant motion, find themselves not distributed symmetrically around the nucleus, thus creating a temporary dipole in the atom or molecule. This dipole then interacts further with neighbouring particles, inducing further dipoles. They are weaker than repulsive interactions (London 1930).

Electrostatics – this force occurs as permanently charged sites of molecules or ions interact with each other. The interaction can be both attractive (particles with opposite charges) or repulsive (particles with same charge).

Polarization – this is a weakly attractive force that arises when a permanently charged particle polarizes another, giving rise to a temporary induced dipole. It is quite expensive to compute, and therefore, with the exception of polarizable force fields (Halgren and Damm 2001), it is only included implicitly in the force field parameters.

2.4.4 van der Waals Interactions

van der Waals interactions include repulsive and dispersive interactions. Dispersive and repulsive interactions between two uncharged particles are commonly expressed together by a single function, called the Lennard-Jones (LJ) potential. It is calculated using Equation 2.21:

$$U(r) = 4\varepsilon[\left(\frac{\sigma}{r}\right)^{12} - \left(\frac{\sigma}{r}\right)^{6}] \qquad \text{Equation 2.21}$$

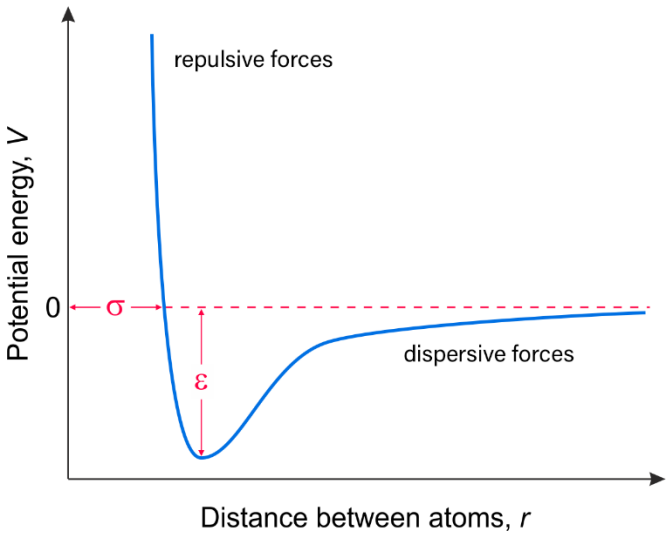

Figure 2.13 – Lennard-Jones potential diagram

Figure 2.13 demonstrates the variation of potential energy of two uncharged atoms depending on the distance between their centres. The value of ε corresponds to the minimum of potential energy which occurs when the distance between the two atom centres is most favourable. As the distance between the centres increases from this minimum, attractive forces are gradually reduced and the potential energy tends to zero at infinite separation. On the other hand, when the distance decreases from the minimum, repulsive forces come into play and the potential energy increases significantly, diverging at zero separation. σ represents the effective atomic radius where the value of the potential energy is zero. Lennard-Jones parameters are used in the simulation to define the strength of the interaction between different species and are typically obtained from force fields, as mentioned above.

The values obtained from force fields normally represent interactions between atoms of the same type, therefore for different atom types it is necessary to calculate the combined values of ε and σ. Most commonly they are calculated using the Lorentz-Berthelot mixing rules shown in Equations 2.21 and 2.23 (Allen and Tildesley 1987).

$$\varepsilon_{ij} = \sqrt{\varepsilon_{ii} \times \varepsilon_{jj}} \qquad \text{Equation 2.22}$$

$$\sigma_{ij} = \frac{(\sigma_{ii}+\sigma_{jj})}{2} \qquad \text{Equation 2.23}$$

In molecular simulation, the contribution of distant atoms can be neglected as the LJ potential approaches zero very quickly for larger separation distances. Therefore, a cut-off

radius is defined and pair interactions beyond the cut-off are neglected for computational efficiency.

To conclude, while the LJ potential is most commonly used, there are many other potentials that can be used to describe these interactions, such as Morse (Morse 1929) or Buckingham (Buckingham 1938). However, most times they are not as convenient and are not included in most available simulation software packages.

2.4.5 Electrostatic Interactions

Electrostatic interactions arise from differences in electronegativity between atoms, caused by the constant motion of electrons around each nucleus. The total electron density for a molecule can be represented by an infinite multipole expansion around the nucleus. Multipole expansion is expressed using terms which become progressively more refined. Multipolar distributions include charge, dipole, quadrupole, octupole etc. The point charge method truncates the expansion at the first term and assigns a point charge value that best represents the overall electron density. Under this approximation, the electrostatic interactions between atoms *ij* can be accounted for using Coulomb's law (Equation 2.24).

$$V_c = k_e \frac{q1 \times q2}{r} \qquad \text{Equation 2.24}$$

where
q - Partial point charge on each site
k_e - Electrostatic constant $1/(4\pi\varepsilon_0)$

Determining the value of the point charge on each interaction sites is one of the most challenging aspects of force field development, mainly because point charges have no direct relation to experimental observables. As a consequence, a multitude of approaches have been suggested over the years, which will be discussed in detail in Section 2.7.

The electrostatic charges exert their effects over longer distances than LJ interactions, and this was accounted for using Ewald summations (Allen and Tildesley 1987) for MOF-adsorbate interactions and Wolf summations (Wolf et al. 1999) for adsorbate-adsorbate interactions. The Ewald summation (Equation 2.25) separately considers short-range interactions in real space and long-range interactions in Fourier space in order to calculate

the overall electrostatic potential. It is a highly accurate method which is used commonly to calculate electrostatic interactions in condensed phase systems.

$$E^{Ewald} = \frac{1}{2}\sum_{i=1}^{N}\sum_{j=1}^{N}\sum_{n=0}^{\infty}\frac{q_i q_j}{|r_{ij}+nL|}\left(erfc\left(\alpha|r_{ij}+nL|\right)\right) - \frac{\alpha}{\sqrt{\pi}}\sum_{i=1}^{N} q_i^2 + \left(\frac{2\pi}{3V}\left(\sum_{i=1}^{N} q_i r_i\right)\right)^2 + \frac{2\pi}{V}\sum_{k\neq 0}^{\infty}\frac{e^{-k^2/4x^2}}{k^2}\sum_{j=1}^{N} q_j e^{-ikr_j}\sum_{j=1}^{N} q_j e^{ikr_j} \quad \text{Equation 2.25}$$

However, the Ewald method is fairly computationally expensive, which makes it unsuitable for calculating the electrostatic potential of a large number of adsorbate molecules on-the-fly. The Wolf summation method is derived from the Ewald method, but involves a novel cut-off scheme ensuring charge neutrality of the system, thus increasing the calculation speed (Equation 2.26).

$$E^{Wolf} = \frac{1}{2}\sum_{i=1}^{N}\sum_{j\neq i}\sum_{r_{ij}<R_c}\frac{q_i q_j}{r_{ij}}\left(erfc\left(\alpha r_{ij}\right)\right) - \lim_{r_{ij}\to R_c}\frac{q_i q_j}{r_{ij}}\left(erfc\left(\alpha r_{ij}\right)\right) - \left(\frac{\left(erfc(\alpha r_{ij})\right)}{2R_c} + \frac{\alpha}{\sqrt{\pi}}\right)\sum_{i=1}^{N} q_i^2 \quad \text{Equation 2.26}$$

2.5 GCMC Computational Method

GCMC adsorption calculations were carried out with MuSiC 4.0 software (Gupta et al. 2003). Before running the simulation, various input files have to be set up (Figure 2.14). Some examples of these files include atom files for each atom in the simulation, which define their individual interaction sites, and molecule files that combine them into indivisible molecules. Atom-atom interaction files contain their intermolecular interaction parameters, calculated from their LJ parameters using the Lorentz-Berthelot mixing rules. The cut-off for intermolecular interactions also has to be specified here.

The control file for the GCMC simulation has to be configured prior to running the simulation. This allows us to input key requirements such as species being simulated, number of iterations, temperature, pressure range, output files etc. Once this is configured, the GCMC simulation can be started. The pressures are converted into fugacity using the Peng-Robinson equation of state (Peng and Robinson 1976), which accounts for the

deviation from the ideal gas behaviour that occurs at higher pressures. This conversion is a pre-processing step carried out using another small utility code.

Once the GCMC simulation is complete, the next step is to run post-processing in order to obtain the results. Here, a percentage of initial results (typically around 40%) at each pressure point is rejected in order to ensure equilibrium conditions. The remainder is then averaged at each pressure to yield an adsorption isotherm.

An optional step prior to running the GCMC simulation is to generate a potential map (PMAP) from the atom-atom interaction files. Where applicable, (in case of polar adsorbates such as CO_2 or H_2O), an electrostatic map (EMAP) would also have to be generated to speed up the calculation of adsorbate-adsorbent electrostatic interactions.

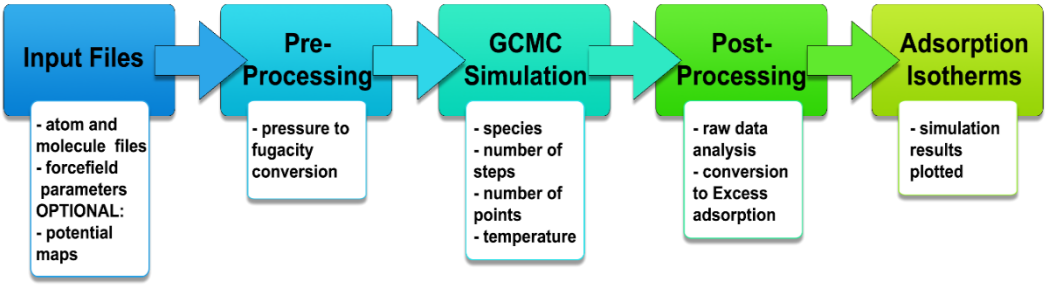

Figure 2.14 – Diagram of the MuSiC GCMC procedure

2.5.1 Potential Maps

Potential mapping is used to simulate the interactions between the adsorbate and the adsorbent in GCMC simulations. A potential map is generated for each atom of the adsorbate, by creating an energy grid within the unit cell consisting of evenly spaced insertions of the atom's LJ interaction site. During the simulation, when a molecule is inserted into the structure by GCMC, rather than calculating the interaction for a specific siting, the potential between adsorbate and framework can easily be interpolated from points on the potential map. This helps to save computational cost as it allows the LJ interactions during the simulation to be calculated from the surrounding grid points by fast interpolation. Generating potential maps is an optional but commonly used step that can be carried out in order to make the simulation process more time-efficient.

Only one PMAP per atom type has to be generated at the start, which can then be used for multiple pressure points and different temperatures. In case of adsorbates that require electrostatics to be included, such as CO_2, an additional EMAP has to be generated. It uses a dummy molecule with a fixed charge, which is compared to the actual adsorbate's point charge in order to calculate the electrostatic interaction. Only one EMAP is required per adsorbate molecule, unlike the case of PMAP which requires one for each LJ interaction site. PMAPS are also used for cavity biasing to enhance sampling of the relevant regions of the system. Favourable locations are identified from the pre-calculated potential map and prioritized for the insertion and deletion moves as was explained previously in section 2.3.4.

2.5.2 Poreblazer

The theoretical pore volumes were calculated using the software Poreblazer (Sarkisov and Harrison 2013). Apart from pore volume, Poreblazer can calculate various other attributes such as accessible surface area, pore distribution or framework density, which makes it suitable for use in computer modelling of MOFs. Poreblazer is based on the grid representation of the porous space (Sarkisov and Kim 2015).

2.6 Quantum Calculations

Quantum mechanical (QM) calculations consider sub-atomic particles rather than atoms such as in classical simulations described above. The aim of QM calculations is to solve the Schrödinger equation and obtain the wavefunction of the system. The wavefunction captures all the observable behaviour of the particle. The Schrödinger equation cannot be solved exactly for any system other than the hydrogen atom, so approximate solutions are achieved which have to be sufficiently accurate to allow reliable comparison between simulations and experimental data. While classical methods depends on the accurate defining of intermolecular interactions, the accuracy of the QM method depends on the details of the theoretical approximations employed, e.g. the selection of the basis set and/or exchange correlation functional (see below). Among many other applications, QM calculations can be used to calibrate force fields and obtain point charges, which is of particular relevance to this thesis. In this section, a brief overview of QM methods will be provided.

The time-independent Schrödinger equation describes the wavefunctions which are stationary states of the system (Equation 2.27).

$$\hat{H}\psi(\vec{r}\,) = E\psi(\vec{r}\,) \qquad \text{Equation 2.27}$$

where

$\hat{H}$ - Hamiltonian Operator

Ψ - Wavefunction, describing quantum state of particles

$\underset{r}{\rightarrow}$ - Position Vectors

E - total energy of the system

The Schrödinger equation has to be solved for every particle (electrons and nuclei) in the system, which quickly becomes non-viable computationally. The Schrödinger equation (Equation 2.28) for a single particle has the form:

$$\left[\frac{-\hbar^2}{2\mu}\nabla^2 + V(r)\right]\Psi(r) = E\Psi(r) \qquad \text{Equation 2.28}$$

where

$\frac{-\hbar^2}{2\mu}\nabla^2$ – kinetic energy

V(r) - potential energy

In order to simplify this problem, the Born-Oppenheimer approximation is employed (Born and Oppenheimer 1927). As nuclei are much larger than electrons and move much slower, the Born-Oppenheimer approximation considers the nuclei to be stationary and the Schrödinger equation can be solved for the electrons in an external static Coulomb potential created by the nuclei. While the use of Born-Oppenheimer approximation does simplify the calculation, it is still not computationally viable to solve the Schrödinger equation for larger systems. There are two main approaches that address this issue – the Hartree-Fock Theory and the Density Functional Theory, which will be briefly described below.

2.6.1 Hartree-Fock Theory

The Hartree-Fock (HF) theory is sometimes referred to as the wavefunction theory. It focuses on solving the time-independent Schrödinger equation once the Born-Oppenheimer approximation has been applied (Hartree 1928) (Fock 1930).

The HF method assumes that the individual electrons do not interact with each other, instead each electron is affected by an average field generated by all electrons. Based on this assumption, the Hamiltonian can be separated into individual one-electron wavefunctions consisting of a collection of spin orbitals, and by combining them, the overall wavefunction of the system can be obtained. The Hamiltonian for each electron then takes the form as described in Equation 2.29:

$$H = \frac{-\hbar^2}{2\mu}\nabla^2 + V(r) + V_H(r) \qquad \text{Equation 2.29}$$

where

$V_H(r)$ – Hartree potential

The Hartree potential describes the average effect of a negative charge field of all electrons on a single electron. In the HF method, the electronic wavefunction is expressed as a single Slater determinant which has the following form for the N-electron system (Equation 2.30) (Slater 1929).

$$\Psi = \frac{1}{\sqrt{N!}}\begin{vmatrix} \chi_1(\mathbf{x}_1) & \chi_2(\mathbf{x}_1) & \cdots & \chi_N(\mathbf{x}_1) \\ \chi_1(\mathbf{x}_2) & \chi_2(\mathbf{x}_2) & \cdots & \chi_N(\mathbf{x}_2) \\ \vdots & \vdots & \ddots & \vdots \\ \chi_1(\mathbf{x}_N) & \chi_2(\mathbf{x}_N) & \cdots & \chi_N(\mathbf{x}_N) \end{vmatrix} \qquad \text{Equation 2.30}$$

where

χ – spin orbital

Each row in the Slater determinant represents an electron and each column corresponds to a spin orbital. The Slater determinant satisfies both the anti-symmetry principle, which states that the sign of the wave function is reversed when two electrons are switched, and the Pauli exclusion principle, which states that the wavefunction is zero when two electrons are in the same orbital at the same time.

With the Slater determinant, the Schrödinger equation can be solved using the variational method (Hanninen 2013). The orbitals are obtained by implementing the variational theorem, which states that the energy calculated for an approximate wavefunction will always be greater than or equal to the true energy. Based on this, different spin orbitals are tried until the lowest possible energy (i.e. the ground state) is obtained. The issue is knowing which orbitals minimize the energy, as infinite possible functions can be tried. To simplify this, a collection of functions and fitting parameters called the basis set is used (Equation 2.31).

$$\chi_i = \sum_{\mu=1}^{K} C_{\mu i}\psi_\mu \qquad \text{Equation 2.31}$$

where

χ_i – spin orbital

C – fitting parameter

Ψ – basis function

By varying the fitting parameter, we can find the minimum energy of the Slater determinant which is made up of spin orbital sets. Large basis sets have the advantage of increased accuracy in describing the spin orbitals, however they incur higher computational cost. The main types of basis sets are plane waves and Gaussian (see Table 2.2).

Gaussian basis sets are localized and consist of Gaussian functions (or Gaussian-type orbitals) centred on each atom. Typically, two or three of these basis sets can be combined to describe an atomic orbital, giving the so-called double-zeta or triple-zeta basis sets. Even larger basis sets are possible (e.g. quadruple-zeta), but they are seldom used because of the very high computational cost. Gaussian basis sets are suitable for individual molecules and they perform well in describing molecular orbitals (Kohanoff 2006). They are, however, prone to the Basis Set Superposition Error (BSSE) (Davidson and Feller 1986). BSSE occurs when atoms in different molecules approach each other and their basis functions overlap. Each molecule then uses the basis function of the neighbouring molecule and increasing its basis set. This leads to inconsistencies and variations in describing the molecular orbitals depending on their distances. Approaches have been developed to compensate for this effect such as the Counterpoise Method (CP) (Boys and Bernardi 1970) and Chemical Hamiltonian Approach (CHA) (Mayer 1983).

Plane wave basis sets are delocalized wavefunctions which are not restricted to a specific atomic position. They are particularly suitable for materials with periodically repeating structures. This method utilizes Fourier transforms to carry out integrals over real-space operators, such as kinetic energy, in a very efficient way. Unlike Gaussian basis sets, plane waves do not suffer from BSSE, as all the functions are mutually orthogonal and not localized to any atom. Their drawback is that in some situations, a large number of plane waves is required – such as in the core region (close to the nucleus) where the electrons are bound more tightly. Furthermore, in this region the valence electron wave functions are rapidly oscillating in order to ensure that they are orthogonal to the core electron wave functions. This is a requirement of Pauli exclusion principle and results in large kinetic energies, which in turn require large number of plane waves.

These issues are addressed by the use of pseudopotentials – a simple effective potential which is designed to eliminate the core region effects within a certain cut-off (Kohanoff 2006). Plane wave basis sets are commonly used in Density Functional Theory (DFT), which will be explained later.

Table 2.2 – Comparison of Gaussian and Plane wave basis sets

Gaussian	**Plane waves**
Atom centred	Delocalized
No pseudopotential	Requires pseudopotential
Basis Set Superposition Error	No Basis Set Superposition Error
Suitable for molecules	Suitable for periodic materials

The main disadvantage of the HF method is that it does not account for electron correlation effects, which leads to overestimation of electron repulsion. Because each electron only interacts with a mean field of all other electrons, the interactions between individual electrons where they would normally not come into proximity with each other are not accounted for. To counteract this, post-HF methods have been developed which introduce an extra term to express the correlation of electrons. Some well-known such methods include Coupled Cluster (CC) (Čížek 1991) and Møller-Plesset Perturbation Theory (MP) (Møller and Plesset 1934). Obviously, the improvements in accuracy in post-HF methods come at much higher computational cost. An alternative approach that attempts to circumvent the limitations of HF in a computationally expedient way is Density Functional Theory.

2.6.2 Density Functional Theory

Density Functional Theory (DFT) approaches the issue by focusing on electron density rather that wavefunction. Like HF, it implements the variational theorem – the aim is to minimize the energy with respect to the density rather than orbitals. The basis for DFT is in the Hohenberg-Kohn theorems (Hohenberg and Kohn 1964). The Hohenberg–Kohn theorems, stated below, relate to any system consisting of electrons moving under the influence of an external potential.

• For non-degenerate ground states, two different Hamiltonians cannot have the same ground-state electron density. Therefore, it is possible to define the ground-state energy as a functional of the electron density: $n(\underset{r}{\rightarrow})$: E = E[n]

• E[n] is minimal when $n(\underset{r}{\rightarrow})$ is the actual ground-state density, among all possible electron densities.

These assumptions allow the DFT method to find the ground state energy by minimizing E[n] instead of going through the determination of the many-electron wavefunction. The variational method can be implemented here – different densities are varied and the resulting energies evaluated – the best solution is that which gives the lowest energy.

DFT calculations implement exchange-correlation functionals to account for electron exchange and correlation, which both arise from the interaction between individual electrons with each other and are not captured by the mean electron density field. The electron exchange energy is a direct consequence of the Pauli exclusion principle, which states that no two fermions can occupy the same spatial as well as spin states. The result of this is that electrons, having the same spin, tend to avoid each other (spatially) even more than they would due to the Coulombic repulsion alone. This results in the lowering of the repulsive energy even further. The HF theory exactly calculates the exchange energy since the anti-symmetry of electrons is accounted for by the use of Slater Determinants in this method. The correlation effect can be described as the motion of each electron being “correlated” to the motion and position of other electrons of the system.

The values of these exchange-correlation functionals are approximated based on the electron density. The accuracy of DFT calculation depends on developing an appropriate exchange-correlation functional. There are four types of these functionals:

- *Local density approximation (LDA)* – this approach uses the form of the uniform electron gas (whose electron density is constant) in order to calculate the exchange-correlation energy density. This is a useful approach for systems where the electron density changes gradually without large differences, such as periodic solid systems. It is less suitable for molecular or cluster systems. Examples of this approach include VWN (Vosko et al. 1980) and PW92 (Perdew and Wang 1992).
- *Generalized gradient approximation (GGA)* – this is a form of the LDA functional further developed to account for electron density gradient, for systems where there are more significant electron density fluctuations. The most common examples of this approach are the Perdew-Wang (PW91) (Perdew and Wang 1991) and Perdew-Ernzerhof (PBE) functionals (Perdew et al. 1996).
- *Meta GGA* – this approach expands upon GGA by also including a term for kinetic energy density. An example of this approach is the M06-L functional (Zhao and Truhlar 2006).
- *Hybrid GGA* – these combine a GGA functional with a percentage of calculated exact energy (from HF theory) which accounts for exchange effects. A common example of this type is the Becke, three-parameter, Lee-Yang-Parr (B3LYP) functional (Becke 1988) (Lee et al. 1988).

Once the exchange-correlation functional is selected, the Kohn-Sham scheme (Equation 2.32) is then used to determine the electron density (Kohn and Sham 1965).

$$H = \frac{-\hbar^2}{2\mu}\nabla^2 + V(r) + V_H(r) + V_{exc}(r) \qquad \text{Equation 2.32}$$

where

$V_{exc}(r)$ – exchange correlation functional

By using exchange-correlation functionals, DFT improves the accuracy of QM calculation by including the correlation energy, although only by approximation. One of the drawbacks is that it is not variational, meaning that improvement of results is not guaranteed by using more complex functionals and there is no systematic way to improve the functionals.

2.6.3 Cluster and Periodic Calculations

QM calculations can be carried out on both periodic and cluster systems. Periodic calculations use periodic boundary conditions and take into account the whole system by using full repeating unit cells of that system, while cluster calculations focus only on the molecule or region of interest. Cluster calculations do not use periodic boundary conditions and are computationally less demanding, but they can be less accurate due to not capturing long range effects of the rest of the system.

2.7 Point Charge Calculation Methods

Determining point charges on interaction sites remains one of the most challenging aspects of force field development, mainly because they have no direct relation to experimental observables. As a consequence, there is currently no universally accepted system of point charge assignment. The approach of assigning point charges is convenient for simulation purposes; however, it has several complexities. For example, it is not possible to exactly reproduce the continuous nature of electron density by a set of fixed point charges, and this can sometimes lead to pronounced artefacts. The charge values may also depend strongly on the quantum mechanical method (e.g. basis set size), on the configuration of the molecule and on the charge determination approach. Indeed, there are various approaches to divide the electron density of the material, and they can generate widely different charges (Watanabe et al. 2011).

A multitude of approaches have been suggested over the years, which can be broadly classified in three categories: 1) empirically fitting the charges to match some set of target experimental properties of the system of interest (e.g. thermodynamic properties in the case of pure fluids, or adsorption isotherms in the case of porous materials) - hereafter termed “Empirical”; 2) extracting the charges from ab initio quantum mechanical calculations - termed “QM-based”; 3) assigning charges based on chemical properties of atoms or small molecular fragments using a set of simple rules (e.g. fragment-based charges; electronegativity equalization methods) - termed “Semi-empirical”. There is also pronounced variability within each class of approaches: class 1 charges will depend strongly on the target properties; class 2 on the details of the underlying QM calculations and on the mathematical procedure to extract the charges; class 3 charges will depend on the properties and set of rules to obtain them. It is not the purpose of this section to provide a comprehensive description of each charge determination method; instead, only the key aspects pertaining to

the methods employed here will be discussed. The reader is referred to previous literature sources for additional technical details (Hamad et al. 2015; Sigfridsson and Ryde 1998; Verstraelen et al. 2016).

By far the most common approach to obtain point charges for MOFs falls into class 2 above - first a QM calculation is carried out on the whole framework or on suitably selected fragments (or "clusters"), followed by a mathematical analysis to extract point charges. This leads us to the first main distinction related to the nature of the QM calculation - periodic or cluster model representations of the molecular systems. Strictly speaking, one should use QM calculations on the entire framework (periodic model approach) to fully capture all electronic effects. Unfortunately, these calculations can become quite computationally demanding as the system sizes increase, and a preferred approach is to run the QM calculation on a smaller molecular fragment that is representative of the MOF functionalities. This, however, introduces a certain degree of arbitrariness in the choice of the cluster(s) and in the choice of atoms to cap the clusters truncated from a periodic framework. As we will see in Chapter 3, this may have a significant effect on the electrostatic interactions in adsorption simulations. It is also important to notice that several charge calculation procedures were not designed to work with periodic QM calculations, and are therefore restricted to cluster calculations. Finally, the level of theory of the QM calculation (e.g., exchange-correlation functional, basis set size) may also have a pronounced effect on the charge values.

Once the QM calculation has been carried out, the question is then how to extract the set of point charges that best represents the electronic environment of the molecule. The multitude of methods to do this can again be broadly classified into 3 types: 1) methods based on population analysis of the QM wavefunction; 2) methods based on partitioning the electron density around each atom; 3) methods based on fitting to the electrostatic potential. The first type is based on the idea of assigning molecular orbitals to individual atoms, and then summing up the population of electrons belonging to each orbital. Population-based methods then differ according to the choice of how to partition shared orbitals. For example, the Mulliken method (Mulliken 1955), one of the earliest charge determination procedures, assigns half of a shared orbital to each atom, regardless of their electronegativity. This makes it relatively simple and computationally efficient to obtain charges using this method, which is why it has been widely used. However, Mulliken charges are not only affected by the

problems related with the different atomic electronegativities but are also very sensitive to changes in basis sets and molecular geometry. These deficiencies led to the elaboration of improved methods, like Löwdin (Löwdin 1950) and Natural Population Analysis (Reed et al. 1985). The more recent LoProp method of Gagliardi et al. (2004) extends this approach by taking into account multipole moments and polarizabilities. An important drawback of these methods is that they cannot be applied to periodic QM calculations using delocalized basis sets. It is possible to perform QM calculations with localized basis sets. These are less common because they are computationally more expensive than calculations with delocalized basis sets.

The second type, of which the Hirshfeld method (Hirshfeld 1977) is the earliest example, does not rely on orbital assignment, but rather on a direct partitioning of the electron density - hence why they are often called "Atoms In Molecules" methods. The Hirshfeld method works by assigning the charge density at each location in proportion to that of reference isolated atoms. This normally leads to rather low charges that tend to underestimate the electrostatic potential around each atom, which has led to the development of numerous improved methods over the years (Verstraelen et al. 2016). One example is the Iterative Stockholder Approach (ISA), in which the partitioning process is optimized iteratively leading to a more realistic representation of the electrostatic potential (Bultinck et al. 2007). Another method that has been widely used in adsorption simulations is DDEC (Density-Derived Electrostatic and Chemical charges) (Manz and Sholl 2010). DDEC has several advantages over the original Hirshfeld method, such as providing a much more accurate representation of the electrostatic potential and being generally applicable to both cluster and periodic QM calculations. A rather different approach of this type are Bader charges, which assign the charges based on a numerical analysis of the gradient and Laplacian of the electron density (Bader et al. 1984). Although they are quite useful to obtain chemical insight, they tend to strongly overestimate the electrostatic potential, and so have rarely been used in adsorption calculations.

Finally, the third type of QM-based charges are obtained through a direct fitting of the electrostatic potential around the molecule (or fragment) of interest. Several methods of this type are available for molecular clusters, with the most prominent examples being ESP (Electrostatic Potential derived charges) (Momany 1978), RESP (Restricted ESP) (Bayly et al. 1993), CHELPG (Charges from Electrostatic Potential using a Grid-based method)

(Breneman and Wiberg 1990), and MSK (Merz-Singh-Kollman) (Singh and Kollman 1984). They differ mostly in the construction of the grid of points in which to fit the electrostatic potential (for example, MSK uses concentric surfaces around each atom, while CHELPG uses a uniform 3-dimensional grid) and in the setting of any constraints to the fitting (for example, RESP imposes constraints on buried atoms to try to ensure chemically realistic charges). This approach has the advantage that the charges are designed to explicitly reproduce the electrostatic potential energy around the molecule/fragment, which is precisely what then goes into the force field calculation. However, the nature of the numerical fitting process means that charges are often quite sensitive to details of the calculation (level of theory, basis set, conformation, etc.). Recently, a generalized version of RESP that is applicable to both clusters and periodic systems, called REPEAT, has been developed (Campana et al. 2009).

Determining point charges through approaches 1 (empirical) or 2 (QM-based) can be quite time consuming and computationally intensive. The advent of high-throughput screening of MOFs has brought the need to develop methods that can yield chemically reasonable charges with low computational requirements. One approach that has been widely used for this purpose is based on charge equilibration (Qeq) (Rappe and Goddard 1991). In a nutshell, this works by assigning point charges that minimize an energy function, which is constructed on the basis of measurable properties like electronegativities or ionization potentials. The choice of energy function separates the different varieties of this method, which include the Extended Charge Equilibration (EQeq) method of Wilmer et al (2012), developed specifically for MOFs. A different approach, also developed for MOFs, is the Connectivity-Based Atom Contribution (CBAC) (Xu and Zhong 2010). This method assigns charges to representative atoms of MOF building blocks with the same bonding environment, and is thus designed to be very fast and highly transferrable. The atomic charge database is itself constructed from QM calculations on a variety of small clusters representative of the most common MOF functionalities.

References

Allen, M.P., Tildesley, D.J.: Computer simulation of liquids. Clarendon Press, Oxford (1987)

Atkins, P.W. 5th ed.; Oxford University Press: Oxford, 1994.

Bader, R. F. W., MacDougall, P. J., Lau, C. D. H.: Bonded and Nonbonded Charge Concentrations and Their Relation to Molecular Geometry and Reactivity. J. Am. Chem. Soc. 106, 1594–1605 (1984)

Bayly, C., Cieplak, P., Cornell, W., Kollman, P.: A well-behaved electrostatic potential based method using charge restraints for deriving atomic charges: the RESP model. J. Phys. Chem. 97, 10269-10280 (1993)

Becke, D.: Density-functional exchange-energy approximation with correct asymptotic behavior, Phys. Rev. A, vol. 38, pp. 3098, (1988)

Belmabkhout, Y., Frère, M. & Weireld, G.D.: High-pressure adsorption measurements. A comparative study of the volumetric and gravimetric methods. Measurement Science and Technology, 15(5), pp.848–858 (2004)

Born, M. and Oppenheimer, R., Zur Quantentheorie der Molekeln. Annalen der Physik, 389(20), pp.457-484 (1927)

Boys, S.F. and Bernardi, F.: The Calculation of Small Molecular Interactions by the Differences of Separate Total Energies. Some Procedures with Reduced Errors. Molecular Physics, 19, 553-566. (1970)

Breneman, C. M.; Wiberg, K. B.: Determining atom-centered monopoles from molecular electrostatic potentials. J. Comput. Chem. 11, 361−373 (1990)

Brunauer, S., Emmett, P. and Teller, E., Adsorption of Gases in Multimolecular Layers. Journal of the American Chemical Society, 60(2), pp.309-319. (1938)

Buckingham, R.A., The classical equation of state of gaseous helium, neon and argon. Proceedings of the Royal Society of London A: Mathematical, Physical and Engineering Sciences 168. 933, pp. 264–283 (1938)

Bultinck, P.; Van Alsenoy, C.; Ayers, P. W.; Carbo-Dorca, R. J. Chem. Phys., 126, (2007)

Campana, C.; Mussard, B.; Woo, T. K.: Electrostatic Potential Derived Atomic Charges for Periodic Systems Using a Modified Error Functional. J. Chem. Theory Comput. 5, 2866−2878 (2009)

Cessford, N., Seaton, N. and Düren, T., Evaluation of Ideal Adsorbed Solution Theory as a Tool for the Design of Metal–Organic Framework Materials. Industrial & Engineering Chemistry Research, 51(13), pp.4911-4921 (2012)

Chen, J., Loo, L.S. and Wang, K., An Ideal Absorbed Solution Theory (IAST) Study of Adsorption Equilibria of Binary Mixtures of Methane and Ethane on a Templated Carbon. Journal of Chemical & Engineering Data, pp. 1209–1212 (2011)

Čížek, J., Origins of coupled cluster technique for atoms and molecules. Theoretica Chimica Acta, 80(2-3), pp.91-94 (1991)

Davidson, E. and Feller, D., Basis set selection for molecular calculations. Chemical Reviews, 86(4), pp.681-696 (1986)

Ebatco, 2020. Thermogravimetric Analysis (TGA). Available at: https://www.ebatco.com/laboratory-services/chemical/thermogravimetric-analysis-tga/ [Accessed January 24, 2022]

Fock, V., Naeherungsmethode zur Loesung des quantenmechanischen Mehrkoerperproblems. Zeitschrift fuer Physik, 61(1-2), pp.126-148 (1930)

Frenkel, D. and Smit, B., Understanding molecular simulation. San Diego: Academic Press (2002)

Gabbott, P.: Principles and applications of thermal analysis. Oxford: Blackwell Pub. (2008)

Gagliardi, L., Lindh, R., Karlström, G.: Local properties of quantum chemical systems: The LoProp approach. J. Chem. Phys. 121, 4494-4500 (2004)

Gelpi, J., Hospital, A., Goñi, R., Orozco, M.: Molecular dynamics simulations: advances and applications, Adv. Appl. Bioinforma. Chem., vol. 8, p. 37 (2015)

Gupta, A., Chempath, S., Sanborn, M. J., Clark, L. A., Snurr, R. Q.: Object-oriented Programming Paradigms for Molecular Modeling. Mol. Sim. 29, 29-46 (2003)

Halgren, T.A., Damm, W.: Polarizable Force Fields. Current Opinion in Structural Biology, 11(2), pp.236–242 (2001)

Hamad, S., Balestra, S., Bueno-Perez, R., Calero, S., Ruiz-Salvador, A.: Atomic charges for modeling metal–organic frameworks: Why and how. J. Solid State Chem. 223, 144-151 (2015)

Hanninen, V.: Introduction to Computational Chemistry, tech. rep., University of Helsinki, (2013)

Hartree, D., The Wave Mechanics of an Atom with a Non-Coulomb Central Field. Part II. Some Results and Discussion. Mathematical Proceedings of the Cambridge Philosophical Society, 24(1), pp.111-132 (1928)

Hirshfeld, F. L.: Bonded-atom fragments for describing molecular charge densities. Theor. Chim. Acta 44, 129-138 (1977)

Hohenberg, P. and Kohn, W., Inhomogeneous Electron Gas. Physical Review, 136(3B), pp.B864-B871 (1964)

Kohanoff, J., Electronic Structure Calculations for Solids and Molecules. Cambridge: Cambridge University Press (2006)

Kohn, W., Sham, L.J.: Self-Consistent Equations Including Exchange and Correlation Effects. Phys. Rev., A1133–A1138 (1965)

Langmuir, I., The constitution and fundamental properties of solids and liquids. Journal of the American Chemical Society, 38(11), pp.2221-2295. (1916)

Larkin, P., 2018. Infrared and Raman Spectroscopy: Principles and spectral interpretation, Amsterdam, Netherlands: Elsevier.

Lee, C., Yang, W., Parr, R. G.: Development of the Colle-Salvetti correlation energy formula into a functional of the electron density, Phys. Rev. B, vol. 37, pp. 785-789, (1988)

Libretexts, 2021. 6.2: Infrared (IR) spectroscopy theory. Chemistry LibreTexts. Available at: https://chem.libretexts.org/Bookshelves/Organic_Chemistry/Organic_Chemistry_I_(Liu)/06%3A_Structural_Identification_of_Organic_Compounds-_IR_and_NMR_Spectroscopy/6.02%3A_Infrared_(IR)_Spectroscopy_Theory [Accessed January 24, 2022]

London, F.: Zur Theorie und Systematik der Molekularkräfte, Zeitschrift für Physik, 63 (3–4): 245, (1930)

Löwdin, P.O.: On the Non-Orthogonality Problem Connected with the Use of Atomic Wave Functions in the Theory of Molecules and Crystals. J. Chem. Phys. 18, 365-375 (1950)

Manz, T. A.; Sholl, D. S.: Chemically meaningful atomic charges that reproduce the electrostatic potential in periodic and nonperiodic materials. J. Chem. Theory Comput. 6, 2455-2468 (2010)

Martin, M. G., Siepmann, J. I.: Transferable Potentials for Phase Equilibria. 1. United-Atom Description of n-Alkanes. J. Phys. Chem. 102, 2569-2577 (1998)

Mason, J.A., Veenstra, M. & Long, J.R.: Evaluating metal–organic frameworks for natural gas storage. Chem. Sci., 5(1), pp.32–51 (2014)

Master Organic Chemistry. Interpreting IR Specta: A quick guide. 2020. Available at: https://www.masterorganicchemistry.com/2016/11/23/quick_analysis_of_ir_spectra/ [Accessed January 24, 2022]

Mayer, I., Towards a "Chemical" Hamiltonian. International Journal of Quantum Chemistry, 23(2), pp.341-363 (1983)

Mayo, S. L., Olafson, B. D., Goddard, W.A.: DREIDING: A Generic Force Field for Molecular Simulations. J. Phys. Chem. 94, 8897-8909 (1990)

Metropolis, N., Rosenbluth, A.W., Rosenbluth, M.N., Teller, A.H., Teller, E.: Equation of State Calculations by Fast Computing Machines. J. Phys. Chem. 21, 1087-1092 (1953)

Mezei, M.: A cavity-biased (T, V, μ) Monte Carlo method for the computer simulation of fluids. Mol. Phys. 40, 901-906 (1980)

MMB group, NAFLEX: Nucleic acids flexibility. Available at: http://mmb.irbbarcelona.org/NAFlex/help.php?id=md [Accessed January 24, 2022]

Møller, C. and Plesset, M., Note on an Approximation Treatment for Many-Electron Systems. Physical Review, 46(7), pp.618-622 (1934)

Momany, F.: Determination of partial atomic charges from ab initio molecular electrostatic potentials. Application to formamide, methanol, and formic acid. J. Phys. Chem. 82, 592-601 (1978)

Morse, P.M., Diatomic Molecules According to the Wave Mechanics. II. Vibrational Levels. Phys. Rev. 34, pp. 57–64 (1929)

Myers, A. and Prausnitz, J., Thermodynamics of mixed-gas adsorption. AIChE Journal, 11(1), pp.121-127 (1965)

Mulliken, R.S.: Electronic Population Analysis on LCAO–MO Molecular Wave Functions. J. Chem. Phys. 23, 1833-1840 (1955)

NASA. Visible light. Available at: https://science.nasa.gov/ems/09_visiblelight [Accessed January 24, 2022]

Pauli, W.: Über den Zusammenhang des Abschlusses der Elektronengruppen im Atom mit der Komplexstruktur der Spektren. Zeitschrift für Physik. 31 (1): 765–783. (1952)

Peng, D. Y., Robinson, D.B.: A New Two-Constant Equation of State. Ind. Eng. Chem. Fundament. 15, 59-64 (1976)

Perdew, J.P. and Wang, Y., Accurate and simple analytic representation of the electron-gas correlation energy, Physical Review B 45, 13244 (1992)

Perdew, J.P., Burke, K. and Ernzerhof, M., Generalized Gradient Approximation Made Simple, Phys. Rev. Lett., vol. 77, pp. 3865-3868, (1996)

Rappe, A. K., Casewit, C. J., Colwell, K. S., Goddard, W. A., Skiff, W. M.: UFF, A Full Periodic Table Force Field for Molecular Mechanics and Molecular Dynamics Simulations. J. Am. Chem. Soc. 114, 10024-10035 (1992)

Reed, A.E., Weinstock, R.B., Weinhold, F.: Natural Population Analysis. J. Chem. Phys. 83, 735-746 (1985)

Rouquerol, F., Adsorption by powders and porous solids. Amsterdam: Elsevier, Academic Press. (2014)

Sarkisov, L. and Harrison, A., Computational Structure Characterisation Tools in Application to Ordered and Disordered porous Materials. Molecular Simulation 37.15, pp. 1248–1257 (2011)

Sarkisov, L. and Kim, J., Computational structure characterization tools for the era of material informatics. Chemical Engineering Science, 121, pp.322-330 (2015)

Sigfridsson, E., Ryde, U.: Comparison of methods for deriving atomic charges from the electrostatic potential and moments. J. Comput. Chem. 19, 377-395 (1998)

Sing, K. S. W., Everett, D.H., Haul, R., Moscou, L., Pieroti, R.A., Rouquerol, J., Siemieniewska, T. Pure Appl. Chem. 57, (1985)

Singh, U., Kollman, P.: An approach to computing electrostatic charges for molecules. J. Comput. Chem. 5, 129-145 (1984)

Slater, J., The Theory of Complex Spectra. Physical Review, 34(10), pp.1293-1322 (1929)

Thommes, M., Kaneko, K., Neimark, A., Olivier, J., Rodriguez-Reinoso, F., Rouquerol, J. and Sing, K., Physisorption of gases, with special reference to the evaluation of surface area and pore size distribution (IUPAC Technical Report). Pure and Applied Chemistry, 87(9-10), pp.1051-1069 (2015)

Verstraelen, T., Vandenbrande, S., Heidar-Zadeh, F., Vanduyfhuys, L., Van Speybroeck, V., Waroquier, M., Ayers, P.: Minimal Basis Iterative Stockholder: Atoms in Molecules for Force-Field Development. J. Chem. Theory and Comput. 12, 3894-3912 (2016)

Vosko, S.H., Wilk, L. and Nusair, M., Accurate spin-dependent electron liquid correlation energies for local spin density calculations: a critical analysis, Canadian Journal of Physics *58 (8), 1200 (1980)*

Wang, Y. and Perdew, J.P., Spin scaling of the electron-gas correlation energy in the high-density limit, Phys. Rev. B, vol. 43, pp. 8911-8916, (1991)

Watanabe, M., Becker, O., MacKerell, A. Roux, B.: Computational Biochemistry And Biophysics. New York: Marcel Dekker, Inc. (2001)

Wikipedia: Ensemble (mathematical physics). Wikipedia. Available at: https://en.wikipedia.org/wiki/Ensemble_(mathematical_physics) 2021 [Accessed January 24, 2022]

Wilmer, C. E.; Kim, K. C.; Snurr, R. Q.: An extended charge equilibration method. J. Phys. Chem. Lett. 3, 2506−2511 (2012)

Wolf, D., Keblinski, P., Phillpot, S.R. and Eggebrecht, J. Exact method for the simulation of Coulombic systems by spherically truncated, pairwise r-1 summation. The Journal of Chemical Physics 110.17 (1999)

Zhao, Y. and Truhlar, D.G., A new local density functional for main-group thermochemistry, transition metal bonding, thermochemical kinetics, and noncovalent interactions, Journal of Chemical Physics *125, 194101 (2006)*

Xu, Q., Zhong, C.L.: A general approach for estimating framework charges in metal organic frameworks. J. Phys. Chem. 114, 5035-5042 (2010)

3. *The Effect of Atomic Point Charges on Adsorption Isotherms of CO_2 and Water in Metal Organic Frameworks*

3.1 Introduction

The immense number of existing and hypothetical combinations of metals and linkers means that MOFs are promising for a wide range of applications, but also poses great challenges for experimental screening (Coudert and Fuchs 2016). As discussed previously, computational methods like Grand-Canonical Monte Carlo offer a viable alternative for MOF screening and design, but they rely strongly on the accuracy of the underlying molecular model. In particular, the assignment of atomic point charges to each atom of the framework is required for modelling Coulombic interactions between the MOF and the adsorbate, which are crucial in adsorption of polar gases like water or carbon dioxide (Nazarian et al. 2016).The aim of this chapter is to investigate the effect of varying framework point charges on adsorption isotherm predictions, identify the underlying trends, and based on this knowledge to improve existing models in order to increase the accuracy of gas adsorption prediction in MOFs.

Adsorption isotherms for CO_2 and water in several MOFs corresponding to the most widely studied "families" (i.e. CuBTC, IRMOF-1, UiO-66, MIL-47, Co-MOF-74 and SIFSIX-2-Cu-I) were generated with GCMC by using several different framework point charge sets. The charge determination methods ranged from purely empirical to Quantum Mechanics (QM) based, including more approximate methods like charge equilibration. Within the QM-based methods, we included charges obtained from both periodic and cluster models, and covering all types of charge calculation approach (electrostatic potential fitting, electron density partitioning and basis set analysis). Our results show that framework charges obtained from QM-based methods using fully periodic models lead to consistent adsorption isotherms regardless of the charge calculation approach. QM-based cluster models, however, can lead to inaccurate adsorption predictions if appropriate care is not taken. More approximate methods offer a faster alternative to calculate point charges, but can often compromise the accuracy of the adsorption predictions. We included both MOFs with and without open metal sites (OMS), specifically to investigate whether this property affects the predicted adsorption behaviour.

3.2 Computational Methods

All adsorption isotherms reported in this thesis were calculated by Grand Canonical Monte Carlo simulations using Music 4.0 software (Gupta et al. 2003) – for details see section 2.5. Each simulation, corresponding to a single pressure point, was set for a total of 5.0×10^7 iterations, composed of a 2.0×10^7 cycle equilibration period, followed by a 3.0×10^7 cycle production run. These lengths are sufficient to ensure convergence (see Figures 3.6 and 3.7 for details) and were kept constant in all runs to enable direct comparison. The sampling period was split into 20 blocks for statistical analysis, and error bars were calculated as a 95% confidence interval - in most cases, they are approximately of the size of the symbols used, so they are not visible in the isotherm plots.

Fluid-fluid and fluid-solid interactions were calculated using models composed of Lennard-Jones (LJ) sites to describe repulsion and dispersion interactions, and partial point charges to describe permanent electrostatic interactions. A LJ cut-off distance was defined as 13 Å. The electrostatic charges exert their effects over longer distances than LJ interactions, and this was accounted for using Ewald summations (Allen and Tildesley 1987) for MOF-adsorbate interactions and Wolf summations (Wolf et al. 1999) for adsorbate-adsorbate interactions. The Universal Force Field (UFF) (Rappe et al. 1992) and DREIDING (Mayo et al. 1990) are frequently used to model gas adsorption in MOFs and they were used in this chapter to describe the interactions with MOF framework atoms. More precisely, LJ parameters for the MOF metal atoms were taken from UFF and for non-metal atoms from DREIDING. For the adsorbate models, the Transferable Potentials for Phase Equilibria (TraPPE) (Martin and Siepmann 1998) model was used for CO_2 and the SPC/E (Berendsen et al. 1987) model for water.

Framework point charge sets generated by different methods were either obtained from literature or calculated in-house (see next section for details). To investigate solely the effect of varying framework point charges on the adsorption isotherms, the adsorbate-adsorbate potential (both LJ and charges), as well as the MOF-adsorbate LJ parameters, were kept constant in all calculations, and only the MOF-adsorbate electrostatic interactions were varied. This means that for each isotherm, a separate electrostatic interaction energy grid was calculated, followed by a full GCMC simulation. We studied IRMOF-1 (also known as MOF-5) (Li et al. 1999), MIL-47 (Barthelet et al. 2002), UiO-66 (in the fully hydroxylated form) (Cavka et al. 2008), $Cu(dpa)_2SiF_6$-i (in the interpenetrated form, abbreviated as

SIFSIX) (Nugent et al. 2013), CuBTC (also known as HKUST-1) (Chui et al. 1999) and Co-MOF-74 (also known as CPO-27-Co or Co_2(dobdc)) (Dietzel et al. 2005), with all framework structures obtained from the Cambridge Structural Database. These MOFs were chosen with the aim of covering the most well-known and comprehensively studied "families" of MOF structures, as well as ensuring a large degree of topological diversity.

3.3 Point charges

We have collected from literature reports a large number of framework point charge sets for all the MOFs under study, spanning all the charge calculation approaches described in section 2.7, as well as different QM levels of theory (in the case of approach 2) including cluster and periodic calculations (computational details are collected in Tables 3.1 - 3.2). These were then used, together with the remaining force field parameters described in section 2.2, to generate individual adsorption isotherms for each point charge set. In some cases (notably for SIFSIX MOF), we have calculated our own framework charges from QM calculations, as follows. DFT calculations using periodic models of selected MOF structures were carried out with both VASP (Kresse and Hafner 1993, Kresse and Hafner 1994, Kresse and Furthmüller 1996) and CP2K (Laino et al. 2006) software. VASP calculations used the PBE functional (Perdew et al. 1996), without spin polarization, Projected Augmented Wave (PAW) potentials (Kresse and Joubert 1999) for core electrons, a cutoff of 415 eV for plane-wave basis sets and a grid of 1×1×2 k-points. CP2K calculations also used the PBE functional with a double zeta plus polarization (DZVP) basis set (Godbout et al. 1992) and optimised Goedecker-Teter-Hutter pseudopotentials (Goedecker et al. 1996). The energy cut-off selected was 500 Ry, the calculations used Γ-point sampling and spin polarization was accounted for. For the SIFSIX MOF, we also carried out cluster calculations using Gaussian 09 (Frisch et al. 2009), with the M06-L functional (Zhao and Truhlar 2006) and a 6-31G** basis set (Hariharan and Pople 1973). DDEC charges were computed using the Chargemol code and the DDEC6 variant (Limas and Manz 2018). Further details of the QM calculations carried out by collaborators of this project are provided in Section A.1.

The vast majority of charge sets were obtained using purely theoretical methods and compared to experiment in original publications. Some specific charge sets were developed empirically against experimental data. As mentioned in Section 1, we intentionally didn't compare our theoretical results with experimental data, in order to avoid the uncertainty inherent to experimental measurements of adsorption in MOFs. The comparison of simulation to experimental data can be viewed in the original publications.

Additional details about the calculations of point charge sets

Table 3.1 – Point charge calculation details for cluster methods.

Charge Set	Charge Method	Functional	Basis set metals	Basis Set non-metals	Cluster details	Saturation	DOI
Yang and Zhong (2006)	CHELPG	B3LYP	LAND2DZ	6-31+G*	1 cluster centred on linker	methyl	10.1021/jp062723w
Yazaydin et al. (2009) (1)	CHELPG	B3LYP	6-31+G*	6-31+G*	1 cluster centred on linker	methyl	10.1021/ja9057234
Sagara et al. (2004)	CHELPG	PBE	6-31+G*	6-31+G*	1 cluster centred on linker	methyl	10.1063/1.1809608
Dubbeldam et al. (2007)	CHELPG	PBE	6-31+G*	6-31+G*	1 cluster centred on linker	methyl	10.1002/anie.200700218
Mu et al. (2010)	CHELPG	B3LYP	LAND2DZ	6-31+G*	1 cluster centred on linker	methyl	10.1016/j.micromeso.2009.10.015
Fischer et al. (2009)	MSK	PBE	DNP	DNP	1 cluster centred on linker	n/a	10.1002/cphc.200900459
Babarao et al. (2007)	RESP	B3LYP	6-31G*	6-31G*	1 large cluster with 4 linkers	hydrogen	10.1021/la062289p
Belof et al. (2009) (1)	MSK	HF	SBKJC	SBKJC	1 cluster centred on metal	hydrogen	10.1021/jp901988e
Belof et al. (2009) (2)	MSK	HF	6-31G*	6-31G*	1 cluster centred on metal	hydrogen	10.1021/jp901988e
Tafipolsky et al. (2007)	MSK	B3LYP	Stuttgart ECP	6-31G**	2 clusters, centred on metal and linker	hydrogen	10.1002/jcc.20648
Finsy et al. (2009)	CHELPG	n/a	n/a	n/a	n/a	n/a	10.1039/b822247a
Yang et al. (2011)	CHELPG	PBE	LAND2DZ	6-31+G*	1 cluster centred on metal-ligand bond	methyl	10.1039/c1cc13543k
Liu et al. (2009) (1)	CHELPG	B3LYP	6-311++G**	6-311++G**	1 cluster centred on metal (30 atoms)	methyl	10.1080/08927020802398926
Liu et al. (2009) (2)	CHELPG	B3LYP	6-311++G**	6-311++G**	1 cluster centred on metal (50 atoms)	methyl	10.1080/08927020802398926
Yazaydin et al. (2009) (2)	CHELPG	PBE	6-31+G*	6-31+G*	1 cluster centred on linker	methyl	10.1021/cm900049x
Babarao et al. (2009)	MSK	B3LYP	LAND2DZ	6-31G*	1 cluster centred on linker	methyl	10.1021/la803074g
Haldoupis et al. (2015)	LoProp	MP2	ANO-RCC	ANO-RCC	several clusters	hydrogen	10.1021/acs.jpcc.5b03700
Pham (CHELPG)	CHELPG	HF	LAND2DZ	6-31G*	several clusters	variable	10.1021/jp402764s
CHELPG (Clusters)	CHELPG	M06L	6-31G**	6-31G**	several clusters	hydrogen	This work
DDEC (Clusters)	DDEC	M06L	6-31G**	6-31G**	several clusters	hydrogen	This work

Table 3.2 – Point charge calculation details for periodic methods.

Charge Set	**Charge Method**	**Functional**	**Code**	**Basis Set**		**Brillouin Zone Sampling**		**DOI**
				Core Electrons	**Valence Electrons[1]**	Grid	k-points	
Manz and Sholl (2010)	DDEC	PW91	VASP	PAW	PW, 400 eV	Γ- point	1	10.1021/ct100125x
Manz and Sholl (2010)	DDEC Uncompensated	PW91	VASP	PAW	PW, 400 ev	Γ- point	1	10.1021/ct100125x
Strathclyde	DDEC	PBE	CP2K	GTH	GPW, 6800 eV, DZVP	Not used	Not used	This work
Campana et al. (2009)	REPEAT	PBE	CPMD	GTH	PW, 1088 eV	Γ- point	n/a	10.1021/ct9003405
Manz and Sholl (2010)	Hirshfeld	PW91	VASP	PAW	PW, 400 eV	Γ- point	1	10.1021/ct100125x
Manz and Sholl (2010)	ISA	PW91	VASP	PAW	PW, 400 eV	Γ- point	1	10.1021/ct100125x
Manz and Sholl (2010)	Bader	PW91	VASP	PAW	PW, 400 eV	Γ- point	1	10.1021/ct100125x
Nazarian et al. (2016)	DDEC	PBE	VASP	n/a	n/a	variable[2]	1000 points per atom	10.1021/acs.chemmater.5b03836
Wilmer et al. (2012)	REPEAT	PW91	VASP	PAW	PW, 520 eV	Monkhorst-Pack	variable [2]	10.1021/jz3008485
Ramsahye et al. (2007)	Mulliken	PW91	DMol	all-electron	G, DNP	n/a	n/a	10.1007/s10450-007-9025-5
Ghosh et al. (2014)	REPEAT	PW91	VASP	PAW	PW, 550 eV	Monkhorst-Pack	n/a	10.1039/c4cc04945d
Zang et al. (2013)	DDEC	PBE-D2	VASP	PAW	PW, 500 eV	Γ- point	1	10.1021/jp310497u
Haldoupis et al. (2015)	DDEC	PBE+U	VASP	n/a	PW, 520 eV	Γ- point	2×2×2 grid	10.1021/acs.jpcc.5b03700
Mercado et al. (2016)	REPEAT	PBE	VASP	PAW	PW, 1000 eV	Γ- point	single k point	10.1021/acs.jpcc.6b03393
DDEC CP2K	DDEC	PBE	CP2K	GTH	GPW, 6800 eV, DZVP	Not used	Not used	This work
REPEAT VASP	REPEAT	PBE	VASP	PAW	PW, 415 eV	Γ- point	1×1×2	This work
DDEC VASP	DDEC	PBE	VASP	PAW	PW, 415 eV	Γ- point	1×1×2	This work

[1]For calculations with Plane Waves (PW), the energy cut-off in units of eV is given; for calculations with Gaussians (G), the basis set is given; for calculations with Gaussian and Plane Waves (GPW), both the cut-off and the Gaussian basis set is given

[2] Different sampling schemes were used for different MOFs, check original papers

3.4 Results & Discussion

3.4.1 IRMOF-1

IRMOF-1 (Figure 1) belongs to a class of MOFs called the isoreticular MOFs (IRMOFs), which are characterised by their cubic topology. It was first reported in 1999 (Li et al. 1999). It forms a cubic network that consists of Zn_4O units joined by linear 1,4-benzenedicarboxylate links (Tranchemontagne et al. 2008). Even though it does not contain OMS, it has been shown to be very water unstable, similarly to other structures with Zn as a central atom, which limits the material's potential applications (Castillo et al. 2008).

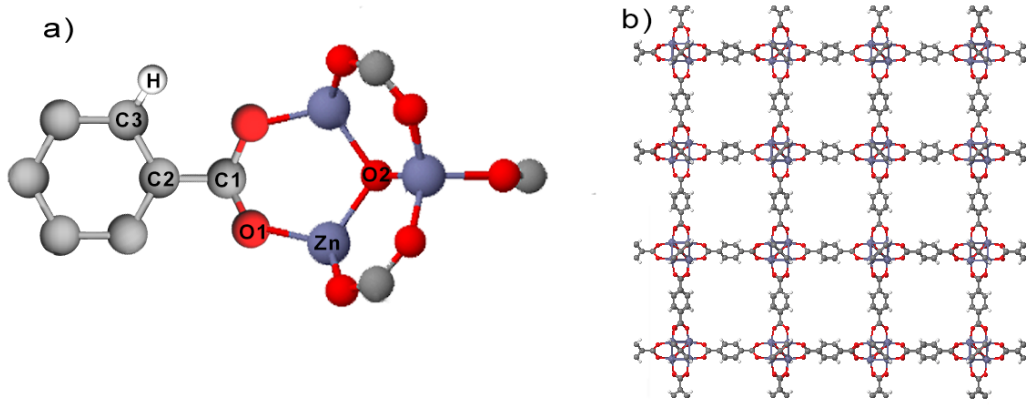

Figure 3.1 – a) IRMOF-1 building block showing the different uniquely charged atoms. The corresponding charges are listed in Table 3.3. b) IRMOF-1 framework structure

Table 3.3 - Charge sets for IRMOF-1 calculated by different methods, obtained from literature sources

Charge Set	**Method**	**Zn**	**O1**	**O2**	**C1**	**C2**	**C3**	**H**
Manz and Sholl (2010)	DDEC	1.121	-0.658	-1.398	0.762	-0.058	-0.148	0.122
Manz and Sholl (2010)	DDEC Uncompensated	1.32	-0.68	-1.68	0.79	-0.16	-0.05	0.12
Strathclyde (This work)	DDEC	0.9864	-0.5512	-1.0220	0.5786	-0.0139	-0.1237	0.1490
Campana et al. (2009)	REPEAT	1.28	-0.61	-1.57	0.52	0.14	-0.18	0.17
Manz and Sholl (2010)	Hirshfeld	0.42	-0.22	-0.34	0.18	-0.01	-0.02	0.04
Manz and Sholl (2010)	ISA	1.27	-0.66	-1.59	0.73	-0.08	-0.10	0.15
Manz and Sholl (2010)	Bader	1.30	-1.13	-1.23	1.37	0.11	0.22	-0.16
Yang and Zhong (2006)	CHELPG	1.501	-0.724	-1.846	0.667	0.072	-0.132	0.140
Yazaydin et al. 2009 (1)	CHELPG	1.333	-0.641	-1.564	0.558	0.106	-0.167	0.162
Sagara et al. (2004)	CHELPG	1.31	-0.63	-1.79	0.62	0.05	-0.12	0.12
Dubbeldam et al. (2007)	CHELPG	1.275	-0.60	-1.50	0.475	0.125	-0.15	0.15
Mu et al. (2010)	CHELPG	1.637	-0.757	-1.996	0.671	0.079	-0.122	0.125
Fischer et al. (2009)	MSK	1.515	-0.708	-1.884	0.606	0.193	-0.234	0.190
Babarao et al. (2007)	RESP	1.10	-0.56	-0.98	0.53	-0.02	-0.10	0.12
Belof et al. (2009) (1)	MSK	1.8529	-1.0069	-2.2568	1.0982	-0.1378	-0.0518	0.1489
Belof et al. (2009) (2)	MSK	1.8833	-1.0144	-2.2684	1.1457	-0.1787	-0.0659	0.1729
Tafipolsky et al. (2007)	MSK	1.26	-0.67	-1.44	0.68	0.06	-0.16	0.16
Wilmer and Snurr (2011) (1)	EQeq	1.16	-0.70	-1.50	0.69	0.07	-0.13	0.19
Wilmer et al. (2012) (2)	EQeq	1.211	-0.482	-0.968	0.321	-0.064	-0.024	0.053
Wilmer et al. (2012)	Qeq	0.450	-0.479	-0.225	0.612	0.033	-0.121	0.146
Xu and Zhong (2010)	CBAC	1.583	-0.802	-1.93	0.797	0.041	-0.139	0.100
	Average	1.2747	-0.6802	-1.4752	0.6858	0.0170	-0.1009	0.1223
	Standard Deviation	0.3614	0.1979	0.5395	0.2656	0.1015	0.0903	0.0750

IRMOF-1 is one of the most widely studied MOFs in the scientific literature. As such, we were able to find a very large number of charge sets for this framework, reported in Table 3.3. We also carried out our own calculations using DDEC based on a periodic QM calculation (see section 2.3). It is clear from Table 3.3 that the point charges on each individual atom show a very wide variability (see also the averages and standard deviations at the bottom of Table 3.3). This is particularly the case for buried atoms, like Zn and O2, which tend to have a small effect on the electrostatic potential.

We proceed to compare the adsorption isotherms for CO_2 and water at 298 K in IRMOF-1, obtained from GCMC simulations using each set of charges (Figures 3.2-3.4). A single plot comparing all charge sets is shown in Figure 3.21b. Figure 3.2a compares adsorption isotherms of CO_2 in IRMOF-1 using framework point charges which were obtained from periodic QM calculations. First of all, our results corroborate previous conclusions that framework charges have a significant effect on adsorption simulations of CO_2 in MOFs (Kadantsev et al. 2013, McDaniel et al. 2015; Yang and Zhong 2006; Zheng et al. 2009), since it is clear that the isotherm calculated without framework point charges lies significantly below all the other isotherms.

All the Manz charge sets were generated from the same underlying DFT calculation, but differ in the method used to extract the point charges, so they make for a particularly interesting comparison. The Hirshfeld method produced much lower magnitude charges than the other methods, but this is consistent over all atoms and the relative difference between atoms is similar (see Table 3.1). Adsorption predictions using the Hirshfeld method are slightly lower than the rest, but the difference is not statistically significant. The ISA charges show very good agreement with DDEC except for C2 and C3 atoms, which are half and double in magnitude compared to DDEC, respectively. However, when translated into adsorption isotherm calculations, these differences in point charge magnitudes turn out to be negligible. In fact, it is quite remarkable that all isotherms obtained using framework charges from periodic calculations (periodic point charges) are statistically consistent with each other, with the exception of the Bader charge set. The latter is markedly different from the rest, both in shape and capacity, indicating much stronger framework/CO_2 interactions at low pressure. The isotherm implies the strength of this interaction is strong enough to overcome the intermolecular CO_2 interactions at low pressure, hence it does not follow the slight inflection of the other isotherms. The fact that experimental isotherms of CO_2 on IRMOF-1 exhibit this pronounced inflexion (Walton et al. 2008), points to the inadequacy

of the Bader method for obtaining point charges for adsorption simulations. The tendency of Bader charges to overestimate adsorption in MOFs was previously reported by Liu et al. (2009). Overall, with the exception of Bader, all the periodic point charge sets should provide consistent adsorption predictions of CO_2 in IRMOF-1. In the following, we will use the DDEC charges from the group of Manz and Sholl as reference points for comparison in all MOFs.

The water isotherms (Figure 3.2b) show a type V shape, where the interaction between the water molecules is stronger than their interaction with IRMOF-1. Very slow uptake is initially observed, which increases once the surface coverage is sufficient to induce water clustering, causing a step-wise increase in the adsorbed amount. This is consistent with the previously reported hydrophobic nature of this material (Walton et al. 2008). We would expect that water, being a much more polar molecule than CO_2 due to a strong permanent dipole moment, would show a stronger effect of framework point charges on adsorption isotherms. It is therefore quite interesting that also in the case of water, all the adsorption isotherms obtained from periodic point charges, with the exception of Bader and Hirshfeld, show very good agreement with each other. The Hirshfeld method showed slightly lower adsorption in the case of CO_2 and this is magnified in the water adsorption isotherm, such that differences are now statistically significant. It is important to note that simulations of water adsorption in hydrophobic materials may suffer from convergence problems (Zhang and Snurr 2017). In this work, we opted to run all isotherms with exactly the same number of MC trials since our aim was to compare simulated isotherms against each other, rather than against experimental data. In any case, we have tested the convergence of individual simulation points, shown in Figures 3.6-3.7. These results, together with the fact that several repetitions of the calculations show close agreement with each other (Figure 3.8), give us confidence that the isotherms represent converged equilibrium uptakes.

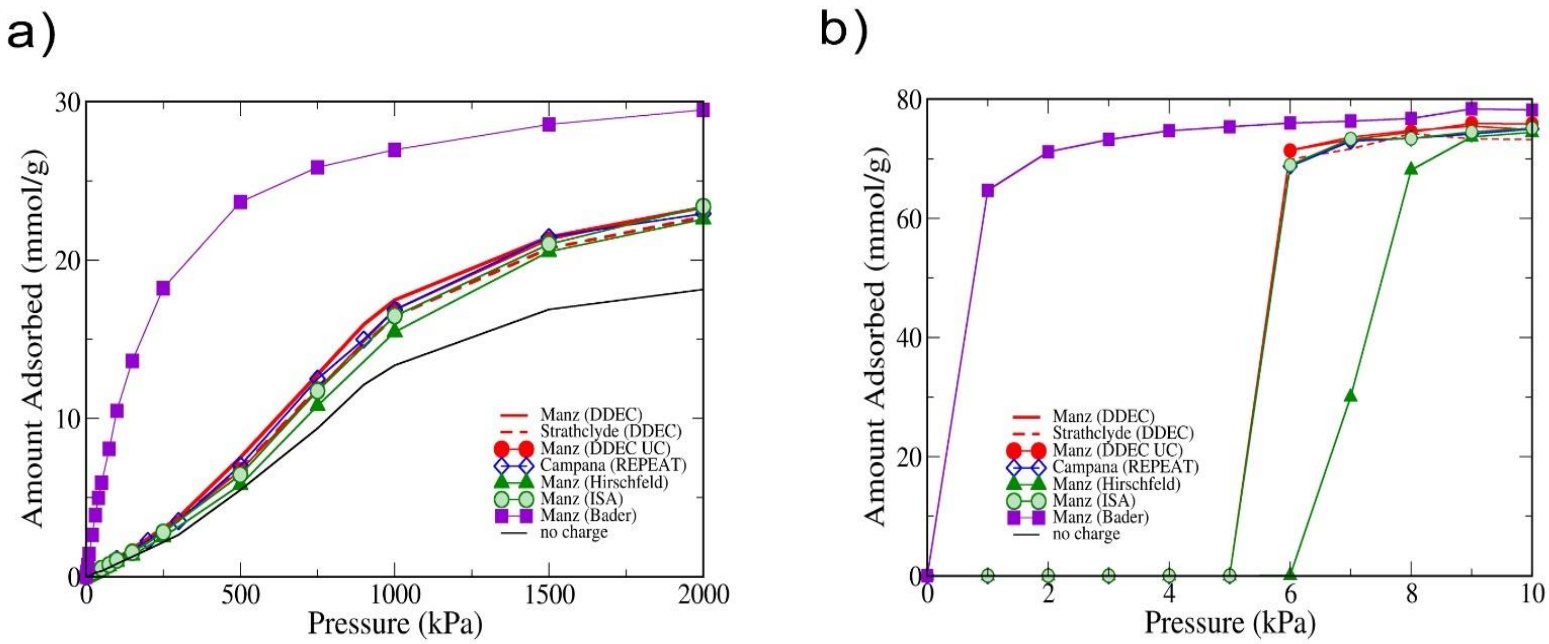

Figure 3.2 – Adsorption isotherms of: a) CO_2; b) water in IRMOF-1 at 298 K using point charge sets obtained by periodic methods. Isotherms calculated without any framework charges are shown as a black line (too low to be visible in the water plot). Error bars are the size of the symbols used.

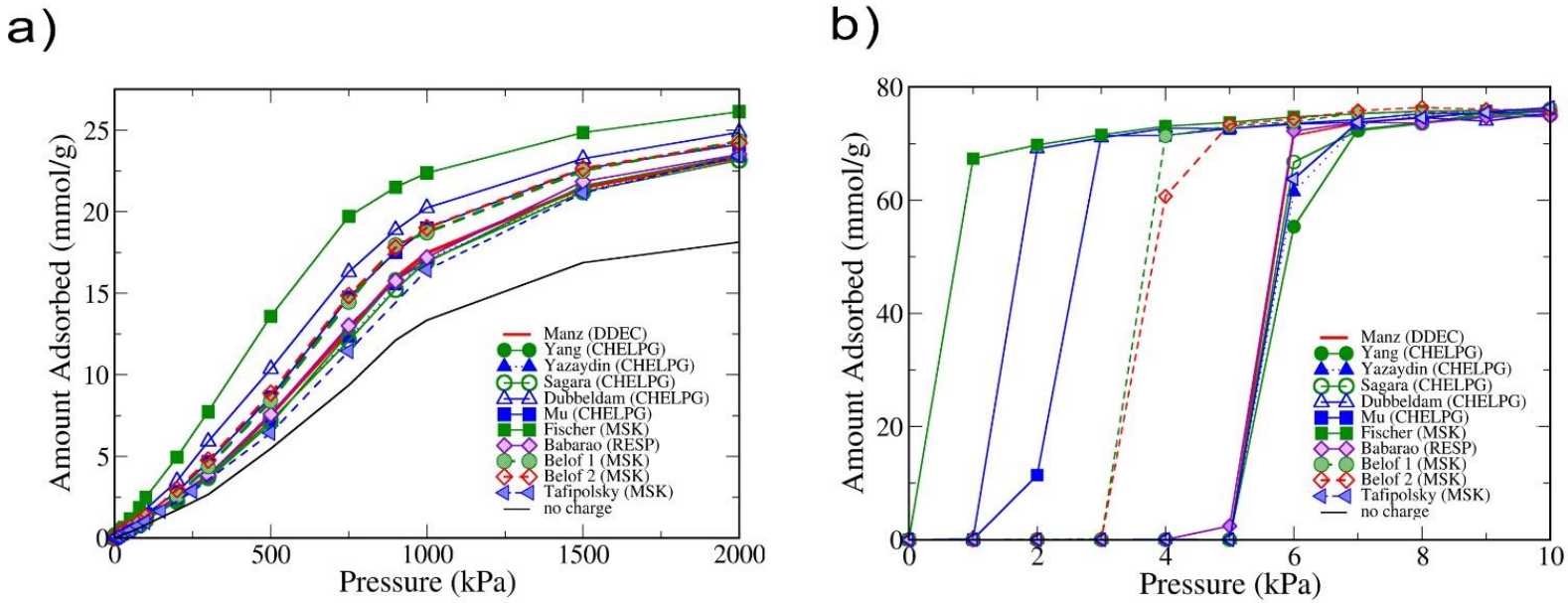

Figure 3.3 – Adsorption isotherms of: a) CO_2; b) water in IRMOF-1 at 298 K comparing DDEC point charges (thick red line) to charges obtained from QM cluster calculations. The charge calculation method for each set is reported in the legend. Isotherms calculated without any framework charges are shown as a black line (too low to be visible in the water plot). Error bars are the size of the symbols used.

Figure 3.3 compares framework point charges obtained by cluster methods, using periodic DDEC charges as reference. The two Belof charge sets use the same charge determination method and are both based on the same underlying Hartree-Fock calculation, but applied different basis sets. The fact that they produce very consistent results suggests that the basis set may not have a strong effect, at least with the MSK charge calculation method. Several data sets (e.g. most CHELPG sets) coalesce around the reference DDEC charges, yielding statistically indistinguishable isotherms for both water and CO_2, despite the fact that individual atomic point charges, such as on the Zn atom, vary greatly among them (see Table 3.3). This implies that the values of individual point charges are somewhat underdetermined, and that the important figure-of-merit for assessment of point charge sets should be how well they reproduce the underlying electrostatic potential. It also emphasises the usefulness of comparing point charge sets on the basis of adsorption isotherms, which is the ultimate goal of adsorption simulations, rather than focusing on the individual charges.

Four of the charge sets (Dubbeldam, Mu and the two Belof sets) lead to slightly stronger adsorption of CO_2, but these effects are magnified for water - as expected, the latter shows a more pronounced dependence on the electrostatic interactions. The Fischer charges produced the highest adsorption isotherms, and also showed the largest magnitude of charges on the aromatic ring atoms (see Table 3.3), possibly caused by over-polarization. CO_2 molecules adsorb quite strongly in the vicinity of the aromatic groups (see Figure 3.4), which means that this enhancement of electrostatic interactions leads directly to higher adsorbed amounts. In fact, when we plot the CO_2 adsorbed amount against the electrostatic component of the fluid-solid interaction energy for both periodic and cluster charge sets (see Figure 3.9), a linear relationship is observed, while the LJ component of the interaction energy is mostly the same (see Table 3.4). Overall, although most simulations using cluster-based framework charges lead to isotherms in agreement with periodic charges, the larger degree of variability observed in the cluster methods suggests that some degree of care should be taken when applying this approach to predict adsorption.

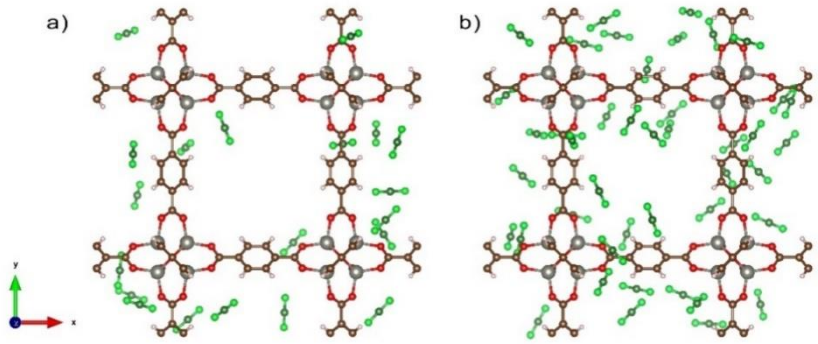

Figure 3.4 – A snapshot of CO_2 (green) adsorption in IRMOF-1 at 298 K and 250 kPa with a) DDEC and b) Fischer charges.

In Figure 3.5, we compare framework point charges obtained by semi-empirical methods, again using periodic DDEC charges from Manz and Sholl as a reference. The original Qeq method yields charges that lead to a significantly lower adsorption isotherm for CO_2, and hence are likely underestimating the electrostatic potential. Interestingly, however, the same effect is not manifested in the water adsorption isotherm, which agrees closely with the reference one. The precise reason for this is unclear at this point. The improved EQeq method of Wilmer et al., designed to reproduce QM charges in MOFs, yields isotherms in excellent agreement with the reference method. It is interesting to see, however, that an earlier version of EQeq actually leads to significantly higher adsorption than the reference isotherm. Finally, the CBAC method produces a CO_2 isotherm that is within statistical error of the DDEC isotherm, which is somewhat expected since this particular system was used as a test case for the development of the method. However, the CBAC water isotherm is significantly shifted to the left, emphasising that small differences in charges can lead to pronounced changes in adsorption of polar molecules. Due to the larger variability and uncertainty of these semi-empirical methods, care should be taken when accurate predictions of individual adsorption isotherms are required. However, they can provide quite useful alternatives to more computationally intensive methods for high-throughput screening of a large number of materials.

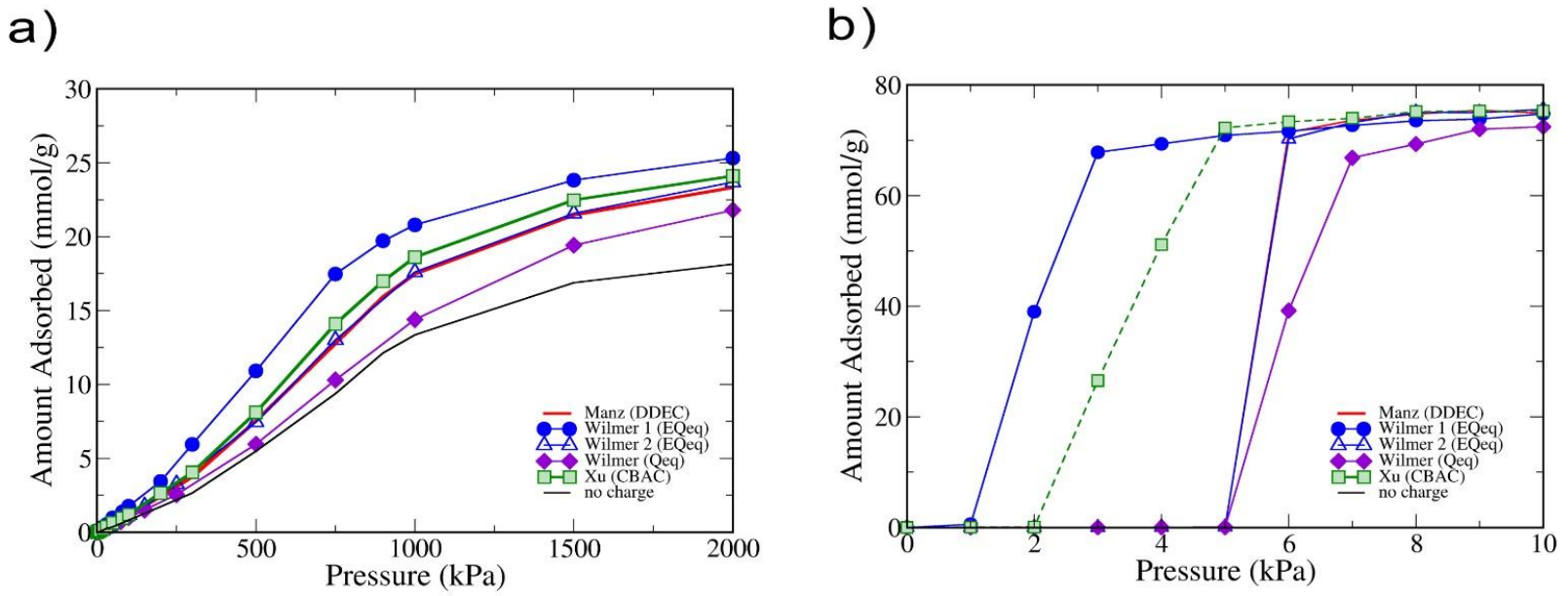

Figure 3.5 - Adsorption isotherms of: a) CO_2; b) water in IRMOF-1 at 298K comparing DDEC point charges to charges obtained by semi-empirical approaches. Isotherms calculated without any framework charges are shown as a black line (too low to be visible in the water plot). Error bars are the size of the symbols used.

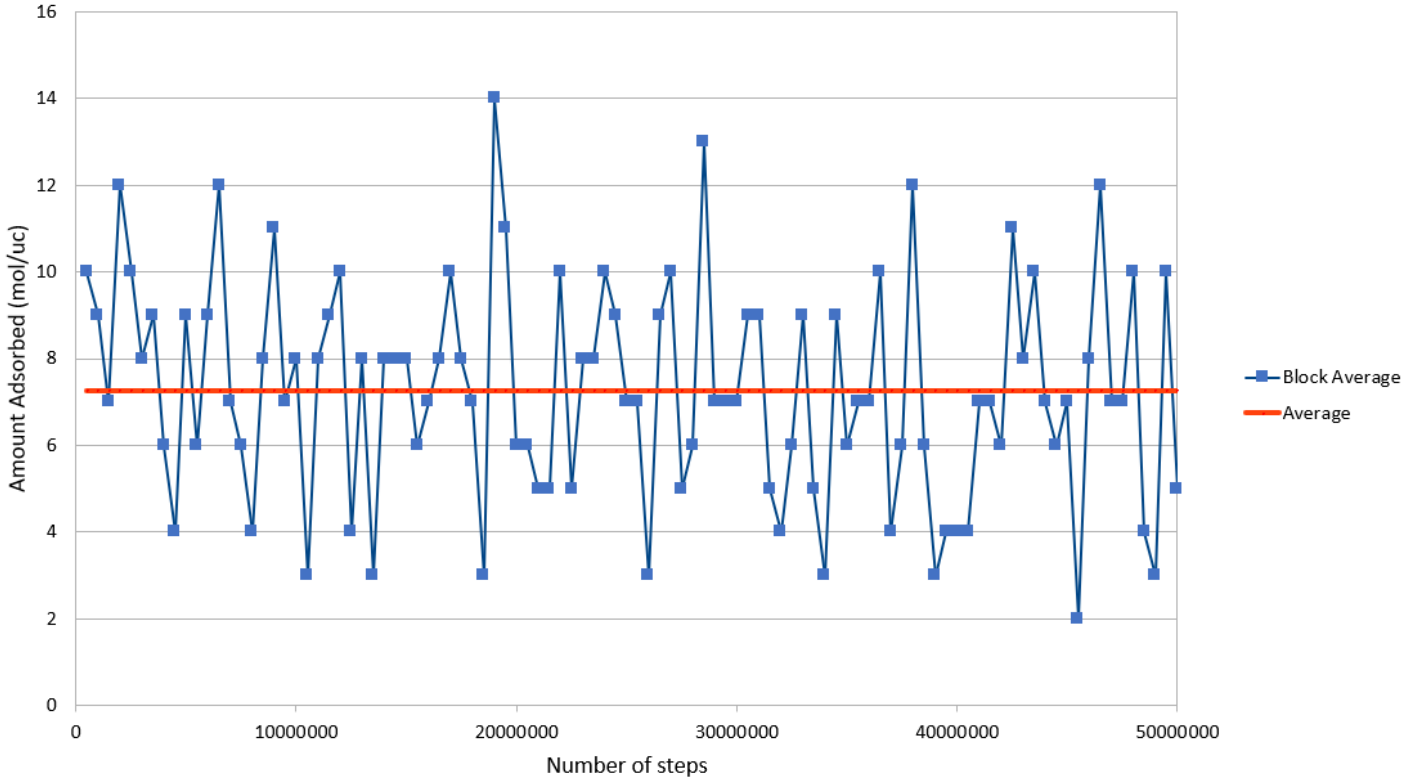

Figure 3.6 – Plot showing convergence of CO_2 adsorbed amount in IRMOF-1 at 298 K and 100 kPa compared with overall average. Only data beyond 20×10^6 steps was used for sampling.

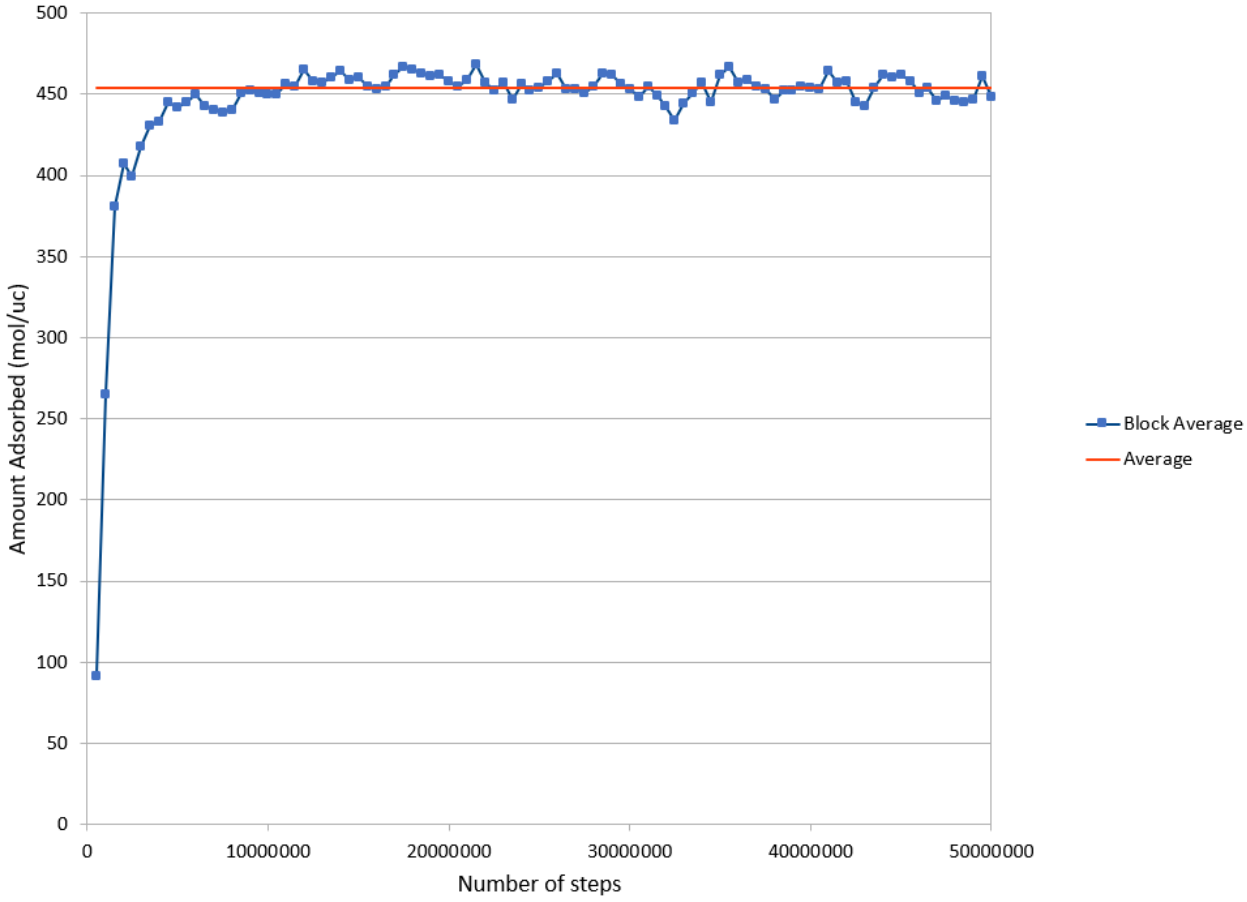

Figure 3.7 – Plot showing convergence of H_2O adsorbed amount in IRMOF-1 at 298 K and 300 kPa compared with overall average. Only data beyond 20×10^6 steps was used for sampling.

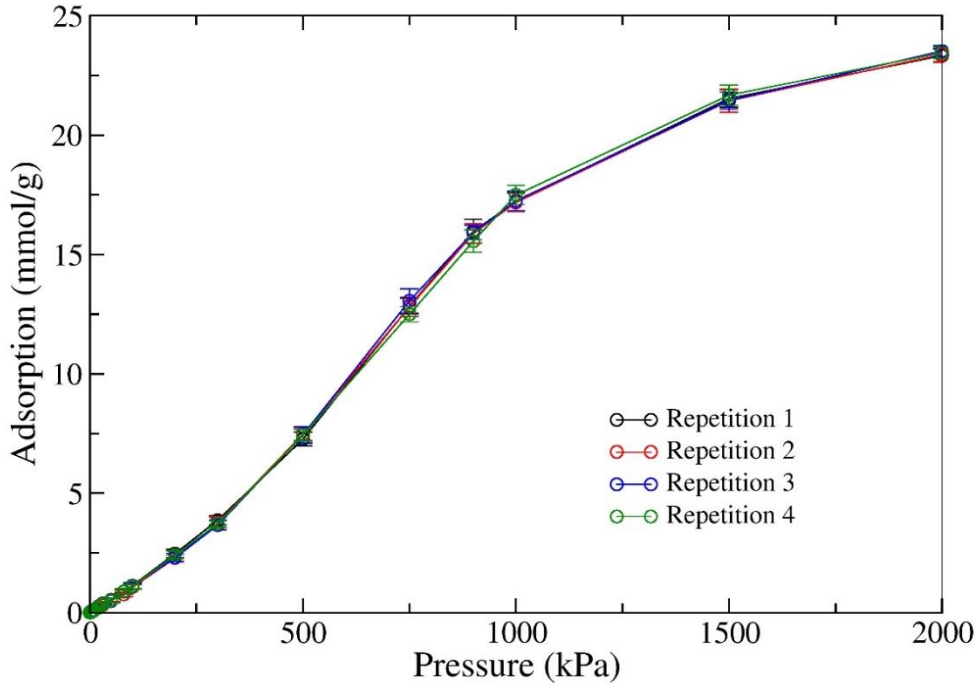

Figure 3.8 – Plot showing adsorption simulation repetitions of CO_2 in IRMOF-1 at 298 K using different random seeds. All repetitions are within statistical error of each other.

Table 3.4 – Energy decomposition (kJ/mol) and amount adsorbed (mol/kg) for adsorption of CO_2 in IRMOF-1 at 298K and 750 kPa using various charge sets and including the neutral framework.

Charge set	**E_{LJ}**	**E_q**	**N_{ads}**
No charge	-9.5055	0.0000	9.1702
Manz (DDEC)	-9.6230	-0.5679	12.0191
Campana (REPEAT)	-9.6770	-0.3896	11.2140
Manz (Hirshfeld)	-9.5591	-0.0404	10.7978
Manz (ISA)	-9.6097	-0.5535	11.7359
Sagara (CHELPG)	-9.7897	-0.3454	11.6510
Yang (CHELPG)	-9.7975	-0.4993	12.1300
Yazayidin 1 (CHELPG)	-9.8368	-0.4465	11.8160
Babarao (RESP)	-9.7855	-0.5951	13.0149
Dubbeldam (CHELPG)	-9.7157	-1.9726	16.3071
Fischer (MSK)	-9.5864	-3.1268	19.7159
Wilmer 1 (Eqeq)	-9.4035	-2.2139	17.4632
Xu (CBAC)	-9.4658	-1.0419	14.0952

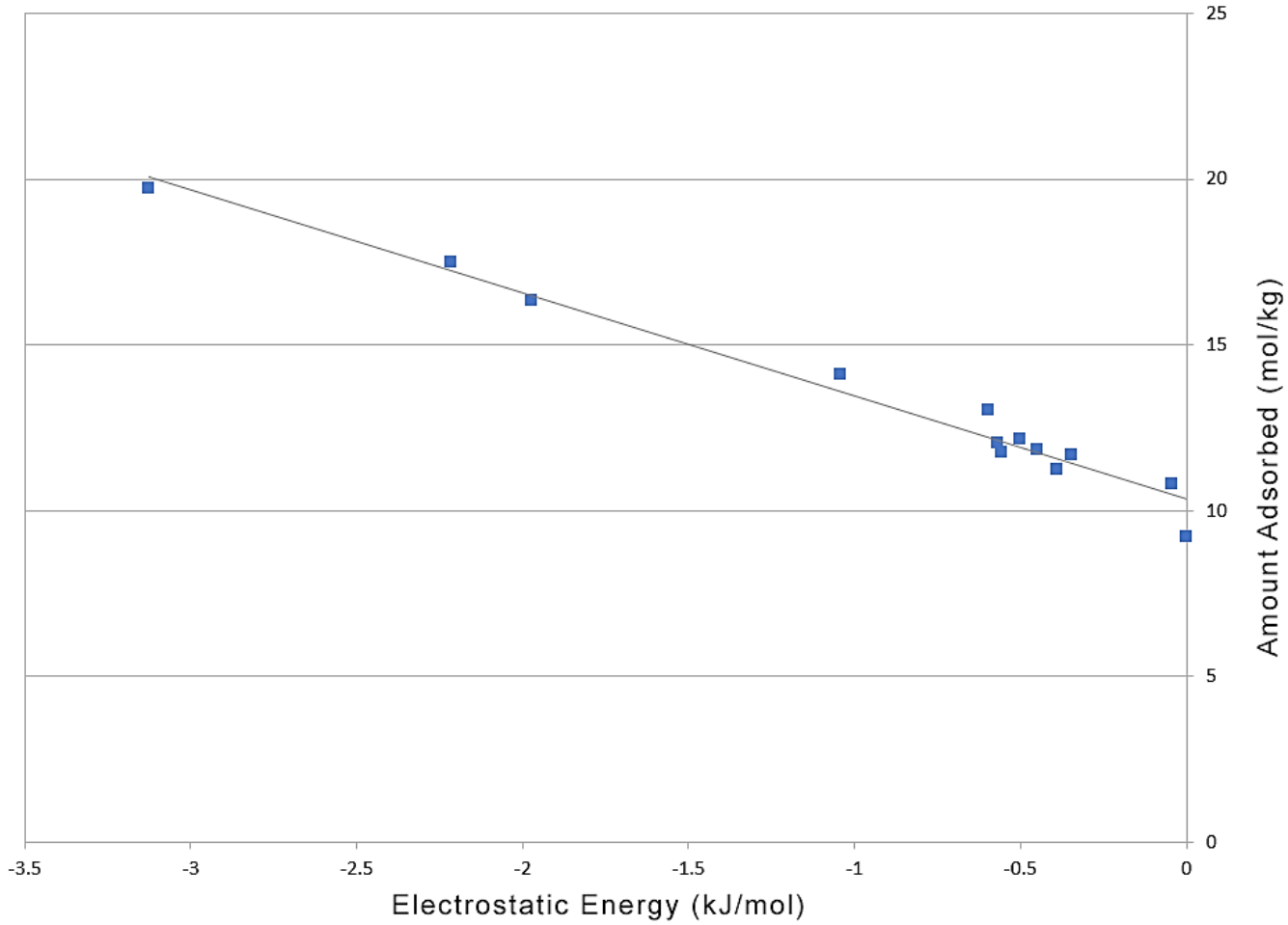

Figure 3.9 – Plot showing a linear increase of amount adsorbed as a function of electrostatic energy contribution for CO_2 in IRMOF-1 at 298 K and 750 kPa.

3.4.2 MIL-47

MIL-47 (Figure 3.10) is classed as a metal dicarboxylate. It forms a three-dimensional network consisting of chains of corner-sharing metal octahedra interlinked by benzene-dicarboxylate groups. Within this network there are one dimensional diamond-shaped pore tunnels. This material has been reported to have hydrophobic character and shows good water stability.[51]

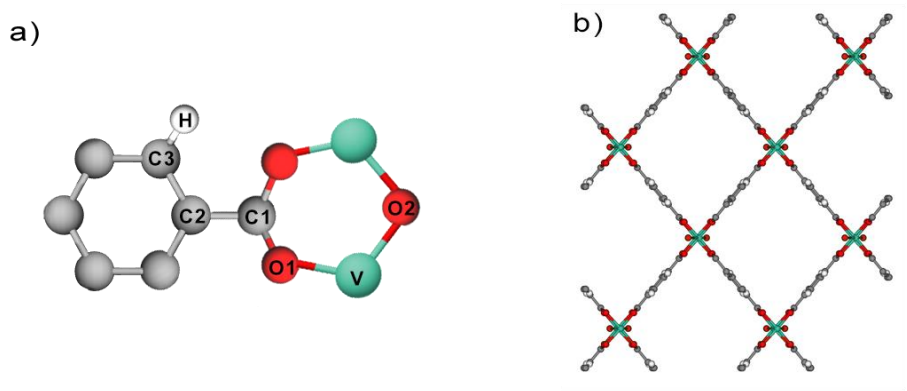

Figure 3.10 –a) MIL-47 building block showing the different uniquely charged atoms. The corresponding charges are listed in Table 3.5. b) MIL-47 framework structure

Several framework charge sets for MIL-47 obtained from literature reports are provided in Table 3.5. It is clear that the charges on the metal atom, which is only weakly exposed to adsorbate molecules, show the greatest degree of variation. Figure 3.11a shows adsorption isotherms for CO_2 and water in MIL-47 obtained using those point charge sets. As for IRMOF-1, most charge sets calculated from QM calculations, either cluster or periodic, yield CO_2 isotherms within statistical error of each other. In particular, the two sets of isotherms from periodic QM calculations show excellent consistency, despite variation in the values of the individual charges. The isotherm obtained with the EQeq method is slightly higher than the rest, which again suggests an inherent loss of accuracy in favour of computational speed. These differences are already statistically significant for CO_2 and are further amplified in the water isotherms (Figure 3.11b), with three of the charge sets now showing a somewhat larger difference relative to the reference case. All simulated isotherms show a characteristic sigmoidal shape, again reflecting the relatively hydrophobic nature of this material.

Table 3.5 - Charge sets for MIL-47calculated by different methods, obtained from literature sources

Charge Set	**Method**	**V**	**O1**	**O2**	**C1**	**C2**	**C3**	**H**
Nazarian et al. (2016)	DDEC	2.010	-0.657	-0.833	0.734	-0.118	-0.056	0.111
Finsyet al. (2009)	CHELPG	1.68	-0.52	-0.60	0.56	0.00	-0.15	0.12
Yazaydin et al. (2009) (1)	CHELPG	1.770	-0.611	-0.662	0.644	0.320	-0.153	0.149
Wilmer et al. (2012)	REPEAT	1.570	-0.533	-0.592	0.635	0.004	-0.136	0.153
Wilmer and Snurr (2011)	EQeq	1.377	-0.591	-0.701	0.689	0.059	-0.131	0.179
Ramsahye et al. (2007)	Mulliken	1.207	-0.496	-0.596	0.604	-0.071	-0.068	0.146
	Average	1.6023	-0.5680	-0.6640	0.6443	0.0323	-0.1157	0.1430
	Standard Deviation	0.2858	0.0617	0.0936	0.0614	0.1540	0.0426	0.0245

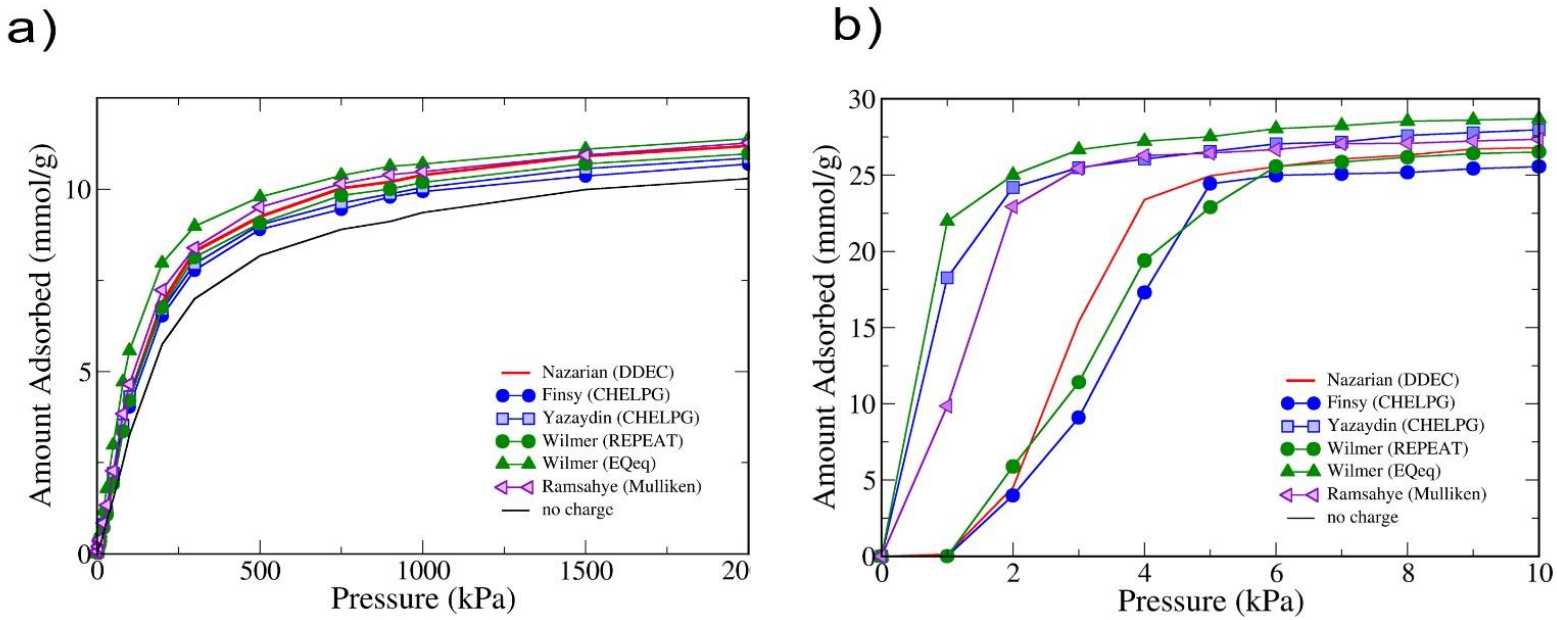

Figure 3.11 – Adsorption isotherms of: a) CO_2; b) water in MIL-47 at 298 K using different point charge sets for the framework atoms. Isotherms calculated without any framework charges are shown as a black line (too low to be visible in the water plot). Error bars are the size of the symbols used.

3.4.3 UiO-66

UiO-66, a zirconium-based MOF, consists of hexa-nuclear $Zr_6O_4(OH)_4$ inorganic nodes which form lattices via 1,4-benzene-dicarboxylate (BDC) linker, forming robust 3D structures (Figure 3.12). This MOF is characterised by a high surface area and very high thermal stability. The inorganic centre contains polar -OH groups and this is reported to be the reason for this MOF's exceptional stability, specifically its ability to undergo a reversible change from its hydroxylated structure to a dehydroxylated form without evoking any changes in the linked carboxylate ligands (Kandiah et al. 2010). DeCoste et al. (2013) investigated the water stability of carboxylate-containing MOFs, including CuBTC and Mg-MOF-74, and found that UiO-66 was the most water stable. This stability is likely to be the result of narrow pores and sterically hindered metal carboxylate sites, making these less accessible to water. The fully saturated metal centres don't have the ability to coordinate with other molecules, unlike structures with OMS. UiO-66 has been known for its tendency to contain a significant number of defects in the form of missing linkers, which would affect the adsorption properties considerably (Ghosh et al. 2014). In this work, a fully hydroxylated structure with no defects was used for simulation purposes, so as to more reliably assess the effect of framework point charges on adsorption isotherms.

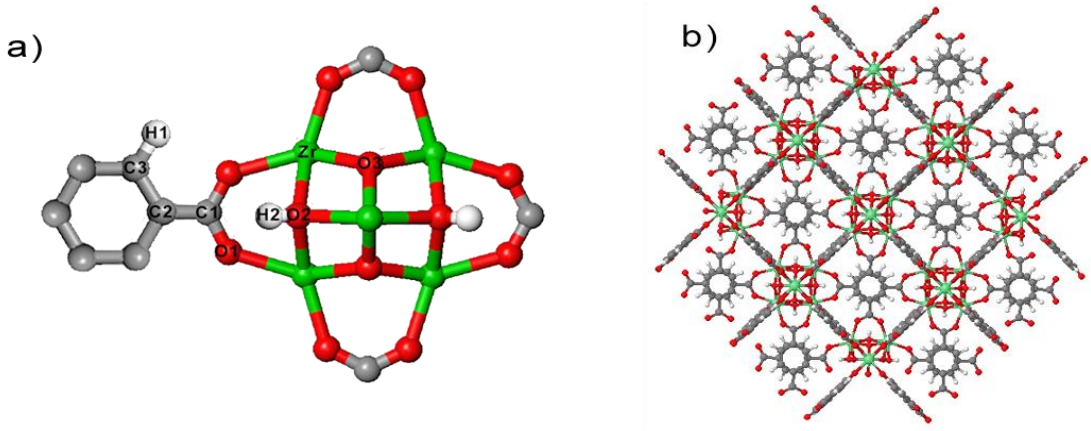

Figure 3.12 – a) UiO-66 building block showing the different uniquely charged atoms. The corresponding charges are listed in Table 3.6. b) UiO-66 framework structure

Table 3.6 - Charge sets for UiO-66 calculated by different methods, obtained from literature sources

Charge Set	**Method**	**Zr**	**O1**	**O2**	**O3**	**C1**	**C2**	**C3**	**H1**	**H2**
Nazarian et al. (2016)	DDEC	2.5730	-0.6761	-1.2300	-1.2370	0.7470	-0.1040	-0.0760	0.1180	0.4810
Wu et al. (2012)	CBAC	2.2576	-0.6324	-1.3024	-1.1494	0.8046	0.0486	-0.1314	0.1076	0.4426
Yang et al. (2011)	CHELPG	2.008	-0.582	-1.179	-0.741	0.625	-0.002	-0.121	0.127	0.495
Ghosh et al. (2014)	REPEAT	2.4490	-0.6983	-1.4330	-0.7187	0.7623	0.0430	-0.1599	0.1460	0.4380
	Average	2.3219	-0.6472	-1.2861	-0.961525	0.7347	-0.004	-0.1221	0.1247	0.4642
	Standard Deviation	0.2462	0.0514	0.1102	0.2700	0.0771	0.0707	0.0348	0.0163	0.0282

We were only able to identify four distinct sets of framework point charges for this MOF in literature (see Table 3.6), but these span all classes of charge calculation methods (semi-empirical, periodic QM-based and cluster QM-based). As for the two previous MOFs under study, the greatest variability in charge values is observed on the buried Zr and O3 atoms, with more exposed atoms exhibiting more consistent charge values. Predicted CO_2 isotherms (Figure 3.13a) are mostly self-consistent with the exception of the CBAC charge set, which shows somewhat lower uptake than the remaining isotherms. The other three isotherms are statistically indistinguishable. Greater variation is seen in the water adsorption isotherms (Figure 13b). Although the three QM-based isotherms show the same sigmoid shape and only slight variations in amount adsorbed, the CBAC isotherm shows a strangely high uptake at low pressure. Interestingly, while the CO_2 isotherm computed without framework charges shows only slightly lower adsorption than the reference DDEC isotherm, it very strongly underestimates water adsorption in the entire pressure range. Once again, this is caused by the pronounced sensitivity of water to details of the electrostatic interactions with the MOF framework.

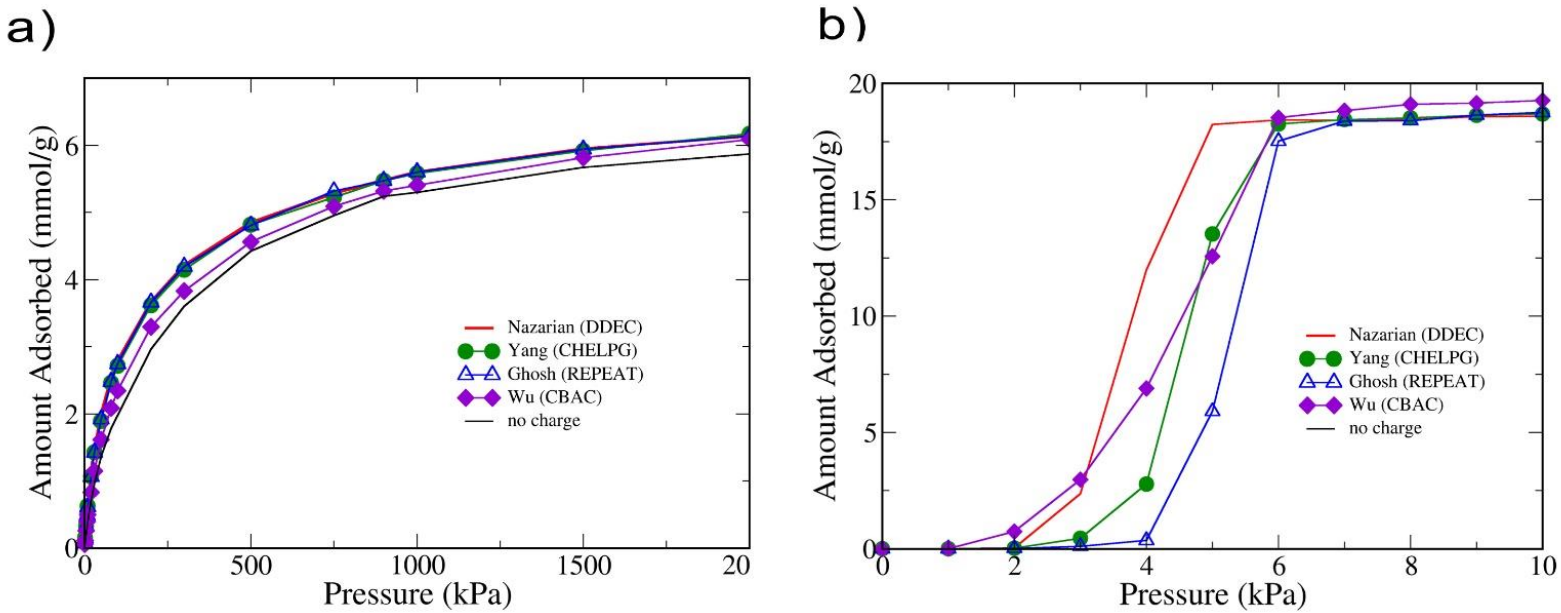

Figure 3.13 – Adsorption isotherms of: a) CO_2; b) water in UiO-66 at 298 K using different point charge sets for the framework atoms. Isotherms calculated without any framework charges are shown as a black line (too low to be visible in the water plot). Error bars are the size of the symbols used.

3.4.4. CuBTC

CuBTC (also known as MOF-199 and HKUST-1) was first discovered by researchers at the Hong Kong University of Science and Technology in 1999 (Figure 3.14) (Chui et al. 1999). It is sold commercially as Basolite C300 and it is one of the most frequently studied MOFs (Moghadam et al. 2017). CuBTC consists of central copper ions linked with 1,3,5-benzenetricarboxylate (BTC) acid ligands. These linkages form a porous crystalline structure with two central copper ions which are bound to 4 BTC ligands via 2 oxygens on each ligand and to solvent (usually water) via 2 oxygens. Activation of CuBTC results in removal of solvent molecules and leaves two coordinatively unsaturated copper ions with available binding sites. The copper ions form open metal sites where the metal atom is exposed, and these sites have a high affinity and selectivity for electron-donating adsorbates. Consequently, CuBTC has a high affinity for water and will readily adsorb moisture (Castillo et al. 2008).

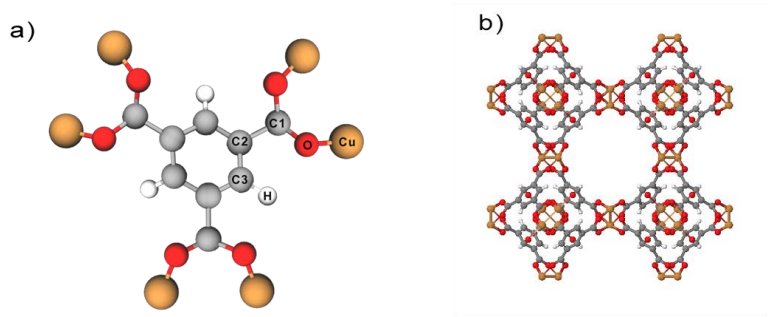

Figure 3.14 – a) CuBTC building block showing the different uniquely charged atoms. The corresponding charges are listed in Table 3.7. b) activated CuBTC framework structure.

Due to the large number of studies carried out on CuBTC, several distinct framework charge sets could be obtained from literature, as shown in Table 3.7. It is interesting to see that in this case, the charge variability is practically uniform among all atoms of the framework. This is because there are no buried atoms in CuBTC, and even the metal sites are exposed to the surface, hence they all contribute significantly to the electrostatic potential. Nevertheless, as we will see below, the observed variation in the charge magnitude at the OMS is likely to have a pronounced effect on adsorption in this MOF.

Table 3.7 - Charge sets for CuBTC calculated by different methods, obtained from literature sources

Charge Set	**Method**	**Cu**	**O**	**C1**	**C2**	**C3**	**H**
Nazarian et al. (2016)	DDEC	0.920	-0.567	0.691	-0.164	0.031	0.117
Zang et al. (2013)	DDEC	0.8682	-0.5436	0.6500	-0.0079	-0.1229	0.1339
Wilmer et al. (2012)	REPEAT	0.940	-0.572	0.704	-0.088	-0.073	0.131
Wilmer and Snurr (2011)	EQeq	0.86	-0.59	0.6	-0.04	-0.06	0.25
Huang et al. (2012)	CBAC	1.065	-0.652	0.792	0.036	-0.148	0.094
Castillo et al. (2008)	Empirical (set IV)	1.248	-0.624	0.494	0.130	-0.150	0.156
Liu et al. (2009) (1)	CHELPG	1.105	-0.659	0.937	-0.320	0.000	0.150
Liu et al. (2009) (2)	CHELPG	1.082	-0.725	0.824	-0.061	-0.004	0.153
Yang and Zhong (2006)	CHELPG	1.098	-0.665	0.778	-0.092	-0.014	0.109
Yazaydin et al. (2009) (1)	CHELPG	1.000	-0.587	0.680	-0.033	-0.110	0.137
Yazaydin et al. (2009) (2)	CHELPG	1.130	-0.645	0.741	-0.070	-0.091	0.145
Babarao et al. (2009)	MSK	1.026	-0.671	0.879	-0.197	0.028	0.123
Fischer et al. (2009)	MSK	1.030	-0.574	0.573	0.215	-0.364	0.209
	Average	1.0286	-0.6211	0.7187	-0.0532	-0.0829	0.1468
	Standard Deviation	0.1110	0.0531	0.1248	0.1364	0.1056	0.0417

As for IRMOF-1, due to the large number of charge sets considered, we have opted to split the comparison in two groups (a single plot showing all isotherms is available in Figure 3.21a). In Figure 3.15 we collect isotherms obtained with periodic QM charges and with semi-empirical charges, while in Figure 3.16 we compare isotherms obtained with cluster QM charges. For CO_2 (Figures 3.15a and 3.16a) all the QM-based charge sets (both periodic and cluster) yield adsorption isotherms in good statistical agreement with each other, with a variability that is certainly well within the observed uncertainty in experimental isotherms reported by Park et al (2017). The EQeq charges also produce an isotherm in agreement with the QM-based ones. However, the CBAC method and the empirically adjusted Castillo charges lead to a statistically significant increase in adsorbed amounts, albeit not by a large extent. In water adsorption (Figures 3.15b and 3.16b), the variation in adsorption isotherms is much more significant. As for the previous MOFs, the isotherms based on periodic QM charges are still in agreement with each other, reinforcing the consistency of this charge determination approach, even for MOFs with OMS. The QM cluster-based isotherms show a much more significant degree of variability, with two of the charge sets leading to a two-fold decrease in the pressure at the isotherm inflection point (from ~3 to ~1.5 kPa). The semi-empirical sets also show rather extreme differences from the reference periodic calculations, even for the EQeq charges, which had yielded CO_2 isotherms in good agreement with DDEC.

The large variety of water adsorption isotherms indicates that the adsorption process of water in CuBTC is different from that of CO_2, which could be due to the large dipole moment of water molecule, as opposed to CO_2 which has only a permanent quadrupole, as well as due to specific interactions with the open Cu site. In fact, one can observe a broad correlation between the steepness of the slope of the water isotherms at low pressure and the point charge on the Cu atom (see Table 3.5). For example, the highest Cu charge of +1.25 is in the Castillo set, which shows one of the strongest water adsorption isotherms. There follows a large group of isotherms with relatively high slopes and Cu charges between +1 and +1.1; finally, the periodic sets of Nazarian, Wilmer and Zang have the smallest slopes and Cu charges around +0.9. The correlation is not perfect, however, with the Yazaydin1 set showing a steep slope and relatively low Cu charge, while the Yazaydin2 set has a relatively smaller slope and a higher Cu charge. Nevertheless, the sensitivity of water adsorption at low pressure on the Cu point charge indicates that the presence of OMS plays a key role in the water adsorption behaviour. This suggests that great care must be taken when selecting framework point charges for simulating adsorption of strongly polar molecules such as

water in MOFs with open metal sites. In this context, it is worth noting that the Castillo charges were specifically designed to match available water adsorption data on CuBTC, yet yield isotherms for both water and CO_2 that are not consistent with QM-based approaches. The same could be said, to some extent, of the CBAC charge set, which attempts to empirically account for the OMS interaction and incorporate it in the charges, resulting in over-polarization and increased adsorption prediction. Based on previous work on MOFs with OMS, a more physically-grounded approach would involve using consistent QM-based charges while separately treating the specific interactions between water and the metal site through a bespoke interaction model (Campbell et al. 2018; Campbell et al. 2017; Fischer et al. 2012; Fischer et al. 2014)

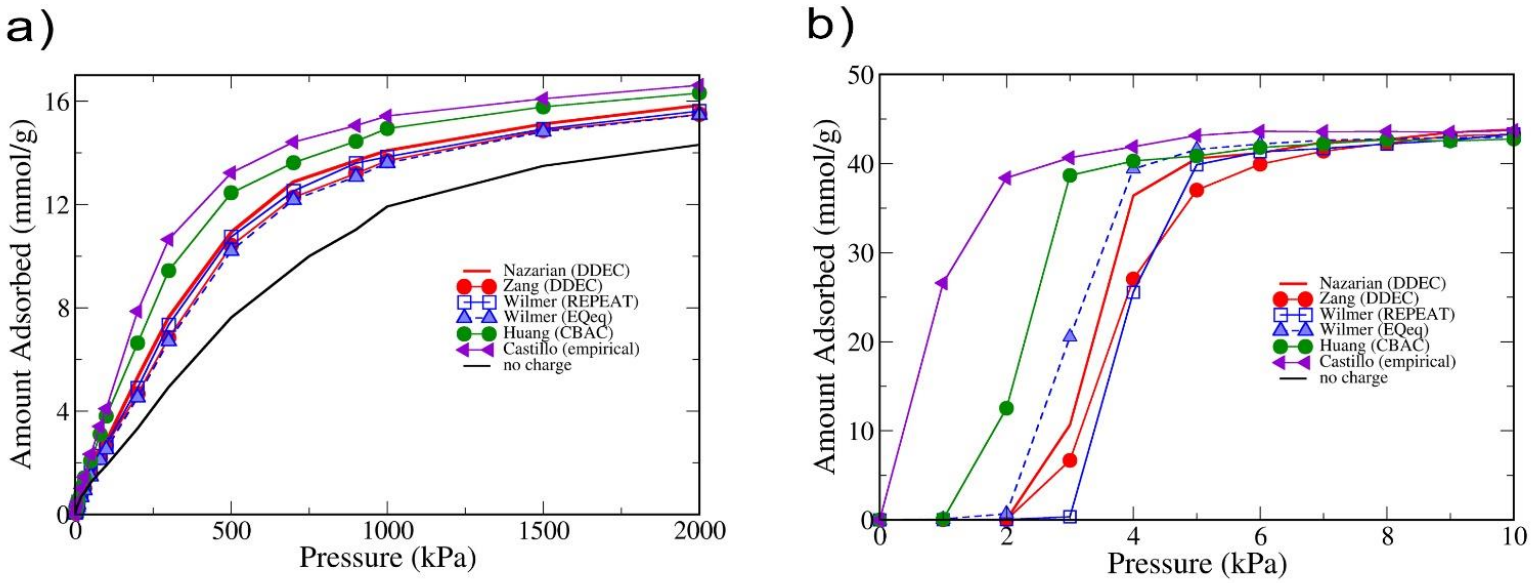

Figure 3.15– Adsorption isotherms of: a) CO_2; b) water in CuBTC at 298 K using point charge sets obtained by periodic QM and semi-empirical methods. Isotherms calculated without any framework charges are shown as a black line (too low to be visible in the water plot). Error bars are the size of the symbols used.

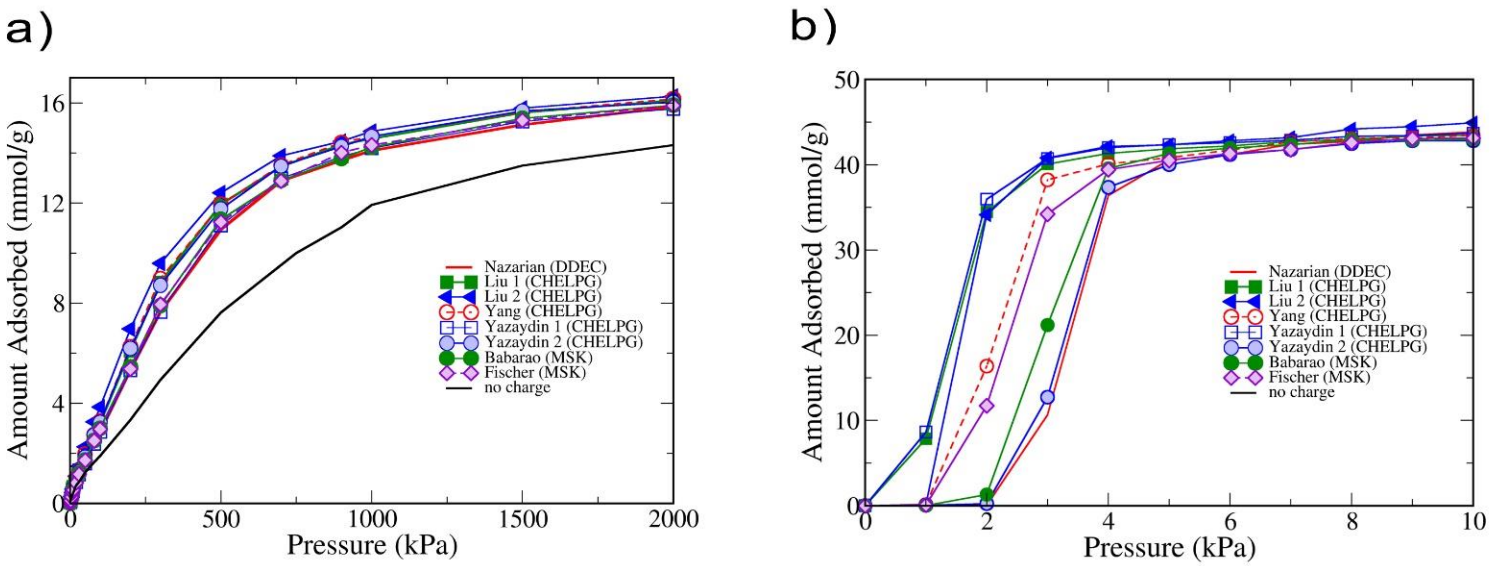

Figure 3.16 - Adsorption isotherms of: a) CO_2; b) water in CuBTC at 298 K comparing DDEC point charges to charges obtained by cluster methods. Isotherms calculated without any framework charges are shown as a black line (too low to be visible in the water plot). Error bars are the size of the symbols used.

3.4.5 Co-MOF-74

Co-MOF-74 (Figure 3.17) belongs to a family of MOFs designated as M-MOF-74 (M = Zn, Ni, Co, Fe, Mg, Mn, Ca, or Sr). It consists of 5-coordinated metal ions linked to 2,5-dioxoterephthalate, forming wide 1-dimensional hexagonal pores around 1.1 nm in diameter. This MOF contains a high concentration of OMS that are formed upon removal of the solvent molecules attached to the metal. Co-MOF-74 and its analogues have been reported to have very low water stability, with their structure degrading after exposure to even small amounts of moisture (DeCoste et al. 2013).

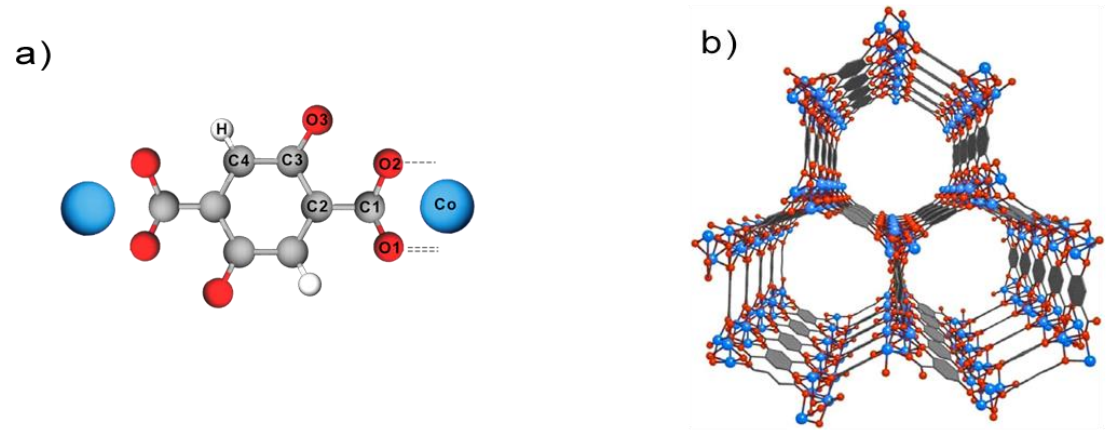

Figure 3.17 – a) Co-MOF-74 building block showing the different uniquely charged atoms. The corresponding charges are listed in Table 3.8. b) Co-MOF-74 framework structure

Six distinct framework point charge sets for this MOF were gathered from literature reports (Table 3.8). Most charges show relatively low variability, with the exception of Co. In fact, comparing with CuBTC (Table 3.7), for which many more data sets were available, the fluctuations in the charge of the unsaturated metal are quite significant for Co-MOF-74. It should be noted, however, that this is mainly due to the unphysically low charge produced by the EQeq method, as well as the rather large charge from LoProp (for which no data was found on CuBTC).

Table 3.8 - Charge sets for Co-MOF-74calculated by different methods, obtained from literature sources

Charge Set	**Method**	**Co**	**O1**	**O2**	**O3**	**C1**	**C2**	**C3**	**C4**	**H**
Haldoupis et al. (2015)	DDEC	1.165	-0.702	-0.617	-0.715	0.760	-0.237	0.381	-0.175	0.141
Yazaydin (2009)	CHELPG	1.139	-0.684	-0.645	-0.731	0.832	-0.292	0.315	-0.110	0.176
Haldoupis et al. (2015)	LoProp	1.4753	-0.7493	-0.6876	-0.8359	0.6104	-0.1258	0.2245	-0.1772	0.2657
Wilmer and Snurr (2011)	EQeq	0.164	-0.532	-0.473	-0.586	0.423	-0.180	0.209	-0.108	0.083
Wilmer et al. (2012)	REPEAT	1.066	-0.648	-0.626	-0.676	0.848	-0.340	0.309	-0.087	0.157
Mercado et al. (2016)	REPEAT	1.189	-0.720	-0.696	-0.785	0.846	-0.308	0.391	-0.177	0.177
	Average	1.0331	-0.6726	-0.6241	-0.7215	0.7199	-0.2471	0.3049	-0.1390	0.1666
	Standard deviation	0.4483	0.0768	0.0807	0.0868	0.1712	0.0821	0.0761	0.0417	0.0596

Figure 3.18 shows simulated adsorption isotherms on Co-MOF-74 using different framework point charge sets. The point charges obtained from the LoProp method carry the highest charge on the metal centre and hydrogen, and the lowest charge on most of the other atoms. In both CO_2 (Figure 3.18a) and water (Figure 3.18b), this isotherm deviates the most from the rest and predicts the highest uptake. Conversely, the EQeq method has by far the lowest charge on the metal, but strangely this does not seem to significantly affect the uptake of both gases. This suggests that the charge magnitude on the metal site has a less pronounced effect on adsorption than observed above for CuBTC. Unlike the rest of the studied MOFs, the type V isotherm due to weak water-adsorbent interactions is not observed here. This is likely to result from the high concentration of OMS pointed directly into the pore channel of Co-MOF-74, facilitating the interaction between these sites and the water molecules. Finally, it is important to note that once again most of the QM-based charge sets, perhaps with the exception of LoProp as discussed above, lead to consistent isotherms for both gases.

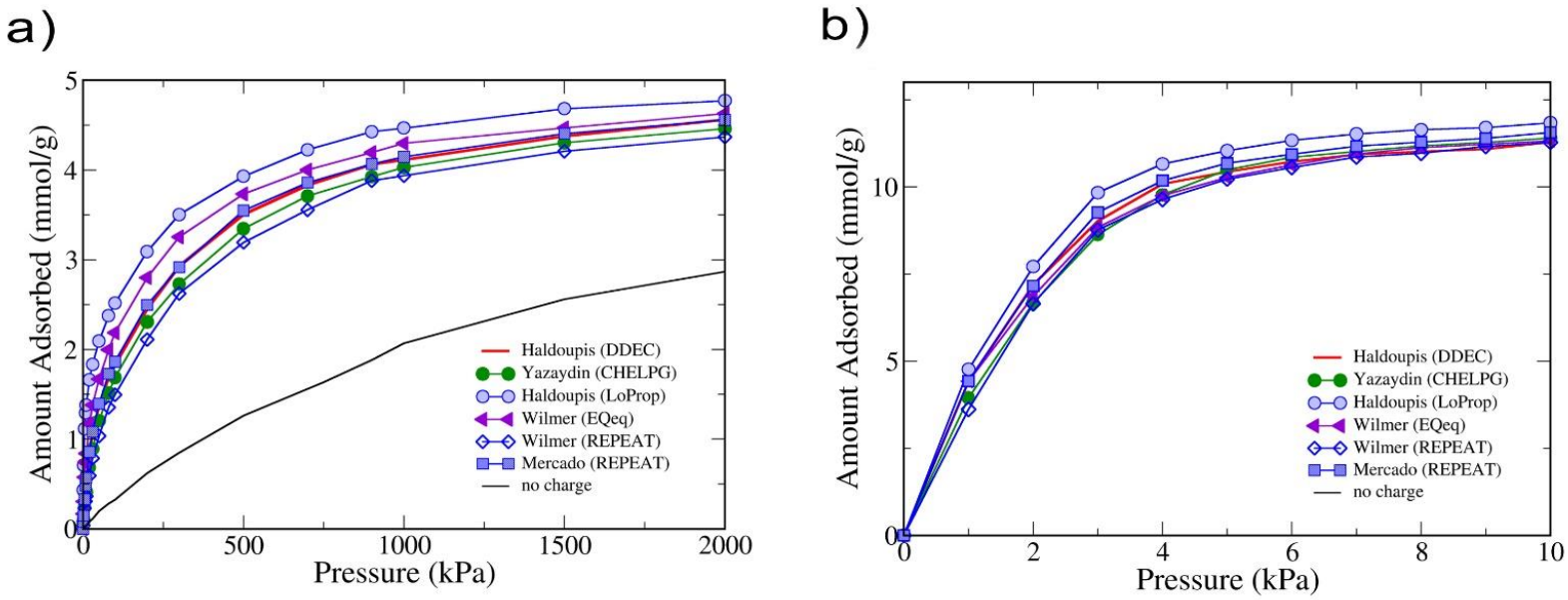

Figure 3.18 – Adsorption isotherms of: a) CO_2; b) water in Co-MOF-74 at 298 K using different point charge sets for the framework atoms. Isotherms calculated without any framework charges are shown as a black line (too low to be visible in the water plot). Error bars are the size of the symbols used.

3.4.6 SIFSIX-2-Cu-I

This MOF belongs to the SIFSIX family and consists of a copper centre and two different ligands, one organic linked to the metal via a nitrogen atom, the other based on silicon surrounded by six fluorine atoms (Figure 3.19). MOFs of this family have orthorhombic unit cells and are prone to interpenetration. In fact, we focused specifically on an interpenetrated member of this family, in order to assess the impact of this feature on the electrostatic interactions.

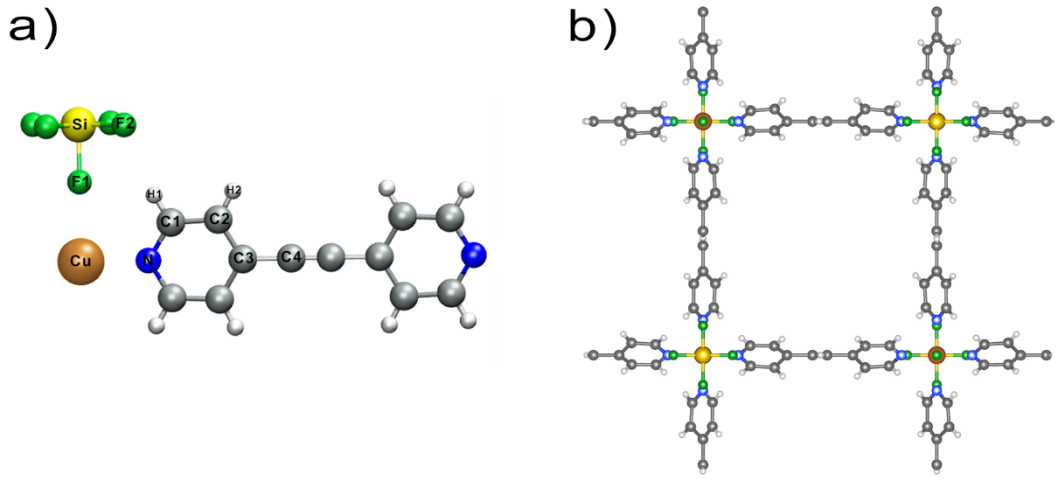

Figure 3.19 – a) Sifsix-2-Cu-I building block showing the different uniquely charged atoms. The corresponding charges are listed in Table 3.7. b) Sifsix-2-Cu-I framework structure.

For this MOF, to the best of our knowledge only one published charge set was available, from Pham et al. (2013). As such, we calculated several sets of framework point charges from both cluster and periodic QM calculations, as described in section 2.3 and A.1. The full sets of charges are provided in Table 3.9. As observed for other MOFs, the largest variation in charge values is for the buried Cu and Si atoms, which are both fully coordinated and barely accessible to adsorbate molecules.

Table 3.9 - Different charge sets for Sifsix-2-Cu-I calculated using different methods. All charge sets were calculated in this work except the first row in the table, which was obtained from the work of Pham et al. (2013)

Charge Set	**Cu**	**Si**	**N**	**F1**	**F2**	**C1**	**H1**	**C2**	**H2**	**C3**	**C4**
Pham (CHELPG)	0.286	1.748	-0.060	-0.537	-0.566	0.142	0.155	-0.324	0.175	0.251	-0.160
DDEC CP2K	0.770	1.923	-0.211	-0.580	-0.594	0.077	0.136	-0.203	0.158	0.160	-0.075
REPEAT VASP	-0.162	2.070	0.148	-0.523	-0.634	-0.019	0.163	-0.288	0.194	0.317	-0.147
DDEC VASP	0.760	1.855	-0.209	-0.568	-0.581	0.073	0.137	-0.199	0.157	0.167	-0.082
CHELPG (Clusters)	0.7742	2.8916	-0.3288	-0.4753	-0.7022	0.2313	0.0044	-0.3291	0.1620	0.3734	-0.1584
DDEC (Clusters)	0.9690	2.0139	-0.2445	-0.6465	-0.6342	0.1058	0.1042	-0.1603	0.1332	0.1834	-0.0930
Average	0.5662	2.0836	-0.1509	-0.5550	-0.6186	0.1017	0.1166	-0.2506	0.1632	0.2420	-0.1192
Standard Deviation	0.4227	0.4120	0.1703	0.0581	0.0495	0.0830	0.0586	0.0722	0.0203	0.0880	0.0400

Adsorption isotherms of CO_2 on SIFSIX MOF are reported in Figure 3.20. The first observation to make is that, as was observed in all the other MOF structures studied in this chapter, all isotherms calculated using periodic QM charges are consistent with each other, despite the fact that the charges themselves show significant fluctuations. This observation is independent of the charge determination method (e.g. compare REPEAT VASP and DDEC VASP, which were both obtained from the same underlying QM calculation) and of the type of basis set employed (e.g. DDEC VASP used plane waves while DDEC CP2K used Gaussian plus plane waves). The framework charges extracted from cluster calculations by Pham et al. show substantially lower adsorption isotherms than any of the periodic charge sets. Our own cluster-based charges, obtained from rather large molecular fragments using two different charge determination methods, yield isotherms that are on either side of the periodic ones, albeit much closer than the isotherm obtained from Pham charges. These differences are larger than the statistical error of the simulations. This reinforces the earlier observations that cluster-based charges lead to much more significant variations in adsorbed amounts, and care should be taken when applying them directly without any prior consistency check. In this context, the very good agreement between simulations and experiments observed in the work of Pham et al. (2013) appears rather fortuitous. A more detailed analysis is needed to clarify this issue, but the fact that this particular MOF has very narrow pore spaces (due to interpenetration) could mean that strong adsorption sites become much more sensitive to details of the electrostatic potential energy surface.

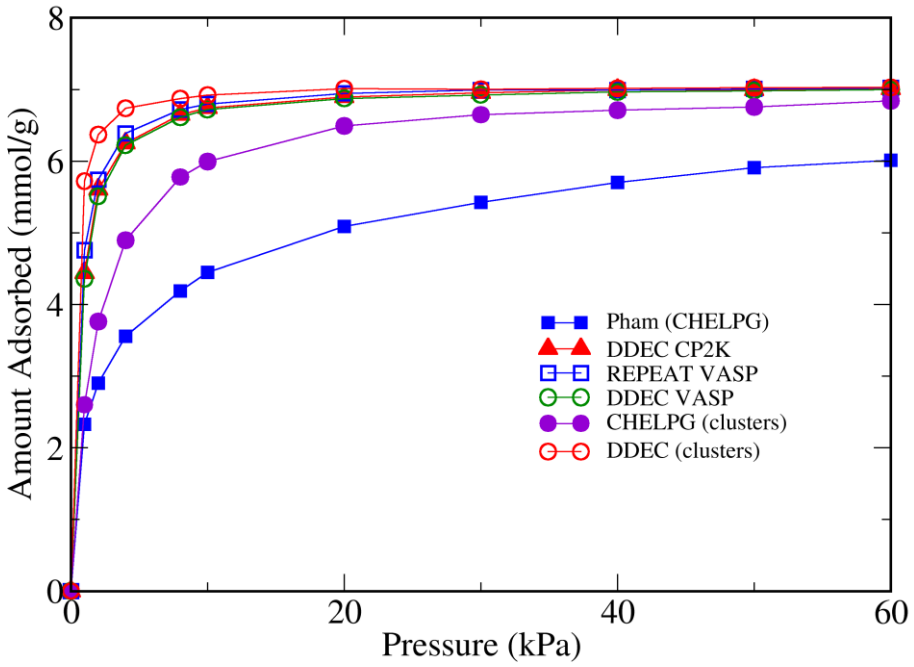

Figure 3.20 – Adsorption isotherms of CO_2 in Sifsix-2-Cu-I at 273 K using different point charge sets for the framework atoms. Error bars are the size of the symbols used.

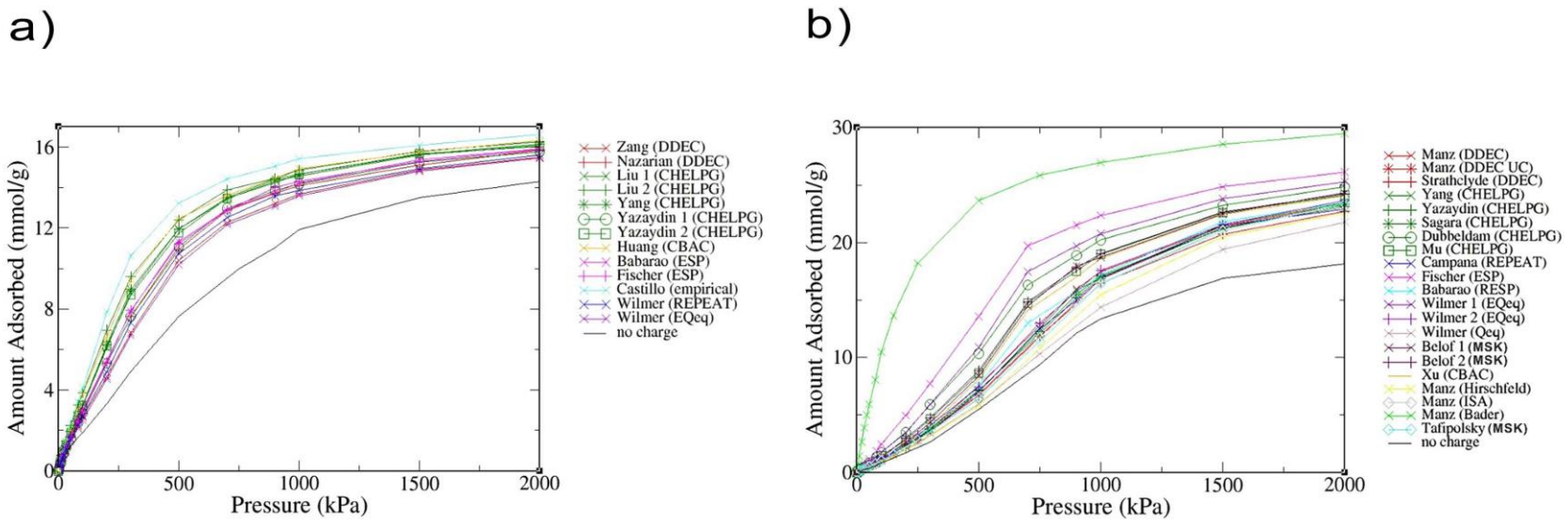

Figure 3.21 – Plot of all point charge set isotherms for CO_2 at 298 K in CuBTC(a) and IRMOF-1(b).

References

Allen, M.P., Tildesley, D.J.: Computer simulation of liquids. Clarendon Press, Oxford (1986)

Babarao, R., Hu, Z., Jiang, J., Chempath, S., Sandler, S.: Storage and Separation of CO_2 and CH_4 in Silicalite, C168 Schwarzite, and IRMOF-1: A Comparative Study from Monte Carlo Simulation. Langmuir 23, 659-666 (2007)

Babarao, R., Jiang, J., Sandler, S.: Molecular Simulations for Adsorptive Separation of CO_2/CH_4 Mixture in Metal-Exposed, Catenated, and Charged Metal−Organic Frameworks. Langmuir 25, 6590-6590 (2009)

Babarao, R., Dai, S., Jiang, D.: Effect of Pore Topology and Accessibility on Gas Adsorption Capacity in Zeolitic−Imidazolate Frameworks: Bringing Molecular Simulation Close to Experiment. J. Phys. Chem. C 115, 8126-8135 (2011)

Bader, R. F. W.: Molecular Fragments or Chemical Bonds? Acc. Chem. Res. 8, 34-40(1975)

Barthelet, K., Marrot, J., Riou, D., Férey, G.: A Breathing Hybrid Organic-Inorganic Solid with Very Large Pores and High Magnetic Characteristics. Angew. Chem. Int. Ed. 114, 291-294 (2002)

Bayly, C., Cieplak, P., Cornell, W., Kollman, P.: A well-behaved electrostatic potential based method using charge restraints for deriving atomic charges: the RESP model. J. Phys. Chem. 97, 10269-10280 (1993)

Belof, J., Stern, A., Space, B.: A Predictive Model of Hydrogen Sorption for Metal−Organic Materials. J. Phys. Chem. 113, 9316-9320 (2009)

Berendsen, H., Grigera, J., Straatsma, T.: The missing term in effective pair potentials. J. Phys. Chem. 91,.6269-6271 (1987)

Borycz, J., Tiana, D., Haldoupis, E., Sung, J., Farha, O., Siepmann, J., Gagliardi, L.: CO_2 Adsorption in M-IRMOF-10 (M = Mg, Ca, Fe, Cu, Zn, Ge, Sr, Cd, Sn, Ba). J. Phys. Chem. C 120,12819-12830 (2016)

Breneman, C. M.; Wiberg, K. B.: Determining atom-centered monopoles from molecular electrostatic potentials. J. Comput. Chem. 11, 361−373 (1990)

Campana, C.; Mussard, B.; Woo, T. K.: Electrostatic Potential Derived Atomic Charges for Periodic Systems Using a Modified Error Functional. J. Chem. Theory Comput. 5, 2866−2878 (2009)

Campbell, C., Ferreiro-Rangel, C.A., Fischer, M., Gomes, J.R.B., Jorge, M.: A Transferable Model for Adsorption in MOFs with Unsaturated Metal Sites. J. Phys. Chem. 121, 441–458 (2017)

Campbell, C., Gomes, J., Fischer, M., Jorge, M.: New Model for Predicting Adsorption of Polar Molecules in Metal–Organic Frameworks with Unsaturated Metal Sites. J. Phys. Chem. Lett. 12, 3544-3553 (2018)

Castillo, J., Vlugt, T., Calero, S.: Understanding Water Adsorption in Cu−BTC Metal−Organic Frameworks. J. Phys. Chem. 112, 15934-15939 (2008)

Castillo Sanchez, J.: Molecular simulations in microporous materials:Adsorption and separation, Ph.D. Thesis, TU Delft (2010)

Cavka, J., Jakobsen, S., Olsbye, U., Guillou, N., Lamberti, C., Bordiga, S., Lillerud, K.: A New Zirconium Inorganic Building Brick Forming Metal Organic Frameworks with Exceptional Stability. J. Am. Chem. Soc. 130, 13850-13851 (2008)

Chui, S.Y., Lo, S.M.F., Charmant, J.P.H., Orpen, A.G., Williams, I.D.: A Chemically Functionalizable Nanoporous Material $[Cu_3(TMA)_2(H_2O)_3]n$. Science 283, 1148–1150(1999)

Coudert, F., Fuchs, A.: Computational Characterization and Prediction of Metal-Organic Framework Properties. Chem. Inform. 47 (2016)

DeCoste, J., Peterson, G., Schindler, B., Killops, K., Browe, M., Mahle, J.: The effect of water adsorption on the structure of the carboxylate containing metal–organic frameworks Cu-BTC, Mg-MOF-74, and UiO-66. J. Mater. Chem. 1, 11922 (2013)

Dietzel, P., Morita, Y., Blom, R., Fjellvåg, H.: An In Situ High-Temperature Single-Crystal Investigation of a Dehydrated Metal-Organic Framework Compound and Field-Induced Magnetization of One-Dimensional Metal-Oxygen Chains. Angew. Chem. Int. Ed. 117, 6512-6516 (2005)

Dubbeldam, D., Walton, K., Ellis, D., Snurr, R.: Exceptional Negative Thermal Expansion in Isoreticular Metal–Organic Frameworks. Angew. Chem Int. Ed. 46, 4496-4499 (2007)

Dunnington, B., Schmidt, J.: Generalization of Natural Bond Orbital Analysis to Periodic Systems: Applications to Solids and Surfaces via Plane-Wave Density Functional Theory. Journal of Chemical Theory and Computation, 8(6), pp.1902-1911 (2012)

Duren, T., Bae, Y.-S., Snurr, R.Q.: Using molecular simulation to characterise metal-organic frameworks for adsorption applications. Chem. Soc. Rev. 38, 1237-1247 (2009)

Li, H., Eddaoudi, M., O'Keeffe, M., Yaghi, O.: Design and synthesis of an exceptionally stable and highly porous metal-organic framework. Nature 402, 276-279 (1999)

Farha, O. K.; Eryazici, I.; Jeong, N. C.; Hauser, B. G.; Wilmer, C. E.; Sarjeant, A. A.; Snurr, R. Q.; Nguyen, S. T.; Yazaydın, A. O¨.; Hupp, J. T.: Metal−Organic Framework Materials with Ultrahigh Surface Areas: Is the Sky the Limit? J. Am. Chem. Soc. 134, 15016−15021 (2012)

Farrusseng, D.: Metal-organic Frameworks: Applications from Catalysis to Gas Storage. Wiley (2011)

Finsy, V., Calero, S., García-Pérez, E., Merkling, P., Vedts, G., De Vos, D., Baron, G., Denayer, J.: Low-coverage adsorption properties of the metal–organic framework MIL-47 studied by pulse chromatography and Monte Carlo simulations. Phys. Chem. Chem. Phys. 11, 3515-3521 (2009)

Fischer, M., Hoffmann, F., Fröba, M.: Preferred Hydrogen Adsorption Sites in Various MOFs - A Comparative Computational Study. ChemPhysChem. 10, 2647-2657 (2009)

Fischer, M., Gomes, J.R.B., Fröba, M., Jorge, M.: Modeling Adsorption in Metal-Organic Frameworks with Open Metal Sites: Propane/Propylene Separations. Langmuir 28, 8537–8549 (2012)

Fischer, M., Gomes, J., Jorge, M.: Computational approaches to study adsorption in MOFs with unsaturated metal sites. Mol. Sim. 40, 537-556 (2014)

Frisch, M. J., Schlegel, B., Scuseria, G.E., Robb, M.A., Cheeseman, J.R., Scalmani, G., Barone, V., Mennucci, B., Petersson, G.A., Nakatsuji, H., Caricato, M., Li, X., Hratchian, H.P., Izmaylov, A.F., Bloino, J., Zheng, G., Sonnenberg, J.L., Hada, M., Ehara, M., Toyota, K., Fukuda, R., Hasegawa, J., Ishida, M., Nakajima, T., Honda, Y., Kitao, O., Nakai, H., Vreven, T., Montgomery, J.A. Jr., Peralta, J.E., Ogliaro, F., Bearpark, M., Heyd, J.J., Brothers, E., Kudin, K.N., Staroverov, V.N., Kobayashi, R., Normand, J., Raghavachari, K., Rendell, A., Burant, J.C., Iyengar, S.S., Tomasi, J., Cossi, M., Rega, N., Millam, J.M., Klene, M., Knox, J.E., Cross, J.P., Bakken, V., Adamo, C., Jaramillo, J., Gomperts, R., Stratmann,

R.E., Yazyev, O., Austin, A.J., Cammi, R., Pomelli, C., Ochterski, J.W., Martin, R.L., Morokuma, K., Zakrzewski, V.G., Voth, G.A., Salvador, P., Dannenberg, J.J., Dapprich, S., Daniels, A.D., Farkas, O., Foresman, J.B., Ortiz, J.V., Cioslowski, J., Fox, D.J.: Gaussian 09, Revision, A.02, 2009

Furukawa, H.; Ko, N.; Go, Y. B.; Aratani, N.; Choi, S. B.; Choi, E.; Yazaydin, A. O.̈; Snurr, R. Q.; O'Keeffe, M.; Kim, J.: Ultrahigh Porosity in Metal-Organic Frameworks. Science 329, 424−428 (2010)

Gagliardi, L., Lindh, R., Karlström, G.: Local properties of quantum chemical systems: The LoProp approach. J. Chem. Phys. 121, 4494-4500 (2004)

Geerlings, P., De Proft, F., Langenaeker, W.: Conceptual Density Functional Theory. Chem. Rev. 103, 1793-1874 (2003)

Ghosh, P., Colón, Y., Snurr, R.: Water adsorption in UiO-66: the importance of defects. Chem. Comm. 50, 11329-11331 (2014)

Godbout, N., Salahub, D., Andzelm, J., Wimmer, E.: Optimization of Gaussian-type basis sets for local spin density functional calculations. Part I. Boron through neon, optimization technique and validation. Can. J. Chem 70, 560-571 (1992)

Goedecker, S., Teter, M., Hutter, J.: Separable dual-space Gaussian pseudopotentials. Phys. Rev. B 54, 1703-1710 (1996)

Gupta, A., Chempath, S., Sanborn, M. J., Clark, L. A., Snurr, R. Q.: Object-oriented Programming Paradigms for Molecular Modeling. Mol. Sim. 29, 29-46 (2003)

Haldoupis, E., Nair, S., Sholl, D.S.: Finding MOFs for Highly Selective CO_2/N_2 Adsorption Using Materials Screening Based on Efficient Assignment of Atomic Point Charges. J. Am. Chem. Soc. 134, 4313-432 (2012)

Haldoupis, E., Borycz, J., Shi, H., Vogiatzis, K., Bai, P., Queen, W., Gagliardi, L., Siepmann, J.: Ab Initio Derived Force Fields for Predicting CO_2 Adsorption and Accessibility of Metal Sites in the Metal–Organic Frameworks M-MOF-74 (M = Mn, Co, Ni, Cu). J. Phys. Chem. 119, 16058-16071 (2015)

Hamad, S., Balestra, S., Bueno-Perez, R., Calero, S., Ruiz-Salvador, A.: Atomic charges for modeling metal–organic frameworks: Why and how. J. Solid State Chem. 223, 144-151 (2015)

Hariharan, P. C., Pople, J. A.: The influence of polarization functions on molecular orbital hydrogenation energies, Theor. Chim. Acta 28, 213-222 (1973)

Hirshfeld, F. L.: Bonded-atom fragments for describing molecular charge densities. Theor. Chim. Acta 44, 129-138 (1977)

Huang, H., Zhang, W., Liu, D., Zhong, C.: Understanding the Effect of Trace Amount of Water on CO_2 Capture in Natural Gas Upgrading in Metal–Organic Frameworks: A Molecular Simulation Study. Ind. Eng. Chem. Res. 51, 10031-10038 (2012)

Kadantsev, E. S.; Boyd, P. G.; Daff, T. D.; Woo, T. K.: Fast and Accurate Electrostatics in Metal Organic Frameworks with a Robust Charge Equilibration Parameterization for High-Throughput Virtual Screening of Gas Adsorption. J. Phys. Chem. Lett. 4, 3056−3061 (2013)

Kandiah, M., Nilsen, M., Usseglio, S., Jakobsen, S., Olsbye, U., Tilset, M., Larabi, C., Quadrelli, E., Bonino, F., Lillerud, K.: Synthesis and Stability of Tagged UiO-66 Zr-MOFs. Chem. Mater. 22, 6632-6640 (2010)

Kenarsari, S., Yang, D., Jiang, G., Zhang, S., Wang, J., Russell, A., Wei, Q., Fan, M.: Review of recent advances in carbon dioxide separation and capture. RSC Advances 3, 22739 (2013)

Kresse, G.; Hafner, J.: Ab initio molecular dynamics for liquid metals. Phys. Rev. B 47, 558-561 (1993)

Kresse, G.; Furthmüller, J.: Efficient iterative schemes for ab initio total-energy calculations using a plane-wave basis set. Phys. Rev. B 54. 11169-11186 (1996)

Kresse, G.; Furthmüller, J.: Efficiency of ab-initio total energy calculations for metals and semiconductors using a plane-wave basis set. Comput. Mater. Sci. 6, 15-50 (1996)

Kresse, G., Joubert, D.: From ultrasoft pseudopotentials to the projector augmented-wave method. Phys. Rev. B 59, 1758-1775 (1999)

Laino, T., Mohamed, F., Laio, A., Parrinello, M.: An efficient linear-scaling electrostatic coupling for treating periodic boundary conditions in QM/MM simulations. J. Chem. Theory Comput. 2, 1370-1378 (2006)

Li, H., Eddaoudi, M., O'Keeffe, M., Yaghi, O. M.: Design and synthesis of an exceptionally stable and highly porous metal-organic framework, Nature, 402 (6759), pp. 276-279 (1999)

Li, J.-R.; Sculley, J.; Zhou, H.-C.: Metal−organic frameworks for separations. Chem. Rev. 112, 869-932 (2012)

Limas, N., Manz, T.: Introducing DDEC6 atomic population analysis: part 4. Efficient parallel computation of net atomic charges, atomic spin moments, bond orders, and more. RSC Advances, 8(5), pp.2678-2707 (2018)

Liu, J., Rankin, R., Karl Johnson, J.: The importance of charge–quadrupole interactions for H_2 adsorption and diffusion in CuBTC. Mol. Simul. 35, 60-69 (2009)

Löwdin, P.O.: On the Non-Orthogonality Problem Connected with the Use of Atomic Wave Functions in the Theory of Molecules and Crystals. J. Chem. Phys. 18, 365-375 (1950)

Ma, S.; Zhou, H.C.: Gas storage in porous metal−organic frameworks for clean energy applications. Chem. Comm. 46, 44-53 (2010)

Manz, T. A.; Sholl, D. S.: Chemically meaningful atomic charges that reproduce the electrostatic potential in periodic and nonperiodic materials. J. Chem. Theory Comput. 6, 2455-2468 (2010)

Martin, M. G., Siepmann, J. I.: Transferable Potentials for Phase Equilibria. 1. United-Atom Description of n-Alkanes. J. Phys. Chem. 102, 2569-2577 (1998)

Mayo, S. L., Olafson, B. D., Goddard, W.A.: DREIDING: A Generic Force Field for Molecular Simulations. J. Phys. Chem. 94, 8897-8909 (1990)

McDaniel, J., Li, S., Tylianakis, E., Snurr, R., Schmidt, J.: Evaluation of Force Field Performance for High-Throughput Screening of Gas Uptake in Metal–Organic Frameworks. J. Phys. Chem 119, 3143-3152 (2015)

Mercado, R., Vlaisavljevich, B., Lin, L., Lee, K., Lee, Y., Mason, J., Xiao, D., Gonzalez, M., Kapelewski, M., Neaton, J., Smit, B.: Force Field Development from Periodic Density Functional Theory Calculations for Gas Separation Applications Using Metal–Organic Frameworks. J. Phys. Chem. 120, 12590-12604 (2016)

Metropolis, N., Rosenbluth, A.W., Rosenbluth, M.N., Teller, A.H., Teller, E.: Equation of State Calculations by Fast Computing Machines. J. Phys. Chem. 21, 1087-1092 (1953)

Moghadam, P. Z.; Li, A.; Wiggin, S. B.; Tao, A.; Maloney, A. G. P.; Wood, P. A.; Ward, S. C.; Fairen-Jimenez, D.: Development of a Cambridge Structural Database Subset: A Collection of Metal− Organic Frameworks for Past, Present, and Future. Chem. Mater. 29, 2618-2625 (2017)

Momany, F.: Determination of partial atomic charges from ab initio molecular electrostatic potentials. Application to formamide, methanol, and formic acid. J. Phys. Chem. 82, 592-601 (1978)

Mu, W., Liu, D., Yang, Q., Zhong, C.: Computational study of the effect of organic linkers on natural gas upgrading in metal–organic frameworks. Micropor. Mesopor. Mater., 130, 76-82 (2010)

Mulliken, R.S.: Electronic Population Analysis on LCAO–MO Molecular Wave Functions. J. Chem. Phys. 23, 1833-1840 (1955)

Nazarian, D., Camp, J., Sholl, D.: A Comprehensive Set of High-Quality Point Charges for Simulations of Metal–Organic Frameworks. Chem. Mater. 28,785-793 (2016)

Nugent, P., Belmabkhout, Y., Burd, S., Cairns, A., Luebke, R., Forrest, K., Pham, T., Ma, S., Space, B., Wojtas, L., Eddaoudi, M., Zaworotko, M.: Porous materials with optimal adsorption thermodynamics and kinetics for CO_2 separation. Nature 495, 80-84 (2013)

Park, J., Howe, J., Sholl, D.: How Reproducible Are Isotherm Measurements in Metal–Organic Frameworks? Chem. Mater. 29, 10487-10495 (2017)

Parr, R., Yang, W.: Density-functional theory of atoms and molecules. New York, NY: Oxford Univ. Press. (1994)

Pham, T., Forrest, K., McLaughlin, K., Tudor, B., Nugent, P., Hogan, A., Mullen, A., Cioce, C., Zaworotko, M., Space, B.: Theoretical Investigations of CO_2 and H_2 Sorption in an Interpenetrated Square-Pillared Metal–Organic Material. J. Phys. Chem. 117, 9970-9982 (2013)

Peng, D. Y., Robinson, D.B.: A New Two-Constant Equation of State. Ind. Eng. Chem. Fundament. 15, 59-64 (1976)

Perdew, J.P., Burke, K., Ernzerhof, M.: Generalized gradient approximation made simple. Phys. Rev. Lett. 77, 3865-3868 (1996)

Ramsahye, N., Maurin, G., Bourrelly, S., Llewellyn, P., Devic, T., Serre, C., Loiseau, T., Ferey, G.: Adsorption of CO_2 in metal organic frameworks of different metal centres: Grand Canonical Monte Carlo simulations compared to experiments. Adsorption 13, 461-467 (2007)

Rappe, A., Goddard, W.: Charge equilibration for molecular dynamics simulations. J. Phys. Chem. 95, 3358-3363 (1991)

Rappe, A. K., Casewit, C. J., Colwell, K. S., Goddard, W. A., Skiff, W. M.: UFF, A Full Periodic Table Force Field for Molecular Mechanics and Molecular Dynamics Simulations. J. Am. Chem. Soc. 114, 10024-10035 (1992)

Reed, A.E., Weinstock, R.B., Weinhold, F.: Natural Population Analysis. J. Chem. Phys. 83, 735-746 (1985)

Sagara, T., Klassen, J., Ganz, E.: Computational study of hydrogen binding by metal-organic framework-5. J. Chem. Phys. 121, 12543-12547 (2004)

Salles, F., Bourrelly, S., Jobic, H., Devic, T., Guillerm, V., Llewellyn, P., Serre, C., Ferey, G., Maurin, G.: Molecular Insight into the Adsorption and Diffusion of Water in the Versatile Hydrophilic/Hydrophobic Flexible MIL-53(Cr) MOF. J. Phys. Chem. 115, 10764-10776 (2011)

Sigfridsson, E., Ryde, U.: Comparison of methods for deriving atomic charges from the electrostatic potential and moments. J. Comput. Chem. 19, 377-395 (1998)

Singh, U., Kollman, P.: An approach to computing electrostatic charges for molecules. J. Comput. Chem. 5, 129-145 (1984)

Snurr, R.Q., Bell, A.T., Theodorou, D.N.: Prediction of Adsorption of Aromatic Hydrocarbons in Silicalite from Grand Canonical Monte Carlo Simulations with Biased Insertions. J. Phys. Chem. 97, 13742-13752 (1993)

Szabo, A., Ostlund, N.: Modern quantum chemistry. Mineola, N.Y.: Dover Publications (2006)

Tafipolsky, M., Amirjalayer, S. and Schmid, R.: Ab initio parametrized MM3 force field for the metal-organic framework MOF-5. J. Phys. Chem. 28, 1169-1176 (2007)

Torrisi, A., Bell, R., Mellot-Draznieks, C.: Functionalized MOFs for Enhanced CO_2 Capture. Cryst. Growth Des., 10, 2839-2841 (2010)

Tranchemontagne, D., Hunt, J., Yaghi, O.: Room Temperature Synthesis of Metal-Organic Frameworks: MOF-5, MOF-74, MOF-177, MOF-199, and IRMOF-0. Tetrahedron, 64 8553-8557 (2008)Verstraelen, T., Vandenbrande, S., Heidar-Zadeh, F., Vanduyfhuys, L., Van Speybroeck, V., Waroquier, M., Ayers, P.: Minimal Basis Iterative Stockholder: Atoms in Molecules for Force-Field Development. J. Chem. Theory Comput. 12, 3894-3912 (2016)

Walton, K.S., Millward, A. R., Dubbeldam, D., Frost, H., Low, J.J., Yaghi, O.M., Snurr, R.Q.: Understanding Inflections and Steps in Carbon Dioxide Adsorption Isotherms in Metal-Organic Frameworks. J. Am. Chem. Soc.130, 406-407 (2008)

Watanabe, T., Manz, T., Sholl, D.: Accurate Treatment of Electrostatics during Molecular Adsorption in Nanoporous Crystals without Assigning Point Charges to Framework Atoms. J. Phys. Chem. 115, 4824-4836 (2010)

Watanabe, T., Sholl, D.: Accelerating Applications of Metal–Organic Frameworks for Gas Adsorption and Separation by Computational Screening of Materials. Langmuir 28, 14114-14128 (2012)

Wilmer, C., Leaf, M., Lee, C., Farha, O., Hauser, B., Hupp, J., Snurr, R.: Large-scale screening of hypothetical metal–organic frameworks. Nature Chem. 4, 83-89 (2011)

Wilmer, C., Snurr, R.: Towards rapid computational screening of metal-organic frameworks for carbon dioxide capture: Calculation of framework charges via charge equilibration. Chem. Eng. J. 171, 775-781 (2011)

Wilmer, C. E.; Kim, K. C.; Snurr, R. Q.: An extended charge equilibration method. J. Phys. Chem. Lett. 3, 2506−2511 (2012)

Wilmer, C., Farha, O., Bae, Y., Hupp, J., Snurr, R.: Structure–property relationships of porous materials for carbon dioxide separation and capture. Energ. Environ. Sci., 5, 9849-9856 (2012)

Wu, D., Yang, Q., Zhong, C., Liu, D., Huang, H., Zhang, W., Maurin, G.: Revealing the Structure–Property Relationships of Metal–Organic Frameworks for CO_2 Capture from Flue Gas. Langmuir 28, 12094-12099 (2012)

Xu, Q., Zhong, C.L.: A general approach for estimating framework charges in metal organic frameworks. J. Phys. Chem. 114, 5035-5042 (2010)

Yang, Q., Zhong, C.: Electrostatic-Field-Induced Enhancement of Gas Mixture Separation in Metal-Organic Frameworks: A Computational Study. ChemPhysChem. 7, 1417-1421 (2006)

Yang, Q., Zhong, C.: Molecular Simulation of Carbon Dioxide/Methane/Hydrogen Mixture Adsorption in Metal−Organic Frameworks. J. Phys. Chem. 110, 17776-17783 (2006)

Yang, Q., Xue, C., Zhong, C., Chen, J.: Molecular simulation of separation of CO_2 from flue gases in Cu-BTC metal-organic framework. AIChE Journal 53,.2832-2840 (2007)

Yang, Q., Wiersum, A., Llewellyn, P., Guillerm, V., Serre, C., Maurin, G.: Functionalizing porous zirconium terephthalate UiO-66(Zr) for natural gas upgrading: a computational exploration. Chem. Comm. 47, 9603-9605 (2011)

Yazaydın, A., Benin, A., Faheem, S., Jakubczak, P., Low, J., Willis, R., Snurr, R.: Enhanced CO_2 Adsorption in Metal-Organic Frameworks via Occupation of Open-Metal Sites by Coordinated Water Molecules. Chem. Mater. 21, 1425-1430 (2009)

Yazaydın, A.Ö., Snurr, R.Q., Park, T-H., Koh, K., Liu, J., Le Van, M.D., Benin, A.I., Jakubczak, P., Lanuza, M., Galloway, D.B., Lowland, J.J., Willis, R.R.: Screening of Metal−Organic Frameworks for Carbon Dioxide Capture from Flue Gas Using a Combined Experimental and Modeling Approach. J. Am. Chem. Soc. 131, 18198-18199 (2009)

Zang, J., Nair, S., Sholl, D.: Prediction of Water Adsorption in Copper-Based Metal–Organic Frameworks Using Force Fields Derived from Dispersion-Corrected DFT Calculations. J. Phys. Chem. 117, 7519-7525 (2013)

Zhang, Y., Li, B., Krishna, R., Wu, Z., Ma, D., Shi, Z., Pham, T., Forrest, K., Space, B., Ma, S.: Highly Selective Adsorption of Ethylene Over Ethane in a MOF Featuring the Combination of Open Metal Site and [Small pi]-Complexation. Chem. Comm. 51, 2714-2717 (2015)

Zhang, H., Snurr, R.: Computational Study of Water Adsorption in the Hydrophobic Metal–Organic Framework ZIF-8: Adsorption Mechanism and Acceleration of the Simulations. J. Phys. Chem. C 121, 24000-24010 (2017)

Zhao, Y.; Truhlar, D. G.: A new local density functional for main-group thermochemistry, transition metal bonding, thermochemical kinetics, and noncovalent interactions. J. Chem. Phys., 125, 194101 (2006)

Zheng, C., Liu, D., Yang, Q., Zhong, C. and Mi, J.: Computational Study on the Influences of Framework Charges on CO_2 Uptake in Metal−Organic Frameworks. Industrial Eng. Chem. Res. *48, 10479-10484 (2009)*

4. Theoretical and Experimental Study of Single Component Adsorption Behaviour in a MOF containing Open Metal Sites

4. 1 Introduction

In this chapter the characterization of CuBTC was performed using several analytical techniques. The results are compared with literature data and show good agreement. Gravimetric methods (section 2.1.5) were used to carry out experimental adsorption measurements of ethane and ethylene on CuBTC at 273K and 323K with comparison of the results to GCMC simulations using the new OMS model (section 4.2.2).

As described in chapter 1, some MOFs contain Open Metal Sites (OMS). CuBTC is one of such materials and it will be the focus of the work in this chapter. The OMS is a complex orbital interaction which the standard force fields were not designed to account for, as they deal only with van der Waals forces. When simulating adsorption with adsorbate species such as ethylene, which interact strongly with the OMS, the simulations fail to describe this process accurately and vastly underestimate the adsorption when compared to experiments. As permanent electrostatics are not relevant with non-polar species such as ethylene, it is reasonable to assume that this increase in adsorption is due to the OMS interaction, which brings about the need for a new fully transferable model to treat OMS interactions consistently. Our group developed such a model to overcome this issue and improve adsorption simulation in MOFs with OMS (Fischer *et al.* 2012) (Jorge *et al.* 2014) (Campbell *et al.* 2016) (Campbell *et al.* 2018). Simulations, implementing the new model, were performed and the results compared to experimental measurements.

4.2 Methodology

4.2.1 Experimental

As described in section 3.4.4, CuBTC (also known as MOF-199 and HKUST-1) has the structural formula Cu3(btc)2 (btc = 1,3,5-benzenetricarboxylate). This MOF consists of central copper ions linked with 1,3,5-benzenetricarboxylate (BTC) acid ligands. These linkages form a porous crystalline structure with two central copper ions, which are bound to

four BTC ligands via two oxygens on each ligand and to solvent (water) via 2 oxygens. The material was purchased from Sigma Aldrich under the commercial name Basolite C300.

The FTIR spectrum of CuBTC was recorded in the range 4000 to 500 cm^{-1} on an attenuated total reflection (ATR) module with an ABB MB 3000 FTIR spectrometer, using a scan interval of 4 cm^{-1}. For the measurements of the CuBTC samples, a moderate pressure was applied to the samples to achieve optimal contact between the solid sample and the ATR crystal. Sixteen scans were averaged to obtain appropriate signal-to-noise ratio. All spectra were background corrected for water and CO_2.

Thermogravimetric analyses (TGA) were carried out with a Netzsch STA (Simultaneous Thermal Analysis) 440 F3 Jupiter thermogravimetric analyser. The temperature range was 25–500 °C with a heating rate of 5 °C/min under an oxygen-free nitrogen atmosphere (BOC, 25 mL/min).

Nitrogen adsorption was performed using a Micromeritics ASAP 2420 instrument operated at -196 °C, using oxygen-free nitrogen (BOC). Before each experiment, the sample was degassed at 180 °C for 12 h to remove any pre-adsorbed species. Isotherms were collected from 0 to 0.99 relative pressure using 40 steps in the adsorption scan and 30 in the desorption scan.

Gravimetric adsorption measurements were made using a Hiden Isochema Intelligent Gravimetric Analyser (IGA). Prior to gas adsorption measurement, the sample was activated at 120 °C under ultra-high vacuum (>10^{-6} mbar) until constant mass was attained (weighing resolution 0.2 mg). Isothermal conditions were achieved using a water jacket maintaining ±0.1 °C throughout.

4.2.2 Computational Methods

The new multiscale approach for describing adsorption at the OMS combines Quantum mechanical calculations with GCMC simulations using a procedure schematically represented in Figure 4.1. First, Quantum calculations of the molecule of interest (in this case, ethylene) adsorbing onto the metal site are carried out. Once the QM calculations have been carried out, the energy profile of the interaction at the open metal site was subsequently obtained. The DFT gives a deeper energy minimum and at a shorter distance than the LJ

models, which demonstrates that the standard models do not show the correct adsorption mechanism (Jorge *et al.* 2014). The next step was to isolate the contribution of the OMS from the energy profile, which was done by energy decomposition. The contributions of dispersion/repulsion, electrostatics where applicable, and OMS interaction were defined and from this the energy contribution of OMS could be isolated from the full DFT energy profile. The obtained OMS energy profile was then fitted to a modified Morse potential function (Equation 4.1). This new interaction function was then included in GCMC simulations. The way this was done was all the previous parameters for repulsion/dispersion interactions were kept the same, but a new interaction site was added at the centre of the double bond of ethylene. This site interacted only with the unsaturated Cu site through the Morse potential described above.

$$U_{function}(r) = D_0.\left[exp\left(\alpha\left(1-\frac{r}{R_0}\right)\right) - 2.exp\left(\frac{\alpha}{2}\left(1-\frac{r}{R_0}\right)\right)\right] - \left(\frac{A}{r}\right)^B \qquad \text{Equation 4.1}$$

All adsorption isotherms reported in this chapter were calculated by GCMC simulations using Music 4.0 software (Gupta *et al.* 2003) – for details see section 2.5. To account for the OMS interaction, the code was modified so that it included the modified Morse potential function described above. Each simulation, corresponding to a single pressure point, was set for a minimum of 1.0 x 10^8 iterations. Each iteration had an equilibration period in which 50% of the steps were ignored, and a production run, which was split into 20 equal blocks for error analysis.

Fluid-fluid and fluid-solid interactions were calculated using models composed of Lennard-Jones (LJ) sites to describe repulsion and dispersion interactions. The LJ interaction cut off distance was defined as 13 Å, with the exception of the interaction between the new OMS site (centre of ethylene double bond) and the unsaturated Cu atom of the framework. Tables 4.1 and 4.2 show the fitted OMS parameters for the ethylene-Cu interaction, including the cut off values for this site. The rationale for these cut off values can be found in previous work by Campbell *et al.* 2016.

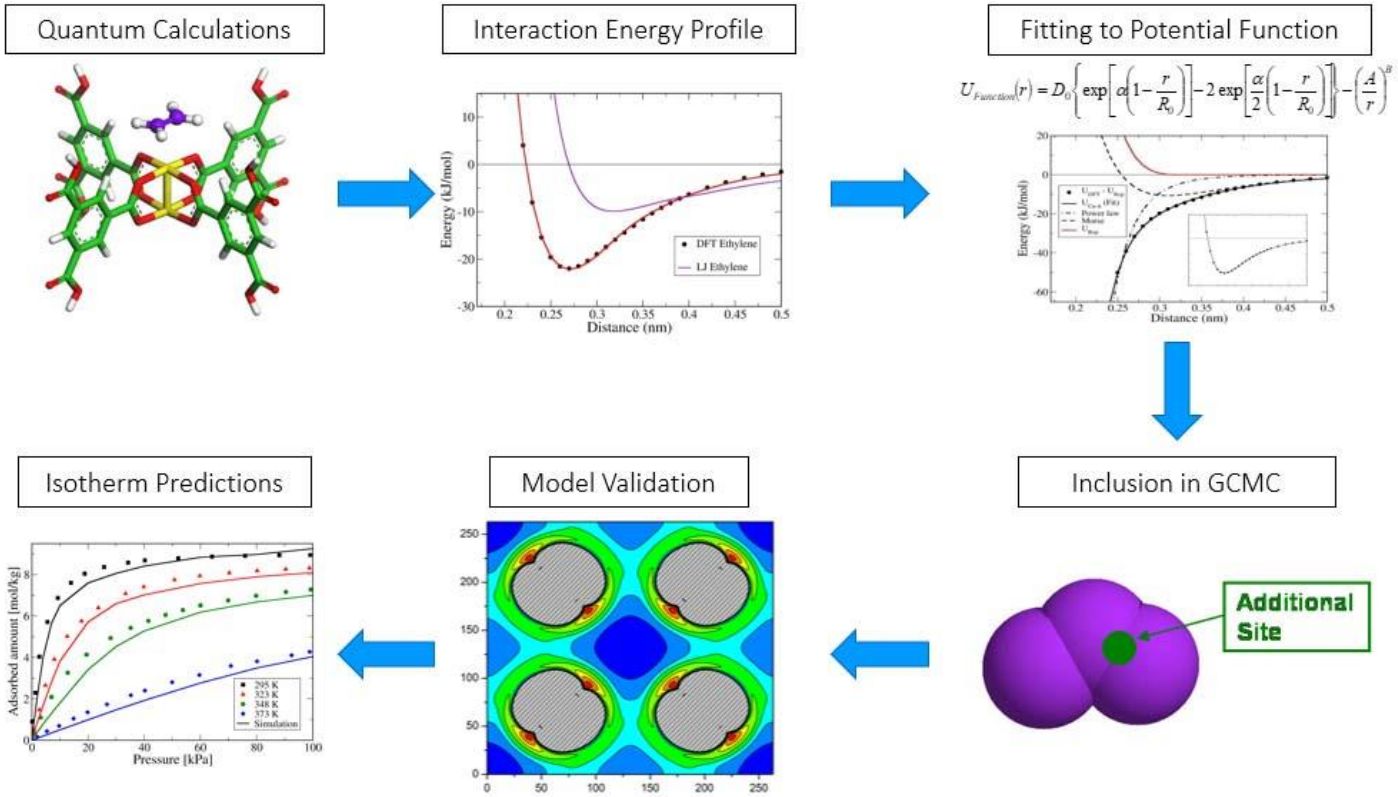

Figure 4.1 – The OMS model (Figure adapted from Campbell et al. 2016)

Table 4.1 – OMS Interaction Parameters (Campbell et al. 2016)

MOF	Complex	R_0 (Å)	D_0 (kJ/mol)	α	A	B
CuBTC	Dimer	3.1030	10.6324	8.0945	3.825	9.2812

Table 4.2 – OMS Cut-Off Values (Campbell et al. 2016)

OMS Interaction Cut Off Values	
Low cut off	1.8 Å
Shift cut off	3.5 Å
High cut off	4.0 Å

The Universal Force Field (UFF) (Rappe *et al.* 1992) and DREIDING (Mayo *et al.* 1990) are frequently used to model gas adsorption in MOFs and they were used in this chapter to describe the interactions with MOF framework atoms. The LJ parameters for the non-metal atoms were taken from DREIDING and for metal atoms from UFF. For the adsorbate models, we used the Transferable Potentials for Phase Equilibria (TraPPE) model (Martin and Siepmann 1998). The framework and the adsorbates were kept rigid throughout the modelling process. Lorentz-Berthelot mixing rules were applied for combining LJ species.

4.3 Results & Discussion

Figure 4.2 shows the results of the FTIR analysis of the CuBTC sample. The peaks below 1200 cm^{-1} correspond to the vibrations of the BTC linker. The bands from 1300 to 1700 cm^{-1} are characteristic of the carboxylate linker, attributed to the coordination of BTC to the copper sites. The CuBTC spectrum shows two small peaks at around 1630 cm^{-1}. assigned to ν (C=O) of the deprotonated benzene tricarboxylic acid. The peaks at 1448 and 1371 cm^{-1} are related to the symmetric stretching vibrations of the carboxylate groups (Seo *et al.* 2009). These stretching vibrations are in good agreement with CuBTC data reported in literature, as shown in Figure 4.2 (Dhumal *et al.* 2016).

Figure 4.3a shows the thermal stability analysis of the CuBTC sample. Dehydration of the material takes place up to approximately 180 °C with around 15% mass loss, corresponding to the presence of water molecules in the framework. The DSC result correlates well to the TGA spectrum showing an endothermic peak (100–280 °C) due to the dehydration of the sample. The third mass loss of approximately 40% is attributed to the decomposition of the

CuBTC framework at around 350 °C. This is in agreement with the theoretical loss of 36.7% (Al Janabi *et al.* 2015). When compared to the reference data (Figure 4.3b), some difference between initial mass loss is observed, which can be accounted for by different amounts of water present in the hydrophilic CuBTC samples.

Figure 4.4 shows the nitrogen adsorption isotherms obtained at 77K for 3 independent samples. A Type I isotherm, characteristic of a microporous material is observed. The three separate runs show good reproducibility. The specific surface area and total pore volume calculated by the BET method are listed in table 4.3.

Table 4.3 – Surface area and pore volume from BET analysis

	Surface Area (m^2/g)	**Pore volume (cm^3/g)**
Sample 1	1804	0.75
Sample 2	1789	0.74
Sample 3	1782	0.74
Reference	1500-2100 *	0.66-0.813 **
Theoretical Pore Volume		0.82 ***

* Lamia *et al.* 2009

** Castillo *et al.* 2008, Hamon *et al.* 2010

*** Liu *et al.* 2007

Pore volume scaling was used according to equation 4.2:

$$N_{scaled} = N_{exp} \frac{V_{p(theoretical)}}{V_{p(experiment)}} \qquad \text{Equation 4.2}$$

The theoretical pore volume refers to the accessible pore volume of a perfect crystal, and the experimental pore volume is the experimentally measured pore volume of the sample. Using this scaling method can help account for reduced adsorption capacity in experiments which can arise due to defects, collapsed pores, remnant solvent molecules or other imperfections (Jorge et al. 2014).

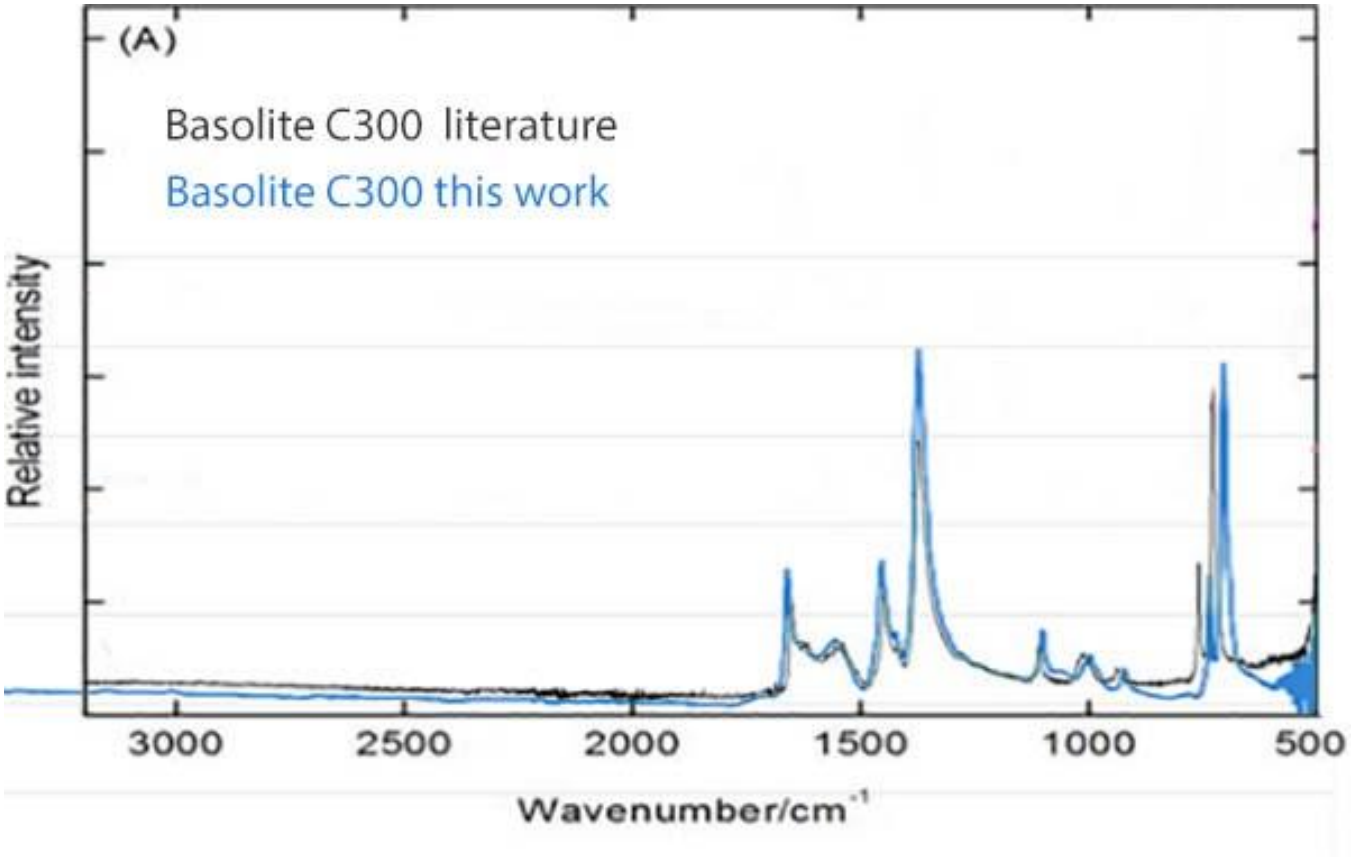

Figure 4.2 – Overlay of this work's FTIR results with literature (Dhumal et al. 2016)

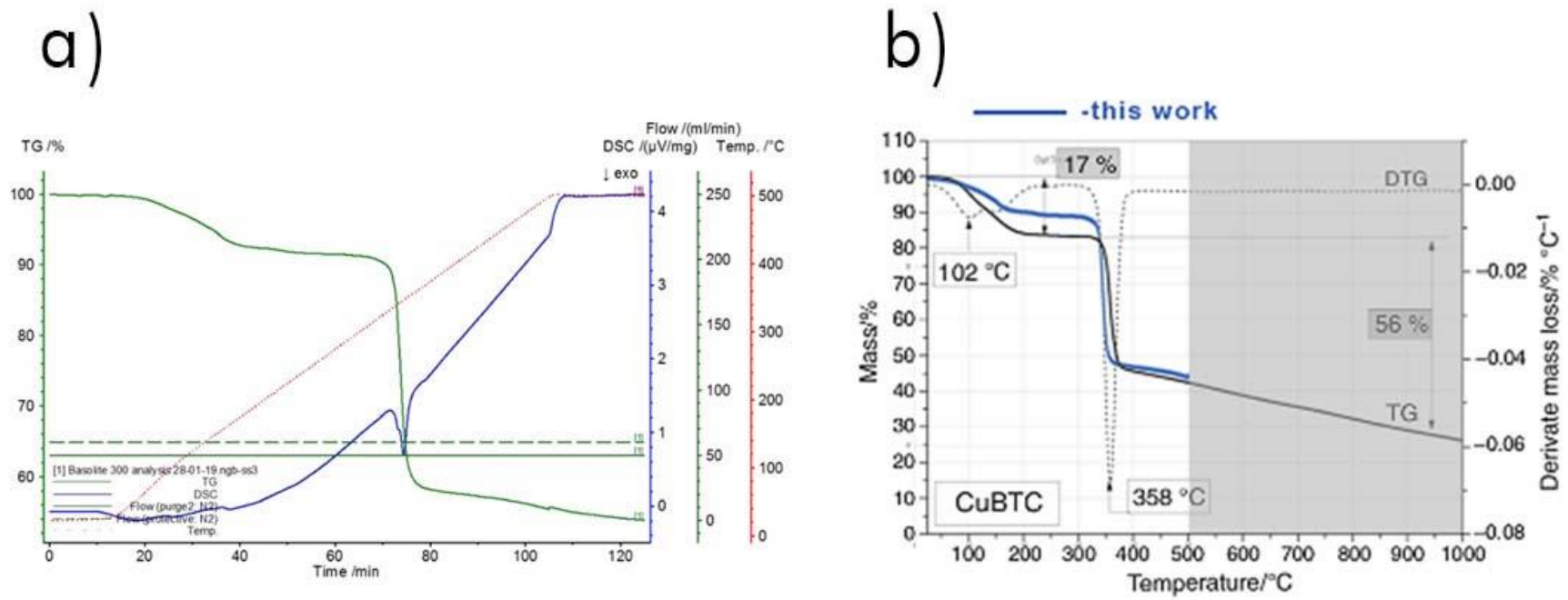

Figure 4.3 – TGA analysis of CuBTC obtained in this work (a) and an overlay of this work's TGA results with literature (Majchrzak-Kucęba and Bukalak-Gaik 2016) (b)

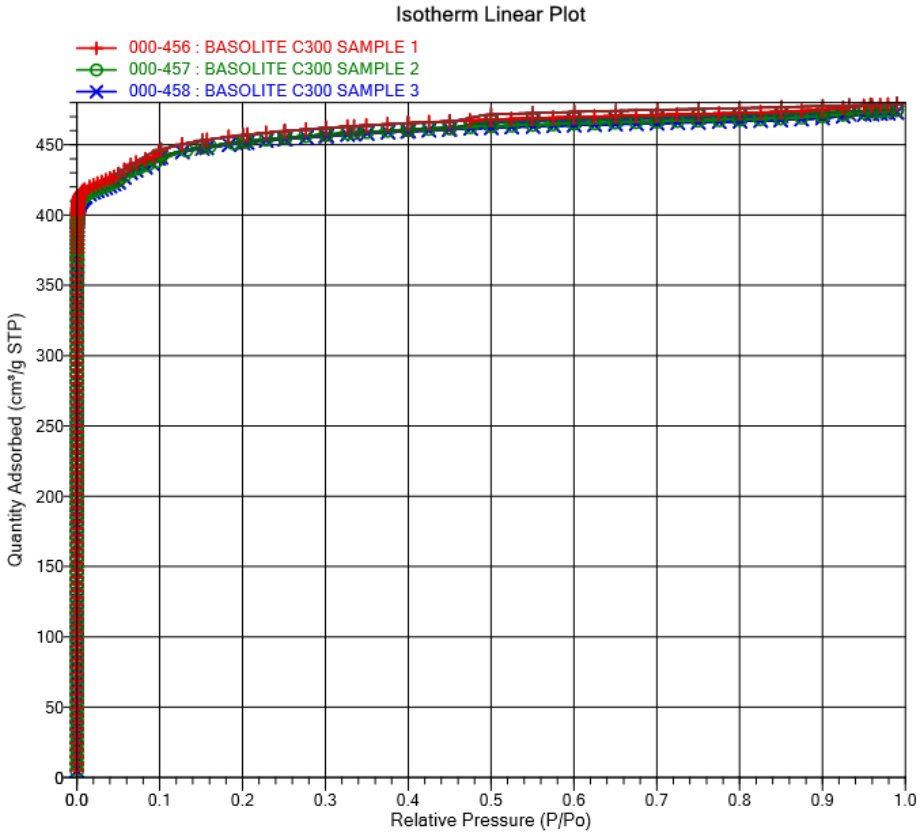

Figure 4.4 – BET analysis of CuBTC obtained on 3 independent samples.

Experimental adsorption measurements of ethane and ethylene on CuBTC were obtained at 273K and 323K (Figure 4.8). The data at 323K can be directly compared with previous measurements on the same commercial material (Basolite C300), reported by Jorge *et al.* (Figures 4.5 and 4.6). The two isotherms agree quite well, suggesting that the activation and measurement process undertaken in this study was performed correctly. As previous work shows (Figure 4.6), the standard models fail to accurately describe the OMS interaction and results in a dramatic underestimation of adsorption for ethylene. Figures 4.5 and 4.6 compares the experimental data against simulations using the OMS model giving good agreement both for ethane and ethylene, clearly indicating that the new model is capturing the OMS interaction in ethylene. In addition to previous work, the experimental adsorption measurements at 273K were also performed and again show good agreement with simulation. This demonstrates that the new OMS model performs well also at low temperatures and will therefore work robustly for a wide range of temperatures.

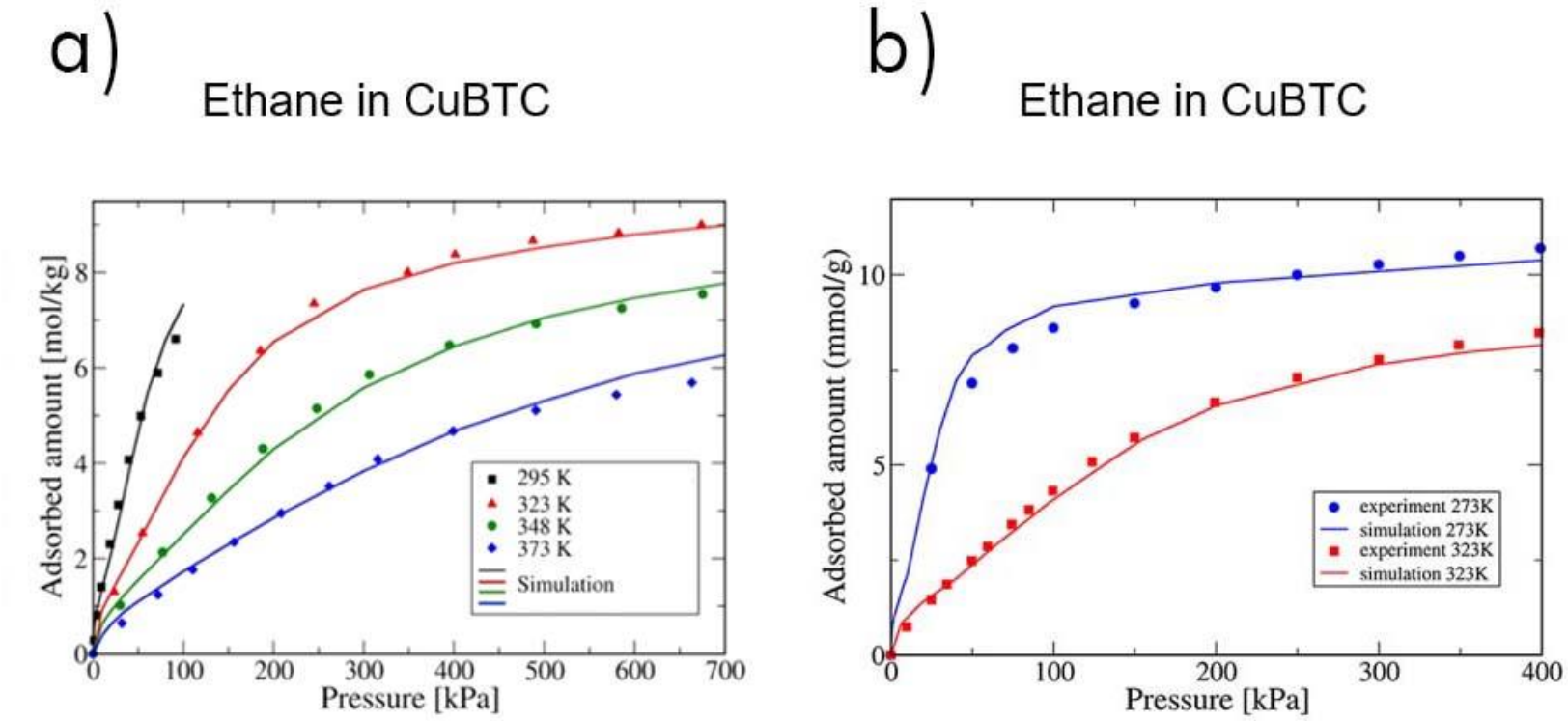

Figure 4.5 – Experimental adsorption measurements (points) for ethane on CuBTC at several temperatures with simulation (lines) using standard models: (a) previous data from Jorge et al. (2014); (b) new data obtained in this work

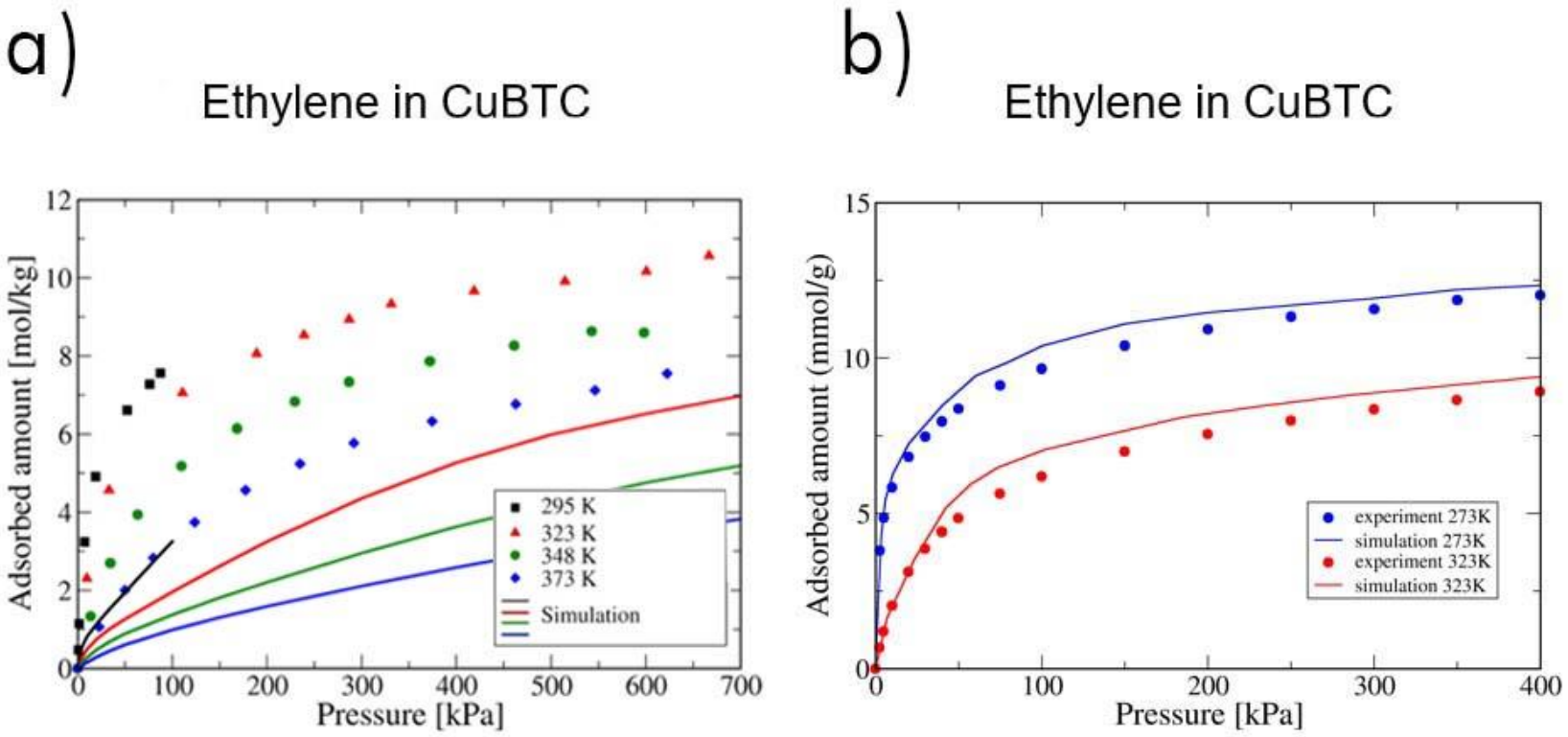

Figure 4.6 – Experimental adsorption measurements (points) for ethylene on CuBTC at several temperatures compared with simulation (lines) using (a) standard models (Jorge et al. 2014) (a); (b) the new OMS model (this work)

References

Al-Janabi, N., Hill, P., Torrente-Murciano, L., Garforth, A., Gorgojo, P., Siperstein, F., Fan, X.: Mapping the CuBTC metal–organic framework (HKUST-1) stability envelope in the presence of water vapour for CO2 adsorption from flue gases, Chem. Eng. J. 281 669–677 (2015)

Campbell, C., Ferreiro-Rangel, C., Fischer, M., Gomes, J. and Jorge, M.: A Transferable Model for Adsorption in MOFs with Unsaturated Metal Sites. The Journal of Physical Chemistry C, 121(1), pp.441-458 (2016).

Campbell, C., Gomes, J., Fischer, M., Jorge, M.: New Model for Predicting Adsorption of Polar Molecules in Metal–Organic Frameworks with Unsaturated Metal Sites. J. Phys. Chem. Lett. 12, 3544-3553 (2018)

Castillo, J., Vlugt, T. and Calero, S., 2008. Understanding Water Adsorption in Cu−BTC Metal−Organic Frameworks. The Journal of Physical Chemistry C, 112(41), pp.15934-15939 (2008)

Dhumal, N., Singh, M., Anderson, J., Kiefer, J. and Kim, H.: Molecular Interactions of a Cu-Based Metal–Organic Framework with a Confined Imidazolium-Based Ionic Liquid: A Combined Density Functional Theory and Experimental Vibrational Spectroscopy Study. The Journal of Physical Chemistry C, 120(6), pp.3295-3304, (2016)

Fischer, M., Gomes, J., Fröba, M. and Jorge, M.: Modeling Adsorption in Metal–Organic Frameworks with Open Metal Sites: Propane/Propylene Separations. Langmuir, 28(22), pp.8537-8549. (2012)

Hamon, L., Jolimaitre, E. and Pirngruber, G.: CO2 and CH4 separation by adsorption using CuBTC metal-organic framework, Ind. Eng. Chem. Res. 2010, 49, 16, 7497–7503 (2010)

Jorge, M., Fischer, M., Gomes, J., Siquet, C., Santos, J. and Rodrigues, A: Accurate Model for Predicting Adsorption of Olefins and Paraffins on MOFs with Open Metal Sites. Industrial & Engineering Chemistry Research, 53(40), pp.15475-15487 (2014)

Lamia, N., Jorge, M., Granato, M., Almeida Paz, F., Chevreau, H. and Rodrigues, A.: Adsorption of propane, propylene and isobutane on a metal–organic framework: Molecular simulation and experiment. Chemical Engineering Science, 64(14), pp.3246-3259 (2009)

Liu, J.; Culp, J. T.; Natesakhawat, S.; Bockrath, B. C.; Zande, B.; Sankar, S. G.; Garberoglio, G.; Johnson, J. K. Experimental and Theoretical Studies of Gas Adsorption in $Cu_3(BTC)_2$: An Effective Activation Procedure J. Phys. Chem. C, 111, 9305 (2007)

Majchrzak-Kucęba, I. and Bukalak-Gaik, D., 2016. Regeneration performance of metal–organic frameworks. Journal of Thermal Analysis and Calorimetry, 125(3), pp.1461-1466 (2016)

Seo, Y.-K.; Hundal, G.; Jang, I. T.; Hwang, Y. K.; Jun, C.-H.; Chang, J.-S. Microwave Synthesis of Hybrid Inorganic−Organic Materials Including Porous Cu3(BTC)2 from Cu(II)-Trimesate Mixture. Microporous Mesoporous Mater. 2009, 119, 331−337

5. Conclusions & Future Work

In this thesis, we reported a detailed and systematic analysis of the effect of the choice of framework point charges on adsorption isotherms predicted by molecular simulations (Chapter 3) and we carried out single component experimental adsorption measurements of ethane and ethylene on CuBTC (Chapter 4) with the ultimate goal of validating molecular simulation models for adsorption in MOFs. We furthermore compared these measurements with simulations implementing the new OMS model previously developed by our group.

In Chapter 3, point charges obtained by different approaches, covering all types of methodology, were used in GCMC simulations of CO_2 and water adsorption in six different MOF structures. The latter covered some of the most widely studied MOF families, and included frameworks with significantly different topologies and surface functionalities, as well as MOFs with and without open metal sites. Our results allow us to draw the following general conclusions:

- The variation in the values of the framework point charges, for any given MOF, is much larger than the variation in the adsorption isotherms themselves. This is particularly the case for QM-derived charges, which suggests that the main property controlling adsorption predictions is the overall electrostatic potential induced by the framework on the adsorbate molecules. As a consequence, assessing the suitability of point charge determination methods solely on the basis of the charges themselves may lead to erroneous conclusions. We recommend diagnosing the suitability of charge sets by comparing predicted isotherms against reference data, whenever possible.
- Charges derived from periodic QM calculations yielded isotherms that were consistent with each other for all charge determination methods, with the exception of Bader and Hirshfeld. This was the case regardless of the details of the underlying QM calculation. In particular, it is noteworthy that consistent charges were obtained from both DDEC (an electron density partitioning method) and REPEAT (an electrostatic potential fitting method) for all MOFs analysed here. It is hard to draw definitive conclusions for other charge determination methods (e.g. LoProp, ISA) due to the small number of instances analysed. As such, we would recommend this approach as the most reliable for obtaining framework charges for adsorption

simulations, at least when the size of the unit cell does not make such calculations prohibitive.

- Framework charges derived from QM cluster calculations were comparatively less reliable – while several sets yielded isotherms in agreement with each other and with periodic charges, there was a significant degree of variation in some cases. Moreover, with one or two exceptions, it was not possible to predict which sets would lead to discrepant isotherms simply by examining the charge values. This means that care should be taken when using charges calculated by this approach, and consistency checks should be sought whenever possible.
- Charges calculated using methods that fit the electrostatic potential (such as CHELPG or REPEAT) or that partition the electron density (such as DDEC or ISA) generally yield isotherms that are statistically consistent with each other. A clear exception are Bader charges, which strongly overestimate the electrostatic potential, and hence the adsorbed amounts. Charges determined from population analysis (e.g. Mulliken) appear to be less reliable, although there are not enough examples in our study to confirm this observation. The decreased reliability of Mulliken charges is reinforced by their significant dependence with the basis set size as reported in the literature.
- Semi-empirical approaches, like EQeq or CBAC, can provide reasonable alternatives to QM-based charges when computational expense is an important limitation (e.g. large-scale screening). However, in some cases, predictions from this class of methods can lead to rather unexpected results (e.g. water in UiO-66). Given the wide variability in MOF framework structures and surface chemistries (including functionalization), we recommend that any charges obtained from semi-empirical methods be validated against reference isotherms obtained from periodic QM charges for prototypical MOFs.
- Water isotherms are much more sensitive to details of the electrostatic interactions than CO_2 isotherms. This was rather expected, due to the significant difference in polarity between these two adsorbates. This effect is emphasised in MOFs that contain open metal sites, as these provide rather strong adsorption sites for water molecules. In such MOFs, attempts to adjust framework point charges (or, indeed, LJ parameters) to implicitly account for coordination bonds at the unsaturated metal site are unlikely to lead to physically consistent adsorption behaviour.

In Chapter 4 we carried out characterization of CuBTC using various analytical techniques and resulting in good agreement with literature, confirming the composition and structural properties of the material. We then performed experimental measurements of single component adsorption of ethane and ethylene on CuBTC at 273K and 323K. The isotherms measured at 323K are consistent with previous literature results on the same material. We compared the experimental results to simulations which were set up to include the OMS interaction and we were able to show that the OMS model previously developed by our group is robust and works well even at low temperatures. The next step in this work was to carry out binary ethane/ethylene experimental adsorption measurements and compare these to simulations, but due to the Covid-19 pandemic restrictions, this was not possible to accomplish in time. As such, this is recommended as a priority for work to be carried out in the near future.

Overall, we believe our work will help to improve the reliability and reproducibility of adsorption simulations by providing a general protocol for testing and validating molecular models. As a first step, we provided useful guidelines to calculate or choose point charges for MOF frameworks – namely, we recommend the use of charges developed by periodic DFT methods as these produced the most accurate and consistent results. By providing a consistent set of adsorption isotherms on reference materials, it should now be possible to systematically assess the effect of other force field parameters (e.g. Lennard-Jones) on the performance of the simulations. More precisely, one could keep the point charges constant (say, using DDEC charges from periodic DFT) and test the effect of varying other force fields parameters, in order to see which model is most suitable for modelling adsorption in MOFs. Together with recent systematic analysis of uncertainty in experimental adsorption measurements (Park et al. 2017), this work would enable a less arbitrary assessment of the suitability of molecular models to provide adsorption predictions that can be used in an industrial context.

References

Park, J., Howe, J., Sholl, D.: How Reproducible Are Isotherm Measurements in Metal–Organic Frameworks? Chem. Mater. 29, 10487-10495 (2017)

A. Appendix

A.1 Determination of cluster-based charges for SIFSIX-2-Cu-I

DFT calculations were carried out by external collaborators on several clusters carved from the SIFSIX periodic cell, as shown in Figures A.1-A.4. Whenever necessary, terminal atoms were capped with hydrogen atoms, as shown in the figures. Calculations were done using Gaussian 09 (Frisch et al. 2009), with the M06-L functional and a 6-31G** basis set. All the atomic positions were frozen at their crystallographic sites with the exception of those corresponding to the hydrogen atoms, which were fully relaxed in the calculations.

Point charges were calculated on each cluster using both CHELPG and DDEC methods, and the values are reported in Tables A.1 and A.2. In an attempt to emulate the procedure of Pham et al. (2013), we have selected the atoms of each type that were surrounded by a chemical environment that was most representative of the fully periodic MOF framework (shown in bold in Tables A.1 and A.2), and calculated the average charge for each atom type. This led to a framework with non-zero overall charge, therefore the remaining charge was uniformly distributed over all atoms, leading to the final charge sets shown in Table 3.9 of the thesis.

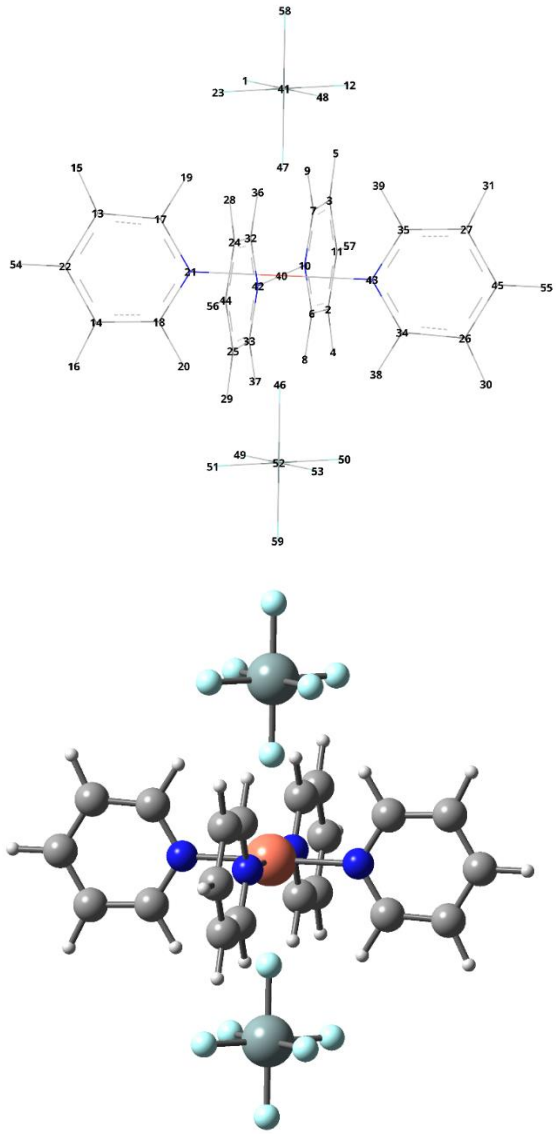

Figure A.1 – Structure of cluster 1 used to calculate charges on the SIFSIX MOF (left – wireframe view; right – ball-and-stick view). Atom labels corresponding to the notation used in Tables S7 and S8 are shown in the wireframe view. Color code for the ball-and-stick view is: Carbon – grey; Hydrogen – white; Copper – orange; Silicon – green; Fluorine – teal.

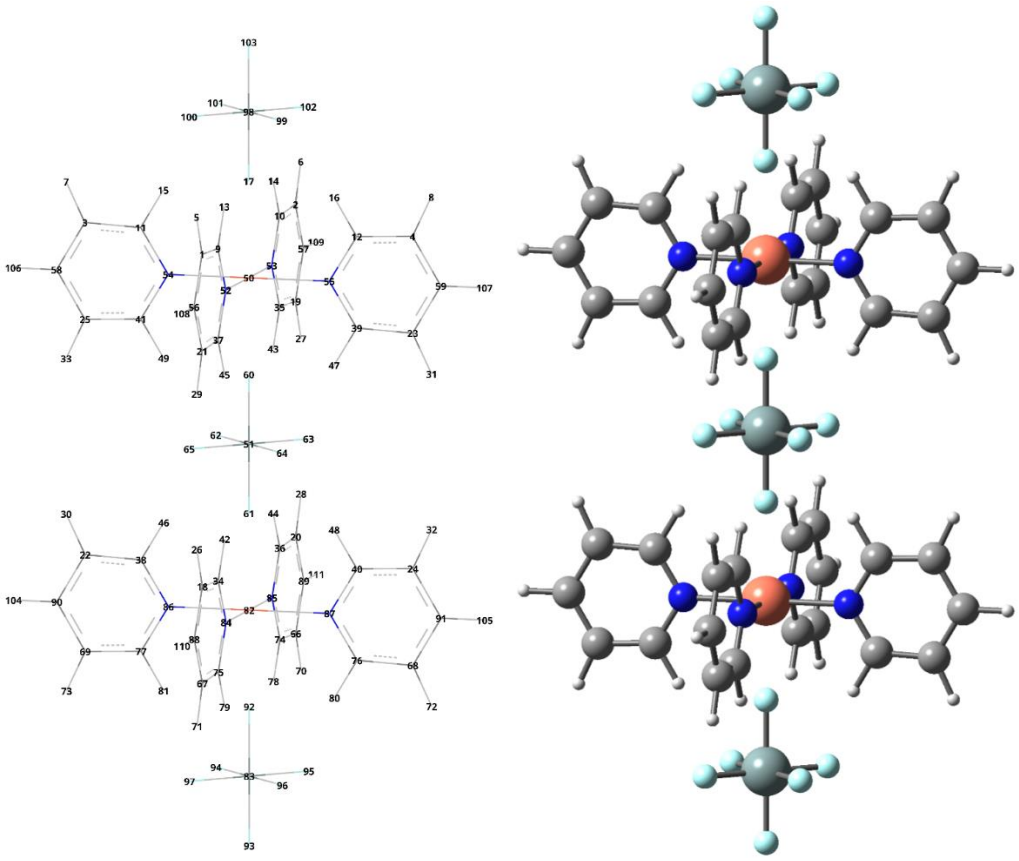

Figure A2 – Structure of cluster 2 used to calculate charges on the SIFSIX MOF (left – wireframe view; right – ball-and-stick view). Atom labels corresponding to the notation used in Tables S7 and S8 are shown in the wireframe view. Color code for the ball-and-stick view is: Carbon – grey; Hydrogen – white; Copper – orange; Silicon – green; Fluorine – teal.

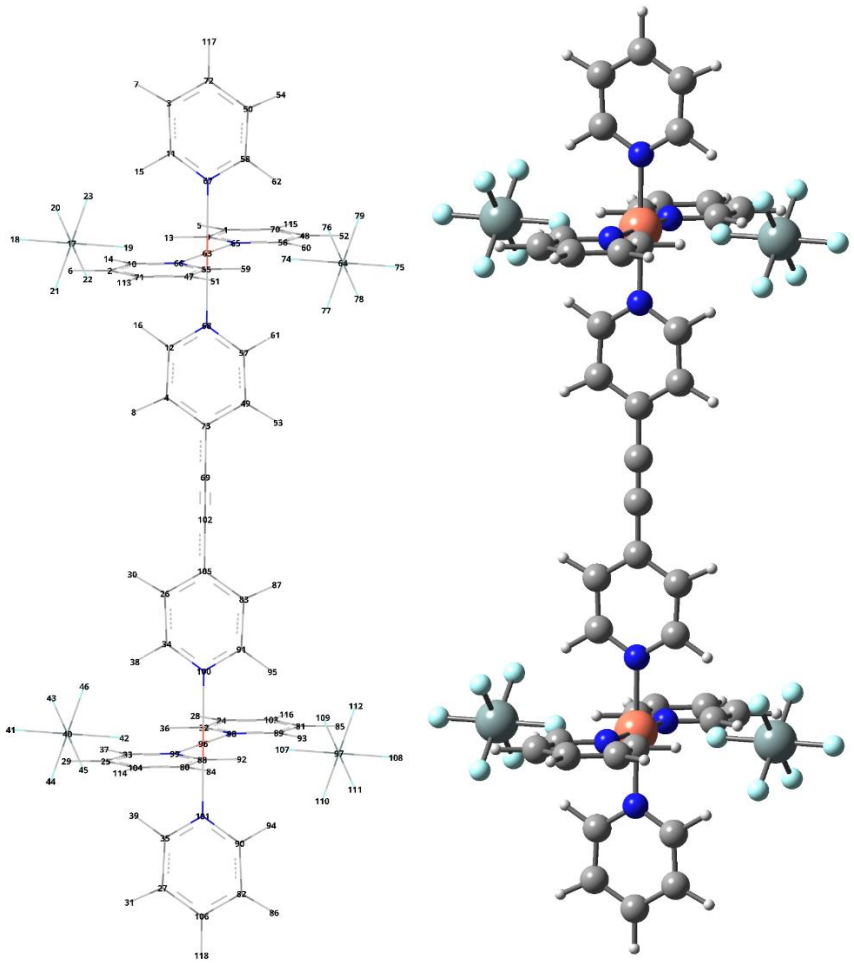

Figure A.3 – Structure of cluster 3 used to calculate charges on the SIFSIX MOF (left – wireframe view; right – ball-and-stick view). Atom labels corresponding to the notation used in Tables S7 and S8 are shown in the wireframe view. Color code for the ball-and-stick view is: Carbon – grey; Hydrogen – white; Copper – orange; Silicon – green; Fluorine – teal.

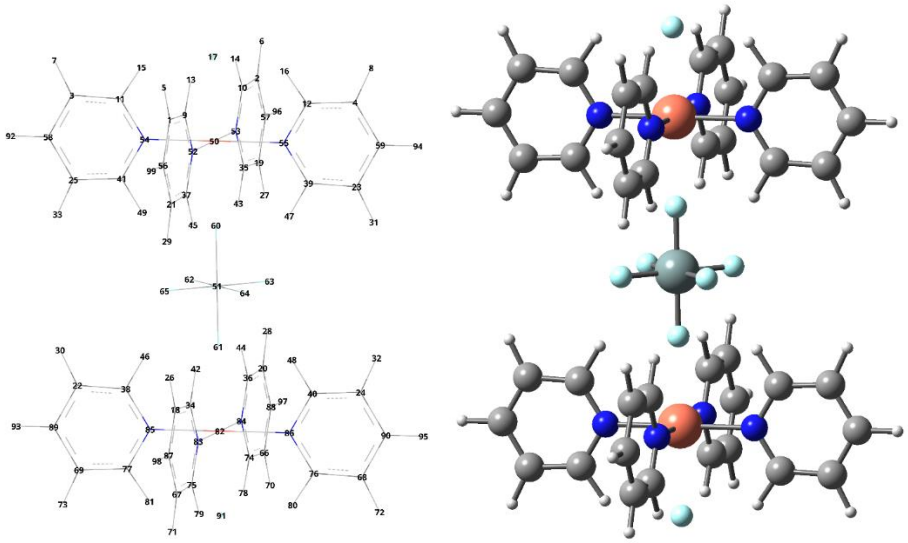

Figure A.4 – Structure of cluster 4 used to calculate charges on the SIFSIX MOF (left – wireframe view; right – ball-and-stick view). Atom labels corresponding to the notation used in Tables S7 and S8 are shown in the wireframe view. Color code for the ball-and-stick view is: Carbon – grey; Hydrogen – white; Copper – orange; Silicon – green; Fluorine – teal.

Table A1 – Point charges for the SIFSIX MOF obtained on the clusters shown in Figures A.1-A.4 using the DDEC method. Atom labels correspond to the notation used in the figures. Charges shown in bold were used to calculate the average framework charges to use in the GCMC simulations.

cluster 1			cluster 2			cluster 3			cluster 4		
label	atom	charge	label	atom	Charge	label	atom	charge	label	atom	charge
1	F	-0.501	1	C	-0.10857	1	C	-0.10162	1	C	-0.13998
2	C	-0.11832	2	C	-0.10937	2	C	-0.10198	2	C	-0.14052
3	C	-0.11832	3	C	-0.10951	3	C	-0.09839	3	C	-0.13989
4	H	0.121666	4	C	-0.10777	**4**	**C**	**-0.14438**	4	C	-0.14039
5	H	0.121666	5	H	0.132769	5	H	0.139104	5	H	0.105406
6	C	0.112357	6	H	0.132558	6	H	0.139034	6	H	0.105746
7	C	0.112357	7	H	0.132894	7	H	0.137233	7	H	0.105496
8	H	0.09155	8	H	0.132444	**8**	**H**	**0.14927**	8	H	0.10543
9	H	0.09155	9	C	0.115866	9	C	0.107106	9	C	0.102308
10	N	-0.27712	10	C	0.118986	10	C	0.111225	10	C	0.102618
11	C	-0.01916	11	C	0.116076	11	C	0.112668	11	C	0.102338
12	F	-0.50189	12	C	0.120272	**12**	**C**	**0.120751**	12	C	0.103164
13	C	-0.10187	13	H	0.123095	13	H	0.126142	13	H	0.095579
14	C	-0.10187	14	H	0.120089	14	H	0.118527	14	H	0.095594
15	H	0.123855	15	H	0.123645	15	H	0.118526	15	H	0.095671
16	H	0.123855	16	H	0.115588	**16**	**H**	**0.120288**	16	H	0.095653
17	C	0.129391	**17**	**F**	**-0.63514**	17	Si	1.978334	17	F	-0.72518
18	C	0.129391	18	C	-0.1222	18	F	-0.46949	18	C	-0.13319
19	H	0.094181	19	C	-0.12287	19	F	-0.64045	19	C	-0.13155
20	H	0.094181	20	C	-0.12182	20	F	-0.54267	20	C	-0.13199
21	N	-0.27449	21	C	-0.12192	21	F	-0.54325	21	C	-0.13315
22	C	-0.02395	22	C	-0.12266	22	F	-0.55088	22	C	-0.13298
23	F	-0.50189	23	C	-0.12415	23	F	-0.54887	23	C	-0.13188

24	C	-0.11832	24	C	-0.12186	24	C	-0.10178	24	C	-0.13184
25	C	-0.11832	25	C	-0.12274	25	C	-0.10157	25	C	-0.13336
26	C	-0.10187	26	H	0.118945	**26**	**C**	**-0.14446**	26	H	0.113462
27	C	-0.10187	27	H	0.118647	27	C	-0.0986	27	H	0.11204
28	H	0.121666	28	H	0.119478	28	H	0.139008	28	H	0.112078
29	H	0.121666	29	H	0.119058	29	H	0.139131	29	H	0.113482
30	H	0.123855	30	H	0.119299	**30**	**H**	**0.149147**	30	H	0.113445
31	H	0.123855	31	H	0.120959	31	H	0.137406	31	H	0.112136
32	C	0.112357	32	H	0.119116	32	C	0.107458	32	H	0.112126
33	C	0.112357	33	H	0.119078	33	C	0.111975	33	H	0.113444
34	C	0.129391	34	C	0.110781	**34**	**C**	**0.123054**	34	C	0.116141
35	C	0.129391	35	C	0.111409	35	C	0.112774	35	C	0.115936
36	H	0.09155	36	C	0.111795	36	H	0.12545	36	C	0.111511
37	H	0.09155	37	C	0.111208	37	H	0.119845	37	C	0.115912
38	H	0.094181	38	C	0.111275	**38**	**H**	**0.120238**	38	C	0.115102
39	H	0.094181	39	C	0.110891	39	H	0.119227	39	C	0.116729
40	Cu	0.919084	40	C	0.1112	40	Si	1.980905	40	C	0.116734
41	Si	1.928124	41	C	0.111732	41	F	-0.4753	41	C	0.111768
42	N	-0.27712	42	H	0.107043	42	F	-0.64018	42	H	0.1039
43	N	-0.27449	43	H	0.106614	43	F	-0.56233	43	H	0.103262
44	C	-0.01916	44	H	0.107085	44	F	-0.54345	44	H	0.110384
45	C	-0.02395	45	H	0.107017	45	F	-0.54935	45	H	0.103931
46	F	-0.56966	46	H	0.107173	46	F	-0.53206	46	H	0.103715
47	F	-0.56966	47	H	0.106853	47	C	-0.10179	47	H	0.104083
48	F	-0.501	48	H	0.107148	48	C	-0.10155	48	H	0.104079
49	F	-0.501	49	H	0.106705	**49**	**C**	**-0.14429**	49	H	0.10998
50	F	-0.50189	50	Cu	0.947216	50	C	-0.09851	50	Cu	0.85961

51	F	-0.50189	**51**	**Si**	**2.031855**	51	H	0.138861	**51**	**Si**	**2.027532**
52	Si	1.928124	52	N	-0.23855	52	H	0.139092	52	N	-0.24403
53	F	-0.501	53	N	-0.24165	**53**	**H**	**0.149136**	53	N	-0.24454
54	H	0.104079	54	N	-0.24048	54	H	0.137264	54	N	-0.24491
55	H	0.104079	55	N	-0.23935	55	C	0.11248	55	N	-0.2462
56	H	0.100758	56	C	-0.01397	56	C	0.107329	56	C	-0.03049
57	H	0.100758	57	C	-0.01483	**57**	**C**	**0.120763**	57	C	-0.03083
58	F	-0.32797	58	C	-0.01453	58	C	0.112952	58	C	-0.03108
59	F	-0.32797	59	C	-0.01459	59	H	0.117609	59	C	-0.03017
			60	**F**	**-0.62891**	60	H	0.127066	**60**	**F**	**-0.62867**
			61	**F**	**-0.62914**	**61**	**H**	**0.120098**	**61**	**F**	**-0.629**
			62	**F**	**-0.61769**	62	H	0.119372	**62**	**F**	**-0.61067**
			63	**F**	**-0.61752**	**63**	**Cu**	**0.984735**	**63**	**F**	**-0.6226**
			64	**F**	**-0.61716**	64	Si	1.980385	**64**	**F**	**-0.6206**
			65	**F**	**-0.61759**	65	N	-0.22512	**65**	**F**	**-0.6224**
			66	C	-0.10871	66	N	-0.22464	66	C	-0.14047
			67	C	-0.10813	67	N	-0.22404	67	C	-0.14
			68	C	-0.10807	**68**	**N**	**-0.22725**	68	C	-0.14042
			69	C	-0.10865	**69**	**C**	**-0.07841**	69	C	-0.13988
			70	H	0.132916	70	C	-0.00732	70	H	0.105743
			71	H	0.132485	71	C	-0.00648	71	H	0.105409
			72	H	0.132622	72	C	-0.0085	72	H	0.105428
			73	H	0.132848	**73**	**C**	**0.199724**	73	H	0.105488
			74	C	0.116395	74	F	-0.63847	74	C	0.102722
			75	C	0.120602	75	F	-0.46784	75	C	0.102298
			76	C	0.12042	76	F	-0.54087	76	C	0.103186
			77	C	0.120839	77	F	-0.54336	77	C	0.102372

			78	H	0.123136	78	F	-0.54898	78	H	0.095623
			79	H	0.115715	79	F	-0.56036	79	H	0.095581
			80	H	0.115658	80	C	-0.10182	80	H	0.095639
			81	H	0.115574	81	C	-0.10134	81	H	0.095654
			82	Cu	0.95044	82	C	-0.09858	82	Cu	0.859652
			83	Si	1.998066	**83**	**C**	**-0.14455**	83	N	-0.24405
			84	N	-0.24042	84	H	0.139007	84	N	-0.24511
			85	N	-0.23852	85	H	0.138844	85	N	-0.24445
			86	N	-0.23879	86	H	0.137421	86	N	-0.24615
			87	N	-0.23899	**87**	**H**	**0.148919**	87	C	-0.0305
			88	C	-0.01477	88	C	0.109493	88	C	-0.03074
			89	C	-0.01429	89	C	0.112342	89	C	-0.03109
			90	C	-0.01391	90	C	0.112568	90	C	-0.03018
			91	C	-0.01446	**91**	**C**	**0.1224**	91	F	-0.72522
			92	**F**	**-0.63255**	92	H	0.122439	92	H	0.091172
			93	F	-0.46496	93	H	0.117655	93	H	0.09117
			94	F	-0.57701	94	H	0.1184	94	H	0.090872
			95	F	-0.57551	**95**	**H**	**0.11978**	95	H	0.090867
			96	F	-0.5752	**96**	**Cu**	**0.984842**	96	H	0.091082
			97	F	-0.57388	97	Si	1.978731	97	H	0.091094
			98	Si	1.996667	98	N	-0.22546	98	H	0.090873
			99	F	-0.57718	99	N	-0.2237	99	H	0.09088
			100	F	-0.57856	**100**	**N**	**-0.22991**			
			101	F	-0.57667	101	N	-0.22471			
			102	F	-0.57657	**102**	**C**	**-0.07584**			
			103	F	-0.46517	103	C	-0.00744			
			104	H	0.103633	104	C	-0.00711			

			105	H	0.103776	**105**	**C**	**0.198948**			
			106	H	0.10375	106	C	-0.00781			
			107	H	0.103416	107	F	-0.63918			
			108	H	0.103566	108	F	-0.47273			
			109	H	0.103498	109	F	-0.54998			
			110	H	0.103622	110	F	-0.54779			
			111	H	0.103984	111	F	-0.5424			
						112	F	-0.54214			
						113	H	0.114523			
						114	H	0.11441			
						115	H	0.114604			
						116	H	0.114796			
						117	H	0.115366			
						118	H	0.115153			

Table A.2 – Point charges for the SIFSIX MOF obtained on the clusters shown in Figures A.1-A.4 using the CHELPG method. Atom labels correspond to the notation used in the figures. Charges shown in bold were used to calculate the average framework charges to use in the GCMC simulations.

cluster 1			cluster 2			cluster 3			cluster 4		
label	atom	charge	label	atom	charge	label	atom	charge	label	atom	charge
1	F	-0.37595	1	C	-0.22238	1	C	-0.1965	1	C	-0.22572
2	C	-0.20276	2	C	-0.22194	2	C	-0.19381	2	C	-0.22589
3	C	-0.20276	3	C	-0.22422	3	C	-0.20946	3	C	-0.22568
4	H	0.143968	4	C	-0.22365	**4**	**C**	**-0.30204**	4	C	-0.22544
5	H	0.143968	5	H	0.16573	5	H	0.166359	5	H	0.122268
6	C	0.212575	6	H	0.164916	6	H	0.165925	6	H	0.122286
7	C	0.212575	7	H	0.165237	7	H	0.168271	7	H	0.122233
8	H	-0.00393	8	H	0.165361	**8**	**H**	**0.188808**	8	H	0.1222
9	H	-0.00393	9	C	0.242215	9	C	0.242863	9	C	0.156073
10	N	-0.26024	10	C	0.245889	10	C	0.238467	10	C	0.156351
11	C	0.059031	11	C	0.257806	11	C	0.271539	11	C	0.156192
12	F	-0.37633	12	C	0.251577	**12**	**C**	**0.256479**	12	C	0.154192
13	C	-0.19336	13	H	0.002823	13	H	0.001198	13	H	0.04497
14	C	-0.19336	14	H	0.001397	14	H	0.009692	14	H	0.044886
15	H	0.145892	15	H	-0.00788	15	H	0.005259	15	H	0.044967
16	H	0.145892	16	H	-0.00489	**16**	**H**	**0.032156**	16	H	0.045711
17	C	0.27726	17	F	-0.17206	17	Si	1.316719	17	F	-0.55533
18	C	0.27726	18	C	-0.2546	18	F	-0.38	18	C	-0.25299
19	H	-0.0271	19	C	-0.25543	19	F	-0.37468	19	C	-0.25293
20	H	-0.0271	20	C	-0.25226	20	F	-0.40926	20	C	-0.25292
21	N	-0.32581	21	C	-0.2525	21	F	-0.41179	21	C	-0.253
22	C	0.050488	22	C	-0.25544	22	F	-0.41382	22	C	-0.25294
23	F	-0.37633	23	C	-0.25375	23	F	-0.4102	23	C	-0.25228

24	C	-0.20276	24	C	-0.25364	24	C	-0.19606	24	C	-0.25228
25	C	-0.20276	25	C	-0.25618	25	C	-0.19457	25	C	-0.25295
26	C	-0.19336	26	H	0.158466	**26**	**C**	**-0.30302**	26	H	0.143723
27	C	-0.19336	27	H	0.158422	27	C	-0.20919	27	H	0.143717
28	H	0.143968	28	H	0.15827	28	H	0.16654	28	H	0.143719
29	H	0.143968	29	H	0.158049	29	H	0.166107	29	H	0.143722
30	H	0.145892	30	H	0.158961	**30**	**H**	**0.188866**	30	H	0.143711
31	H	0.145892	31	H	0.157967	31	H	0.168026	31	H	0.14338
32	C	0.212575	32	H	0.158253	32	C	0.237398	32	H	0.143382
33	C	0.212575	33	H	0.158817	33	C	0.236852	33	H	0.14371
34	C	0.27726	34	C	0.3104	**34**	**C**	**0.26251**	34	C	0.282897
35	C	0.27726	35	C	0.310985	35	C	0.272198	35	C	0.28283
36	H	-0.00393	36	C	0.306597	36	H	0.011228	36	C	0.282822
37	H	-0.00393	37	C	0.306012	37	H	0.005886	37	C	0.282901
38	H	-0.0271	38	C	0.31169	**38**	**H**	**0.027149**	38	C	0.28321
39	H	-0.0271	39	C	0.308484	39	H	0.005963	39	C	0.281947
40	Cu	0.647588	40	C	0.30947	40	Si	1.321001	40	C	0.28194
41	Si	1.25335	41	C	0.312887	41	F	-0.38538	41	C	0.283214
42	N	-0.26024	42	H	-0.12205	42	F	-0.37928	42	H	-0.09297
43	N	-0.32581	43	H	-0.12289	43	F	-0.42758	43	H	-0.09274
44	C	0.059031	44	H	-0.12024	44	F	-0.39645	44	H	-0.09277
45	C	0.050488	45	H	-0.12115	45	F	-0.4191	45	H	-0.09295
46	F	-0.23454	46	H	-0.1216	46	F	-0.39975	46	H	-0.09292
47	F	-0.23454	47	H	-0.12145	47	C	-0.19288	47	H	-0.09263
48	F	-0.37595	48	H	-0.12108	48	C	-0.19667	48	H	-0.09265
49	F	-0.37595	49	H	-0.12288	**49**	**C**	**-0.30232**	49	H	-0.0929
50	F	-0.37633	50	Cu	0.232363	50	C	-0.20939	50	Cu	0.317408

51	F	-0.37633	**51**	**Si**	**2.964441**	51	H	0.165521	**51**	**Si**	**2.872139**
52	Si	1.25335	52	N	-0.17497	52	H	0.166419	52	N	-0.1594
53	F	-0.37595	53	N	-0.18205	**53**	**H**	**0.188793**	53	N	-0.15966
54	H	0.087247	54	N	-0.18864	54	H	0.168233	54	N	-0.16006
55	H	0.087247	55	N	-0.1838	55	C	0.235707	55	N	-0.15867
56	H	0.081397	56	C	0.066738	56	C	0.242786	56	C	0.060252
57	H	0.081397	57	C	0.064502	**57**	**C**	**0.256503**	57	C	0.060296
58	F	-0.23525	58	C	0.06522	58	C	0.271076	58	C	0.060207
59	F	-0.23525	59	C	0.066588	59	H	0.012061	59	C	0.061354
			60	F	-0.30991	60	H	0.001523	**60**	**F**	**-0.4487**
			61	F	-0.31517	**61**	**H**	**0.032543**	**61**	**F**	**-0.44854**
			62	F	-0.69807	62	H	0.005823	**62**	**F**	**-0.6755**
			63	F	-0.69805	**63**	**Cu**	**0.800135**	**63**	**F**	**-0.67548**
			64	F	-0.69819	64	Si	1.318458	**64**	**F**	**-0.67542**
			65	F	-0.69782	65	N	-0.24248	**65**	**F**	**-0.67537**
			66	C	-0.2223	66	N	-0.24559	66	C	-0.22587
			67	C	-0.22085	67	N	-0.30037	67	C	-0.2257
			68	C	-0.22341	**68**	**N**	**-0.30073**	68	C	-0.22542
			69	C	-0.22415	**69**	**C**	**-0.13234**	69	C	-0.22566
			70	H	0.165798	70	C	0.062542	70	H	0.122284
			71	H	0.164902	71	C	0.061199	71	H	0.122265
			72	H	0.165419	72	C	0.072865	72	H	0.122197
			73	H	0.165448	**73**	**C**	**0.400466**	73	H	0.122231
			74	C	0.242771	74	F	-0.3762	74	C	0.156296
			75	C	0.241032	75	F	-0.38016	75	C	0.156017
			76	C	0.251102	76	F	-0.4097	76	C	0.154136
			77	C	0.257899	77	F	-0.4124	77	C	0.156138

			78	H	0.002768	78	F	-0.41409	78	H	0.04494
			79	H	0.004685	79	F	-0.41065	79	H	0.045024
			80	H	-0.00386	80	C	-0.19485	80	H	0.045766
			81	H	-0.00819	81	C	-0.19458	81	H	0.045016
			82	Cu	0.242943	82	C	-0.20976	82	Cu	0.317151
			83	Si	1.334378	**83**	**C**	**-0.30219**	83	N	-0.15933
			84	N	-0.18083	84	H	0.165826	84	N	-0.15958
			85	N	-0.17666	85	H	0.165777	85	N	-0.15998
			86	N	-0.1879	86	H	0.168188	86	N	-0.1586
			87	N	-0.185	**87**	**H**	**0.188619**	87	C	0.06024
			88	C	0.065049	88	C	0.240256	88	C	0.060285
			89	C	0.066989	89	C	0.23755	89	C	0.060194
			90	C	0.065365	90	C	0.272959	90	C	0.061344
			91	C	0.06684	**91**	**C**	**0.256551**	91	F	-0.5554
			92	F	-0.17525	92	H	0.002058	92	H	0.071278
			93	F	-0.36914	93	H	0.010431	93	H	0.071279
			94	F	-0.45667	94	H	0.005387	94	H	0.070639
			95	F	-0.45432	**95**	**H**	**0.03258**	95	H	0.070639
			96	F	-0.45534	**96**	**Cu**	**0.801621**	96	H	0.071256
			97	F	-0.45219	97	Si	1.31679	97	H	0.071256
			98	Si	1.333462	98	N	-0.24405	98	H	0.071273
			99	F	-0.45696	99	N	-0.23808	99	H	0.071273
			100	F	-0.45566	**100**	**N**	**-0.30344**			
			101	F	-0.45481	101	N	-0.30367			
			102	F	-0.45361	**102**	**C**	**-0.13093**			
			103	F	-0.37337	103	C	0.063275			
			104	H	0.090377	104	C	0.061308			

			105	H	0.089513	**105**	**C**	**0.39968**			
			106	H	0.090176	106	C	0.072882			
			107	H	0.089345	107	F	-0.37655			
			108	H	0.089288	108	F	-0.38003			
			109	H	0.089852	109	F	-0.41355			
			110	H	0.089904	110	F	-0.41024			
			111	H	0.08946	111	F	-0.40902			
						112	F	-0.41186			
						113	H	0.100605			
						114	H	0.100818			
						115	H	0.100723			
						116	H	0.100169			
						117	H	0.100253			
						118	H	0.100264			